

**ENCAPSULATION AND CONTROLLED RELEASE OF ACTIVE DNA
FROM UNCROSSLINKED GELATIN MICROSPHERES**

A Dissertation
Presented to
The Academic Faculty

by

James Otey Hardin IV

In Partial Fulfillment
of the Requirements for the Degree
Doctor of Philosophy in Materials Science and Engineering

Georgia Institute of Technology

May 2012

Encapsulation and Controlled Release of Active DNA from Uncrosslinked Gelatin Microspheres

Approved by:

Dr. Valeria T. Milam, Advisor
School of Material Science and
Engineering
Georgia Institute of Technology

Dr. Ken H. Sandhage
School of Material Science and
Engineering
Georgia Institute of Technology

Dr. Vladimir Tsukruk
School of Material Science and
Engineering
Georgia Institute of Technology

Dr. Ken Gall
School of Material Science and
Engineering
Georgia Institute of Technology

Dr. Niren Murthy
School of Biomedical Engineering
Georgia Institute of Technology

Date Approved: November 15, 2011

ACKNOWLEDGEMENTS

I would like to thank all my friends, family and coworkers, who have supported, advised, cajoled and harassed me throughout the years of my PhD work. Specifically, I would like to thank Dr. Bryan Baker for providing constant intellectual, logistical, physical and philosophical support, Dr. Valeria Milam for constant patience and faith in my ability to accomplish this work even when I was prepared to accept failure, and Ceil and Jim Hardin for all the love, wise advice, and friendship that a son could hope for. I would also like to thank Dr. Chris Tison, Didi Eze, Alex Weller, Rick Sullivan, and Maeling Tapp for making work a joy most of the time and patiently listening to my stories of gerbil mixers and flesh-eating bacteria. Furthermore, without the early support of my pursuit of research during my high school and undergraduate education from Drs. David Stone, Marvin Payne, Jing-Yuan Zhang, Chuck Carr, Mary Lynn Realff, and Heungsup Park it is unlikely I would have pursued this path. Finally, I would like to thank Rachel Frieswick for her love and cookies which have kept me moving and motivated during the last phase of my thesis work.

I would also like to gratefully acknowledge the financial support of this research from the Georgia Cancer Coalition Distinguished Scholars Program, Emory-Georgia Tech Center for Cancer Nanotechnology Excellence (National Cancer Institute), NSF CAREER, Army Research Office and the GAANN fellowship through Georgia Tech's Center for Drug Design, Development and Delivery (CD4). Without their belief in the potential of this work, it would have remained just a dream. Flow cytometry and confocal microscopy were performed at the Institute of Bioengineering and Biosciences (IBB) Core Lab facilities and was supported by Jonafel Crowe and Steven Woodard who were always available and helpful.

TABLE OF CONTENTS

	Page
ACKNOWLEDGEMENTS	iii
LIST OF TABLES	viii
LIST OF FIGURES	ix
LIST OF SYMBOLS AND ABBREVIATIONS	xii
SUMMARY	xiii
CHAPTER 1: INTRODUCTION	1
1.1 DNA Encapsulation	4
1.1.1 Current Methods	4
1.1.2 Gelatin Properties.....	7
1.1.3 Gelatin Particle Synthesis	8
1.1.4 Drug Delivery with Gelatin Particles.....	13
1.1.5 Gelatin Hybrids.....	15
1.1.6 Layer by Layer Deposition	16
1.2 Controlling Functionality of Colloids with DNA	19
1.2.1 DNA Hybridization.....	19
1.2.2 Modeling Primary Hybridization in Solution	22
1.2.3 Modeling Competitive Hybridization in Solution	23
1.2.4 Hybridization on Surfaces	25
1.3 DNA-Mediated Colloidal Assembly.....	30
1.3.1 Nonspecific Colloidal Forces.....	30
1.3.2 DNA-mediated Colloidal Assembly	31

1.4 References.....	38
CHAPTER 2: DNA ENCAPSULATION IN GELATIN MICROSPHERES.....	50
2.1 Overview.....	50
2.2 Materials and Methods.....	51
2.2.1 Materials	51
2.2.2 Preparation of DNA-Gelatin Blocks.....	51
2.2.3 Preparation and DNA Loading of Gelatin Microspheres	53
2.2.4 Zeta Potential Measurements of GMS.....	55
2.2.5 Release of Encapsulated DNA Strands.....	55
2.2.6 Preparation and Hybridization of DNA-Functionalized Polystyrene Microspheres.....	56
2.2.7 Flow Cytometry	56
2.2.8 Determination of GMS Concentration.....	57
2.2.9 Microscopy	58
2.3 Results and Discussion	58
2.3.1 Oligonucleotide Release from Gelatin Blocks.....	58
2.3.2 Oligonucleotide Gelatin Microspheres	65
2.4 Conclusions.....	72
2.5 References.....	73
CHAPTER 3: INVESTIGATING DNA HYBRIDIZATION AT SURFACES.....	74
3.1 Overview.....	74
3.2 Materials and Methods.....	75

3.2.1 DNA Sequences	75
3.2.2 Post washing Hybridization Experiments	75
3.2.3 <i>In situ</i> Hybridization Experiments	77
3.2.4 Analysis of Competitive Displacement Activity	78
3.3 Results and Discussion	80
3.3.1 <i>In situ</i> Primary Kinetics	80
3.3.2 Investigation of Electrostatics of Hybridization	84
3.3.3 Secondary Post Washing Hybridization Experiments	88
3.3.4 <i>In situ</i> Secondary Displacement Studies	95
3.4 Conclusions	101
3.5 References	102
CHAPTER 4: TRIGGERED CHANGES IN SURFACE FUNCTIONALITY OF GMS-BASED COLLOIDAL ASSEMBLIES	103
4.1 Overview	103
4.2 Materials and Methods	103
4.2.1 Materials	103
4.2.2 Construction of Device	104
4.2.3 Generation of Microspheres	105
4.2.4 GMS Processing	108
4.2.5 Preparation of PS Microspheres	108
4.2.6 Optimization of DNA hybridization	109
4.2.7 Assembly on GMS	109
4.2.8 Release of Competitive DNA	110

4.3 Results and Discussion	110
4.3.1 GMS Synthesis.....	110
4.3.2 Investigation of Competition at Elevated Temperature	114
4.3.3 Assembly.....	116
4.4 Conclusions.....	121
4.5 References.....	122
CHAPTER 5: CONCLUSIONS AND FUTURE WORK.....	123
5.1 Gelatin Microsphere Synthesis	124
5.2 Gelatin-Polyelectrolyte Interface	125
5.3 Intrinsic Colloidal Disassembly	126
5.4 Surface Hybridization	127
5.5 Alternate Applications	128
5.6 References.....	130
APPENDIX A: FURTHER DISCUSSION OF KINETICS AND ENERGETICS OF HYBRIDIZATION	131
A.1 ΔS Changes Due to Immobilization.....	131
A.2 Reaction at the Surface	135
A.3 Kinetics of Hybridization.....	136
A.4 References	141
VITA	142

LIST OF TABLES

	Page
Table 1.1 Examples of LbL films substrates and a substrate shapes.	17
Table 3.1 List of the function and nomenclature for all DNA sequences employed.....	76
Table 3.2 Observed rate of primary duplex formation.....	82
Table 3.3 Measured displacement rates	91

LIST OF FIGURES

		Page
Figure 1.1	Goals of this work.....	4
Figure 1.2	Strategies of delivering DNA and controlling its release	5
Figure 1.3	Illustration of the gelatin matrix	8
Figure 1.4	Example of GMS made using a W/O emulsion.....	9
Figure 1.5	Example of GMS made using a desolvation technique	10
Figure 1.6	Gelatin nanoparticles produces via coacervation of gelatin.	11
Figure 1.7	A simplistic model of a DNA duplex	20
Figure 1.8	Description of the terms used to describe the function of DNA sequences and pathways of competitive displacement	24
Figure 1.9	Schemes used to induce DNA-mediated particle assembly.....	33
Figure 2.1	Graphical description of study involving DNA release from gelatin blocks	53
Figure 2.2	W/O emulsion synthesis of GMS	54
Figure 2.3	Concentration of P14-F DNA released from uncoated gelatin-DNA blocks of varying gelatin concentration	59
Figure 2.4	Concentration of P14-F DNA released from gelatin-DNA blocks coated with varying numbers of PAH/PAA bilayers	62
Figure 2.5	Release of DNA from 20% gelatin blocks coated with 1 to 3 bilayers	62
Figure 2.6	Concentration of P14-F DNA released from uncoated and coated gelatin- DNA blocks loaded with either 2 μ M or 10 μ M solution of DNA	64
Figure 2.7	Histogram of GMS diameters before and after washing steps	66

Figure 2.8	Phase contrast and fluorescence micrographs showing GMS suspensions at various processing stages	68
Figure 2.9	Phase contrast micrographs of an individual GMS.....	69
Figure 2.10	Concentration of P14-F DNA released from GMS	71
Figure 2.11	Impact of incubation at room temperature on GMS	72
Figure 3.1	Schematic diagram of the hybridization reactions and pathways examined in this work.....	78
Figure 3.2	<i>In situ</i> measurements of primary duplex formation.....	82
Figure 3.3	Surface density of fluorescently labeled primary targets.....	85
Figure 3.4	Comparison between the calculated solution-based and experimentally observed ΔG values.....	87
Figure 3.5	The difference between observed and calculated energetics as a function of number of bases in primary target.....	89
Figure 3.6	Fraction of various primary targets displaced.....	90
Figure 3.7	Observed displacement rates as a function of total number of base-pair matches	91
Figure 3.8	<i>In situ</i> measurements of the fraction of fluorescently labeled primary target	96
Figure 3.9	Fraction of primary target, M11-F , displaced by P15 secondary targets ..	99
Figure 3.10	Investigation of the effect of the fluorescent label on hybridization	100
Figure 4.1	Top view schematic and photograph of microfluidic device.....	105
Figure 4.2	Arrangement of microfluidic GMS production apparatus.....	106
Figure 4.3	Picture of the various device types investigated in this project.....	111

Figure 4.4	The three flow arrangements mentioned in this work	112
Figure 4.5	Phase contrast micrograph showing the uniform gelatin microspheres...	113
Figure 4.6	Bar graphs of primary targets remaining	115
Figure 4.7	Phase contrast micrographs of the colloidal satellite assemblies.....	117
Figure 4.8	Evidence of intrinsic DNA-mediated change in surface functionalization	119
Figure 4.9	A series of micrographs depicting the structure of the assemblies used in an attempt to induce DNA-mediated disassembly	120
Figure A.1	Fraction of allowed conformations as a function of the initial height above the surface.....	134
Figure A.2	Examples of hypothetical fractions of primary target released in the presence of noncomplementary or competitive DNA	140

LIST OF SYMBOLS AND ABBREVIATIONS

DNA	Deoxyribonucleic Acid
ssDNA	Single Stranded DNA
dsDNA	Double Stranded DNA
A	Adenine
T	Thymine
C	Cytosine
G	Guanine
GMS	Gelatin Microsphere
PS	Polystyrene
PAH	Poly(allylamine hydrochloride)
PAA	Poly(acrylic acid)
EDC	1-ethyl-3-(3-dimethylaminopropyl) carbodiimide
PE	Polyelectrolyte
bL	Polyelectrolyte Bilayer
LbL	Layer-by-layer

SUMMARY

This thesis work investigates the encapsulation of DNA in gelatin microspheres (GMS) and the subsequent temperature controlled release of the encapsulated DNA from these GMS. DNA-loaded GMS were then used as templates for colloidal satellite assemblies and the released DNA was shown to competitively displace the original partner strands of immobilized DNA on the surface of the assemblies. To support these investigations, hybridization of DNA at colloidal surfaces was also investigated using *in situ* measurements. DNA hybridization is of particular interest as means of controlling the functionality of colloidal structures because it is uniquely reversible and tunable as well as biocompatible. Gelatin was chosen as the encapsulation matrix for its superior biocompatibility, convenient gel to liquid phase transition at $\sim 35^{\circ}\text{C}$, and economical availability.

This thesis is divided into five chapters. Chapter 1 covers the motivation of this work and provides a general background for the materials used. Chapter 2 details the synthesis of GMS and the use of these uncrosslinked GMS as controlled release matrices for active DNA. Bare GMS were not found to be able to inhibit DNA release on their own. With the addition of a polyelectrolyte bilayer, however, clear inhibition of DNA release at room temperature and permitted release at 37°C was observed. Chapter 3 is an investigation of the thermodynamics and kinetics of primary and secondary DNA hybridization at colloidal surfaces. Flow cytometry was used to quantify the hybridization reaction *in situ* and compare it to more conventional measurement protocols involving washing steps. The post washing results illuminated the importance of the toehold region and demonstrated changes in kinetics with changing toehold length which are consistent with published solution studies of toehold-mediated strand

displacement. The *in situ* studies enabled the measurement of primary hybridization rate as well as secondary hybridization rate. Despite the significant deviation in degree of hybridization that washing steps can induce, the *in situ* and post washing results were still similar in their overall trends. Chapter 4 details the use of microfluidics to manufacture monodisperse GMS as well as the subsequent assembly of colloidal satellite structures using these GMS. DNA released from the GMS template particle was found to competitively displace fluorescently labeled primary hybridization partners on the DNA-functionalized satellite particles, thus changing the duplex “expression” of the surface of the colloidal assembly. Chapter 5 offers some concluding remarks and some areas for future exploration.

CHAPTER 1

INTRODUCTION

Cancer is a disease that varies dramatically from person to person due to the specifics of the individual's physiology and the source of the cancer. In most cases, the origin of the cancer can be determined (only 2 to 4% of cancer cannot be traced to a primary site of origin)¹ but metastasis can lead to tumors anywhere and thus many cancers require treatment of the whole body. Since many of the drugs that are used to treat cancer are toxic to healthy cells as well as cancerous ones, there has been considerable interest in developing ways to convey the drug specifically to the cancer cells with minimal exposure to healthy cells. Colloid drug delivery vehicles have shown considerable progress toward this end,² while also reducing degradation of the drug prior to delivery to targeted sites (particularly important for oligonucleotide and protein therapeutics), and controlling release rates.

Targeting cancerous tumors with colloidal particles can be done through either passive or active modes. Colloidal particles are reported to passively target tumors due to the enhanced permeability and retention effects of the tumor environment (given a particle diameter less than ~200 nm) or by accumulating in portions of the body responsible for the clearance or filtration of small foreign particulates (liver, spleen and bone marrow). Significant passive accumulation is usually accomplished through a stealth coating which minimizes interactions with the body's natural means of disposing of such particles (macrophages). Functionalization of the surface of the particle with ligands for receptors specific to the tumors cells can be used to actively target the tumor

but also increase clearance of the particles. Switching between an initial passive stealth coating and subsequent active targeting ligands would provide an ideal combination of these targeting modes but requires specific timing of the switch from passive to active mode to be effective.

Tunability (to get the right timing), reversibility (to be able to form and break the linkage), and specificity (to reduce chance of side reactions) are important qualities for whatever linking scheme is used to attach a shedable functionality like the stealth coating discussed above. Nature provides a great example of such a linking scheme, DNA hybridization. DNA duplexes could be used to attach a stealth coating to a colloidal particle, thus supporting passive targeting, and subsequent displacement of these duplexes by competitive hybridization could specifically remove the stealth coating, thus unveiling surface-immobilized targeting ligands for active targeting. The kinetics of this competitive DNA displacement reaction are highly tunable. Even if other linking systems later prove to be more commercially effective, the ability to tune the energetics of a linkage (by tuning the energetics of the primary and secondary hybridization events) enables rational explorations of the design space.

Although tunable and controlled changing of the functionalization of a colloidal assembly has many applications, there is still the issue of how to introduce the competitive DNA required to induce this change. Following the injection of the colloids with a second injection of large amounts of competitive DNA seems impractical in addition to the concerns about possible side effects such a large amount of DNA might induce. By encapsulating the competitive DNA inside a semipermeable particle, the release mechanism becomes intrinsic to the assembly, unnecessary exposure to excess

DNA can be significantly reduced, and another mechanism for controlling the kinetics of release is introduced. As above, DNA can be viewed as a model payload molecule, functioning as a release agent in this case, for exploring a colloidal controlled release system with applications beyond controlling surface functionalization.

The overall goals of this project are represented in Figure 1.1. The first goal is to encapsulate DNA in a gelatin microsphere. Once the DNA is loaded, it needs to be trapped by a barrier which controls the release of DNA. Ideally, this barrier is impermeable (to DNA) at room temperature but permeable at 37 °C. This step is followed by the possible addition of another layer to permit DNA functionalization. This second layer is not necessary if the first layer can be functionalized with DNA without losing its controlled release properties but nonspecifically adsorbed DNA-functionalized particles are used in this work. These particles may already possess the additional functionality of interest (such as fluorescence or stealth coating) or that functionality can be added at this step. This additional functionality could also include other drug loaded particles or diagnostic particles to permit treatment with an easily defined ratio of drugs. The last goal is to use the DNA released at 37 °C to elicit DNA-mediated release of the additional functionalities added in the previous steps.

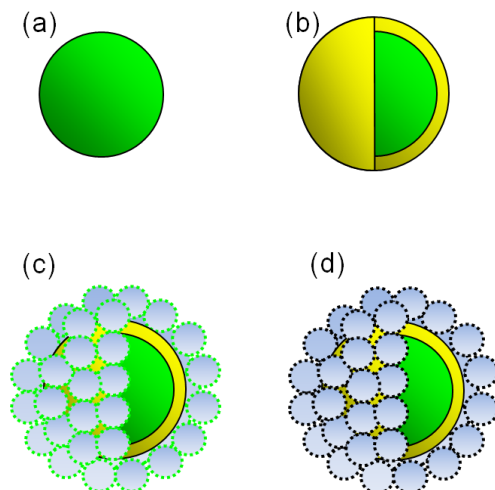


Figure 1.1. Goals of this work. (a) Infiltration of competitive DNA into a template gelatin microsphere is followed by (b) temporarily trapping DNA through deposition of a polymeric capsule. (c) DNA functionalization of the surface is achieved by adsorbing one layer of polystyrene microspheres functionalized with fluorescently-labeled DNA duplexes. (d) Finally, upon heating to 37 °C, the infiltrated competitive DNA escapes from the template gelatin particle and displaces the original fluorescently-labeled hybridization partner thus reducing the fluorescence of the satellite particles.

1.1 DNA Encapsulation

1.1.1 Current Methods

Successful encapsulation of DNA in a manner that permits its temperature-triggered release *in vivo* is the first step in developing the colloidal drug delivery vehicle described in Figure 1.1. Many different materials have been used as a controlled release reservoir for DNA. Polymers such as poly(lactic acid) (PLA)³, poly(lactic-co-glycolic acid) (PGLA)³⁻⁵, are often used to encapsulate DNA as depicted in Figure 1.2 (a).

Liposomes, though very effective for delivering other pharmaceuticals, appear to be more limited in terms of effective, stable DNA loading. Recent progress in liposomes-based carriers for DNA may help alleviate these issues by using improved DNA loading techniques or using negatively charged liposomes.^{6,7} Polymersomes reportedly enable

better transfection than liposomes as well as expand the possibility for release triggered by pH changes incurred during endocytosis.⁸ Layer-by-layer (LbL) capsules provide another means for encapsulating DNA.⁹ LbL capsules, liposomes and polymersomes all house the DNA in an aqueous core surrounded by a barrier as depicted in Figure 1.2 (b). Complexation of DNA with both natural and synthetic polycations, as depicted in Figure 1.2 (c), has proven an effective means of trapping DNA, but covalent crosslinking of the polycations is usually necessary to maintain stability for more than a few hours in serum.^{10, 11 12} The distortion of the DNA strand during complexation or crosslinking steps can also impede its later function.¹³ DNA-b-PPO (poly(propylene oxide)) micelles, with the DNA presented on the surface, were tested as targeted drug delivery vehicles, but were found to significantly reduce cell viability.¹⁴ DNA has also been loaded onto the surface of gold nanoparticles to promote gene knock down.¹⁵ In DNA-b-PPO micelle and gold nanoparticle cases, the DNA is attached to the surface of a particle, as depicted in Figure 1.2 (d). While there is a very rich spectrum of delivery strategies with the various carriers illustrated above, hydrogel-based carriers represent a less explored, but promising DNA carrier candidate.

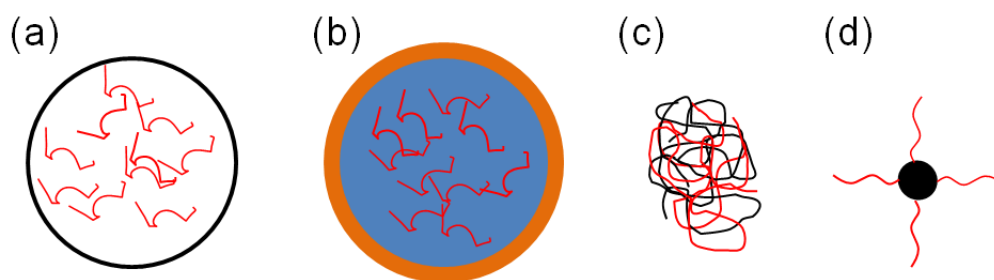


Figure 1.2. Strategies of delivering DNA and controlling its release can involve (a) simple entrapment of DNA in a biodegradable solid; (b) a protective shell around an aqueous DNA-containing core; (c) DNA complexation with polycations or other species that bind strongly with DNA to facilitate cell transfection; (d) grafting DNA to the carrier surface.

Hydrogel-based particles, also called microgels or nanogels, are another class of carriers with generally high biocompatibility and the potential for tuning the release rates of encapsulated agents.¹⁶ This tunability is typically achieved by changing the pore size of the semipermeable matrix. The high biocompatibility is due the high water content of hydrogels and their structural similarity to the extracellular matrix.¹⁶ Poly(*N*-isopropylmethacrylamide) (pNIPMAm) is a temperature responsive polymer that can be crosslinked to form hydrogel particles for the purposes of drug delivery.¹⁷ By polymerizing a copolymer shell around a pNIPMAm particle, the particle can be imparted with surface localized functionality while trapping the therapeutic payload inside the core. As one example, PNIPMAm particles have been functionalized with a targeting protein and loaded with siRNA via a “breathing-in” method.¹⁷ Another popular microgel material for biomaterial applications is alginate. Alginate microspheres loaded with calf thymus DNA were shown to be stable enough to survive passage through the entire GI tract although significant damage to the microspheres was reported.¹¹ Plasmid DNA has also been encapsulated in a poly(ethylene glycol) or PEG-based polymer network using photocrosslinking.¹⁸ Although this method can lead to some delayed burst release profiles, it also leads to chemical changes in the plasmid that may be detrimental to its function. As an alternative to using chemical crosslinks, natural polymers that form physical crosslinks are being explored. Of these natural polymers, gelatin is probably the most well known.

1.1.2 Gelatin Properties

Gelatin is a ubiquitous, but complex material. It is produced by degrading collagen from various animal sources in hot alkali or acid baths. This process modifies many of the amino acids and breaks down the amino acid chains yielding a very polydisperse solution of collagen fragments, however, the ability to form triple helices between chains via secondary interactions remains intact for many of these fragments. These triple helices mediate hydrogel formation as shown in Figure 1.3. The polydispersity of the amino acid chains that make up and these triple helix forming regions leads to a broad and very history dependent gel transition, however the “melting” temperature is usually in the range from 30 °C to 35 °C.¹⁹ This phase transition between room temperature and body temperature is convenient for long term storage purposes as well as many drug delivery applications. Gelatin is also amphiprotic (able to have both positive and negative charges) due to the amine and carboxyl groups in some of the residues, which further complicates its interactions. Gelatin is generally regarded as safe by the US FDA and has been used in intravenous injections²⁰, implants,²¹⁻²⁴ and ingested drug formulations although its use as a plasma expander has been banned because it reduced clotting²⁵ (a significant problem in that application but not an issue in many others). Gelatin has also been used as a coating to reduce the cytotoxicity of quantum dots.²⁶ Gelatin microspheres and nanospheres are of particular relevance to the current work as potential matrices for temporarily storing, then releasing oligonucleotides.

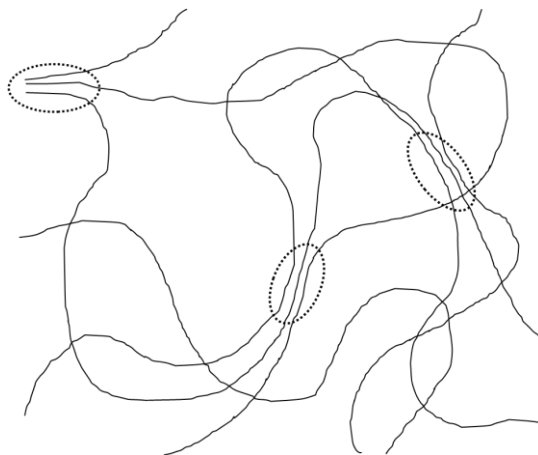


Figure 1.3. Schematic illustration of the gelatin matrix showing amorphous or random coil regions as well as triple helices (circled).

1.1.3 Gelatin Particle Synthesis

The most common gelatin microsphere (GMS) synthesis technique involves water in oil (W/O) emulsions. While gelatin microspheres made from W/O emulsions have been investigated for decades, Yasuhiko Tabata has pioneered many of the recent advances.²⁷ Mixing liquid gelatin with a large volume of oil yields gelatin droplets. By lowering the temperature, the liquid droplets solidify into gelatin particles as shown in Figure 1.4. The resulting particle sizes depend on the oil phase viscosity, aqueous volume to oil volume ratio, surfactant concentration, and degree of agitation. Many different hydrophobic liquids have been used, such as mineral oil²⁸, olive oil²⁹, sesame oil³⁰, toluene³¹, chloroform³¹, and isooctane³². Despite the large number of different oil phases used in literature, the only side-by-side comparative study of unique oil phases (not involving mixtures) was for isostrearylisostearate, isopropylpalmitate, and paraffin.³³ Of these three oils, isostrearylisostearate was reported to be the best choice for microsphere production. In general, higher viscosity oils are reported to yield smaller particles.²⁹ Gelatin concentrations in the aqueous phase typically range from 10 to 30

wt%^{29-31, 34, 35} Larger fractions of gelatin in the emulsion are reported to produce larger particles.³³ Once the oil and gelatin phases have been selected, the next step is to mix the two phases. Greater agitation through either increased mixing rates or sonication typically produces smaller particles.^{29, 32, 33, 35} The process of breaking the gelatin into small droplets generates a large amount of surface area which reduces the propensity for further break-up of the particles while increasing the possibility of coalescence. To retain smaller particle sizes, the surface energy can be reduced with either surfactants or the addition of smaller particles to form a Pickering emulsion³⁶. Span and poly(methyl methacrylate) (PMMA)³⁷ have been used individually to increase the emulsion stability, however, combinations of multiple surfactants (Span and Tween, for example) have been used as well.³² In general, more surfactant yields smaller droplets. Although most W/O emulsion-based synthesis approaches for gelatin microspheres use surfactants to stabilize the droplets prior cooling them, surfactants are not always necessary if the emulsion is cooled while being adequately agitated.²⁹ In general, the W/O emulsion technique has been shown to be very flexible but results in a polydisperse size population of spherically shaped particles.

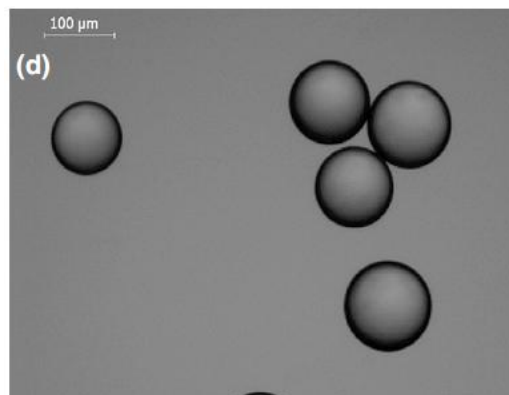


Figure 1.4. Example of GMS made using a W/O emulsion. Taken from reference 35.

By taking advantage of gelatin's poor solubility in alcohol or acetone, gelatin nanoparticles can be formed by precipitating gelatin from solution.^{12, 38, 39} The one step precipitation approach is known for producing polydisperse particles that tend to aggregate.^{40, 41} Dissolving this first precipitate in water and precipitating it again appears to increase the stability and decrease the polydispersity of the particles, as shown in Figure 1.5.⁴⁰ This repeated precipitation approach is thought to remove lower molecular weight gelatin chains which are less prone to gelation.⁴⁰ In some cases, two macromolecules can be precipitated together such as gelatin and bovine serum albumin (BSA).⁴² Strongly-charged polyelectrolytes can also accomplish this effect if the gelatin has a significant net charge.⁴³

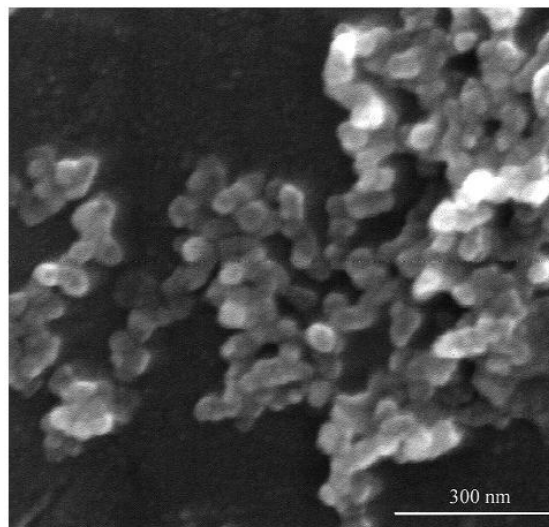


Figure 1.5. Example of GMS made using a desolvation technique. Scanning electron microscope image of gelatin nanoparticles produced using a 2-step desolvation technique. Taken from reference 40.

Before the gelatin precipitates to form a more solid-like particle, it can go through a liquid-liquid phase separation step to form a coacervate. The gelatin rich phase, or coacervate, is reported to form spherical nanoparticles on cooling although there is some evidence that the morphology is more irregular as seen in Figure 1.6.⁴⁴ Simple gelatin coacervates have been used to coat microparticles of sulphamerazine, aspirin, and phenolphthalein⁴⁵ or to produce gelatin particles.⁴⁴ Coacervation in the presence of two oppositely-charged polymers or complex coacervation is often seen between gelatin and polysaccharides⁴³ or between different types of gelatin (Type A and Type B gelatin for example).⁴⁶ Since the coacervate is a liquid, encapsulation by coacervation-based approaches should be less harsh than precipitation. As an example, complex coacervation of gelatin (positively charged) and negatively-charged DNA successfully led to the protection of DNA from nucleases while still permitting transfection.^{10, 47}

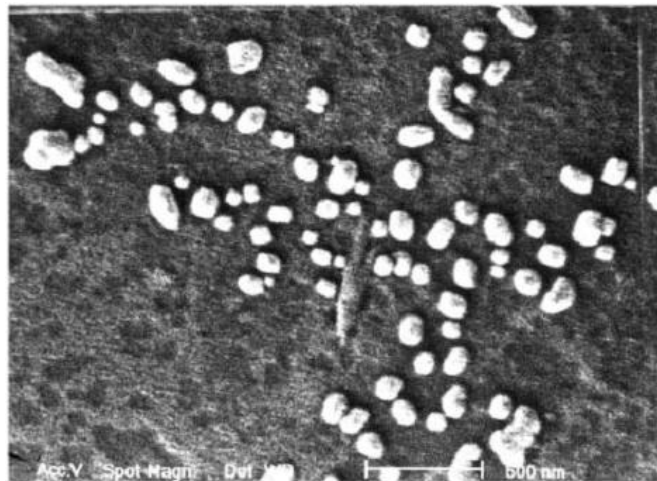


Figure 1.6. Gelatin nanoparticles produced via coacervation of gelatin. Taken from reference 44.

Although W/O emulsion, precipitation, and coacervation are the most common approaches for producing gelatin particles, sprays, microfluidics, and lyophilization-based techniques have also been used. Spray drying of gelatin microparticles containing propolis was reported to have a relatively high entrapment efficiency of ~40%.⁴⁸ Large amounts of mannitol were necessary to generate regular, spherical particles shapes and to prevent aggregation. Microfluidic production of gelatin or collagen microspheres by microfluidics has generally been limited to aqueous diameters over 50 μm .⁴⁹⁻⁵¹ Lyophilization of gelatin and PEG 6000 mixtures was reported to produce gelatin microspheres, though the particle sizes were polydisperse.^{52, 53} Although these methods are not common in literature, they do demonstrate the broad range of processing possibilities available with gelatin.

The vast majority of gelatin particles are covalently crosslinked with glutaraldehyde^{12, 29, 40, 54, 55}, formaldehyde^{28, 45, 54}, EDC^{10, 35}, genipin⁴², or glyoxal⁵⁶⁻⁵⁸, to increase their stability. Thermal hardening at temperatures above 80°C has also been used to reduce the solubility of the gelatin and, thus, increase the stability of the microspheres.³³ Although the conventional wisdom is that uncrosslinked gelatin is too unstable to be used in biomedical applications⁵⁹ (due to the poor mechanical properties at 37 °C), liquid-like droplets such as liposomes have proven to be quite effective drug delivery vehicles. Crosslinking also reduces the temperature sensitivity of the physical properties of the gel⁵⁹ as well as the overall charge of the particles, which can promote aggregation.⁴⁹ Payload molecules present during the crosslinking reaction may become covalently attached to matrix. In the case of doxorubicin loaded gelatin particles, crosslinking was reported to lead to significant covalent binding between doxorubicin

and the gelatin matrix.⁴⁴ Such modifications to the drug can compromise its therapeutic function and are, therefore, of interest to regulatory agencies like the US FDA. Studies of uncrosslinked GMS are few in number but hold promise as an alternative to crosslinked gelatin matrices.^{28, 54, 60}

1.1.4 Drug Delivery with Gelatin Particles

Although gelatin solutions were shown to have some limitations (increased blood viscosity and reduced clotting) as a plasma expander (Knox gelatin plasma expander was removed from the market in 1978 because it was ineffective)²⁵, gelatin-based particles have demonstrated significant advantages in terms of biocompatibility. Gelatin nanoparticles, for example, are more readily taken up by SP-1 and EMT 6 cells than albumin nanoparticles.⁴¹ Several other cell types such as human macrophages⁴⁰, 143B osteosarcoma³⁹, and murine bone marrow dendritic cells⁵⁵ also readily take up gelatin nanoparticles. Although lipofectamine has a higher transfection effectiveness than gelatin nanoparticles, there is some evidence that the expression of the transfected plasmid from gelatin is higher.¹⁰ Gelatin nanoparticles are also reportedly less cytotoxic than other DNA vectors such as lipofectamine and poly(ethyleneimine).⁶⁰ Additionally, gelatin microspheres are an effective adjuvant for vaccines, but do not appear to be immunogenic or cytotoxic on their own.^{31, 61, 62}

Many different pharmaceuticals have been encapsulated with gelatin and some size based targeting has been observed. Gelatin has used to encapsulate sulfanilamide²⁸, riboflavin²⁸ and sulphamerazine⁴⁵ particles. Drugs such as Mitomycin C³⁰, muramyl dipeptide³¹, insulin³⁴ and methotrexate^{37, 63} doxycycline³⁵ have been encapsulated in

gelatin either through mixing with initial gelatin solution or “breathing” into dehydrated gelatin particles^{34, 44, 64}. Small gelatin particles are removed by the reiticuloendothelial system (RES) relatively quickly, but gelatin microspheres are reported to accumulate in the capillary beds of the lungs and liver as well.³⁰ Smaller gelatin microspheres appear to be more susceptible to phagocytosis by macrophages than larger ones (>10 μm)³¹ and also release their payload faster.⁶² On the other hand, larger, 23 μm GMS were used to specifically target ischemic areas with angiogenesis promoting bFGF (basic fibroblast growth factor).⁶⁴

Since gelatin particles are usually crosslinked, release of encapsulants is typically induced through protease degradation of the gelatin matrix. Enzymatic release is generally unique to a physiological environment. This degradation route is limited by the requirement that the crosslinked gelatin be readily accessible to proteases. This requirement can limit possibilities of particle surface modification. Additionally, many *in vitro* studies have shown a significant reduction in release rate occurs with increasing crosslinking.^{31, 34, 45} This same trend has been reported from *in vivo* studies in both oral²⁸ and intramuscular³⁴ administration routes. Since the release of DNA from uncrosslinked gelatin is usually quite fast, such a reduction in release rate is usually advantageous. As an alternative to loading drugs inside the gelatin particle, payload molecules have also been loaded onto the particle carrier surface.³⁸

Although gelatin (crosslinked or uncrosslinked) is relatively stable at room temperature, retention of encapsulants often depends on the tortuosity of the diffusion path through the gelatin matrix. Simple tortuous diffusion is well modeled and is primarily dependent on the pores size of the gel and the hydrodynamic radius of the

encapsulated species, however gelatin gels are not a simple gels. Gelatin has many charged groups that can interact with a charged, flexible macromolecule, such as DNA, as it diffuses through the gel.²⁹ The net charge of the gelatin and, therefore, the interaction between the diffusing species and the gel is also dependent on the pH. Regardless, molecules or encapsulated particles that are larger than the pore size of the matrix have little mobility as long as the matrix remains intact. Saltzman et al measured an interfiber distance of 12 nm for 10 wt% gelatin. Furthermore, this distance is inversely proportional to the square root of the gelatin concentration⁶⁵. For small macromolecules, such as short oligonucleotides, the gelatin matrix alone may not be sufficient to prevent premature release. Coatings of alginate or chitosan have been used by other groups to control the release profiles of encapsulated species³⁷ but layer-by-layer coatings of polyelectrolytes provide a more tunable alternative for controlling permeability.

1.1.5 Gelatin Hybrids

Gelatin has many functional groups (primary amines and carboxyl groups) that are convenient for chemically modifying gelatin. Cationic gelatin has been generated by coupling of cholamine^{66, 67}, chitosan⁶⁸, or ethylenediamine²³ to gelatin. Such cationic gelatin is likely to have stronger attractive interactions with negatively charged macromolecules such as DNA. A more anionic gel has been formulated by coupling chondroitin sulfate to gelatin.⁶⁹ PEG has been added to the gelatin by either coupling to the gelatin prior to^{56, 57, 60} or following^{58, 70} the formation of gelatin particles. PEG modification of gelatin can be used to extend the circulation lifetime of nanoparticles

without impeding transfection.^{56, 57} Gelatin particles have also been coated with alginate³⁷, chitosan³⁷, silica³², or nylon⁷¹ to regulate its release properties. Coupling avidin to gelatin allows for subsequent functionalization with biotinylated species.⁷² Thiolation of the gelatin has been used to facilitate further modification with avidin⁷² or PEG.⁵⁸ Although the details of these chemical modifications are beyond the scope of this work, their prevalence speaks to the flexibility of gelatin as a material.

1.1.6 Layer by Layer Deposition

Layer-by-layer (LbL) deposition of alternating polycationic and polyanionic polymers was pioneered by Decher and Hong in the early 1990's⁷³ and has since been used with a variety of different polyelectrolytes on many flat substrates as well as particle morphologies as shown in Table 1. Although the term "layer-by-layer" deposition (LbL) has been extended to include hydrogen bonded^{74, 75} and click chemistry⁷⁶ mediated depositions, this section focuses on electrostatically mediated LbL deposition. In addition to the flexibility in deposited material and substrate, LbL deposition allows for relatively precise control of layer thickness as a function of the number of deposition cycles, as well as pH, and ionic strength of deposition solutions.^{77, 78} Despite its popularity, LbL deposition on hydrogel surfaces has received little attention⁷⁹, perhaps due in part to the potential complications of using a water-swollen polymer network as a substrate instead of a non-porous homogenous surface. Gelatin itself has been used as the polyanionic species for constructing an LbL film. Hollow LbL capsules of gelatin and poly(dimethyl diallylammonium chloride) (PDDA) were prepared by Ai and Gao that had diameters down to 392 nm⁸⁰. In separate work, capsules comprised of poly(styrene sulfonate)

Table 1.1. Examples of LbL films substrates and a substrate shapes.

Polyanion Name	Polycation Name	Substrate		Reference
		Name	Shape	
poly(acrylic acid)	poly(allylamine)	Silica	Sphere	91
PSS/HSA	poly(allylamine)	erythrocyte	ellipsoid	9
poly(styrene sulfonate)	poly(allylamine)	dex-HEMA	Sphere	92
poly(styrene sulfonate)	poly(diallyldimethylammonium)	PNiPAM	microgel	93
poly(styrene sulfonate)	poly(allylamine)	Catalase	biocrystal	94
poly(styrene sulfonate)	poly(allylamine)	α -Chymotrypsin	particle	95
Hyaluronic acid	poly(L-lysine)	gold or silica titanate	plate	96
poly(glutamic acid)	poly(L-lysine)	Glass	plate	97
poly(acrylic acid)	poly(allylamine)	Glass	plate	78
poly(styrene sulfonate)	gelatin	Furosemide	microcrystal	81
gelatin	poly(diallyldimethylammonium)	melamine formaldehyde	particle	80
glucose oxidase	poly(diallyldimethylammonium)	Nafion	Network	98
poly(styrene sulfonate)	poly(allylamine)	melamine formaldehyde	Sphere	99
poly(acrylic acid)	poly(diallyldimethylammonium)	Silicon	wafer	100
alginate	poly(L-lysine)	Silica	wafer	101
poly(styrene sulfonate)	poly(diallyldimethylammonium)	Dodecane	droplet	102
dextran sulfate	chitosan	Silica	Sphere	103
poly(styrene sulfonate)	decomposed MF	melamine formaldehyde	Sphere	104
Silica nanoparticles	poly(diallyldimethylammonium)	Poly(styrene)	Sphere	105
poly(acrylic acid)	poly(allylamine)	Alginate	Sphere	106
poly(acrylic acid)	PAH/P4VP	Silica	plate	107
poly(acrylic acid)	poly(allylamine)	Silicon	plate	108
poly(styrene sulfonate)	diazoresin	PS	sphere	109
dextran sulfate	chitosan	Silica	plate	88
poly(styrene sulfonate)	poly(allylamine)	Silica	Sphere	84
alginate	chitosan	Indomethacin	microcrystal	86
poly(glutamic acid)	poly(L-lysine)	Mesoporous Silica	particles	89
poly(styrene sulfonate)	poly(diallyldimethylammonium)	Dodecane	Sphere	102

(PSS) and gelatin bilayers were used by Ai and coworkers to control the release of furosemide.⁸¹

The permeability of a LbL film depends on the number of layers, ionic strength, and pH of the solution. More layers typically decrease the permeability of the film.^{81, 82} Higher ionic strength weakens the electrostatic attractions that stabilize LbL films and thus tend to increase the permeability.^{83, 84} Increasing the temperature has been reported to either increase or decrease the permeability.^{83, 85, 86} Hollow LbL capsules (usually made on a sacrificial template) appear to decrease in permeability with increasing temperature due to an increase in film thickness as the polymers relax from initially more stretched states.^{83, 85} LbL coated microcrystals, on the other hand, show an increase in permeability with increasing temperature.⁸⁶ This discrepancy in temperature-dependent permeability could be due to the inability of a supported film to contract in the same way as an unsupported or hollow capsule. To compensate for the lack of radial contraction, supported film may form pores. Similar pores have also been observed with pH changes.⁷⁸ Reversible pore formation based on pH changes are on the order of 100 nm in size.^{83, 87} Although the results above appear to be generally applicable to different systems, quantitative control of the permeability of LbL films has yet to be achieved.⁸²

The use of LbL films *in vivo*, is limited by the well-known cytotoxic effects of many polycationic polymers. In order to overcome this problem, many biocompatible polycationic materials from biological sources, such as chitosan⁸⁸, gelatin⁸¹, and poly(lysine)⁸⁹, have been used. Despite the trends in the literature towards using

biopolymers, PAA/PAH bilayers are reported to be relatively bioinert when constructed under certain conditions, especially low pH.⁹⁰

1.2 Controlling Functionality of Colloids with DNA

As a tunable recognition-based assembly tool, DNA presents several advantages including its relative ease of handling. In order to effectively use DNA as a means of controlling the functionality, assembly, and disassembly of colloidal particles, one must first understand how immobilization affects its hybridization activity.

1.2.1 DNA Hybridization

The double helical structure of DNA was first described by Watson and Crick in 1953.¹¹⁰ Each strand of DNA consists of a deoxyribose (sugar) and phosphate backbone with one of four nucleosides attached to each sugar. The nucleosides are either adenine (A), thymine (T), cytosine (C), or guanine (G). At neutral pH, the phosphates are negatively charged and spaced at ~0.6 nm intervals along the backbone. Due to charge and double helical structure, double-stranded DNA (dsDNA) has a persistence length of ~10 nm.¹¹¹ Single-stranded DNA (ssDNA) is considerably more flexible with a persistence length of ~2 nm.¹¹² The mechanical properties of DNA are sequence and solution dependent.^{112, 113} A simplistic model of DNA is depicted in Figure 1.7. At neutral pH, DNA is a relatively stable macromolecule, however, the purine bases (adenine and guanine) can be hydrolyzed at low pH and elevated temperature¹¹⁴ while the sugar phosphate backbone can degrade under strong alkaline conditions.¹¹⁵ Due to the biological relevance of DNA, there are also many enzymes that degrade DNA but most

of these require specific ions to be present in solution to be active. Synthetic oligonucleotides with modified backbones such as locked nucleic acids and peptide nucleic acids, are resistant to protein degradation and form more stable duplex, but are beyond the scope of this work.



Figure 1.7. A simplistic model of a DNA duplex showing the double helical structure and base pairing between color-coded bases (guanine is brown, cytosine is green, adenine is purple and thymine is yellow). Red and blue represent the deoxyribose and phosphate backbone proceeding in two different directions (5' to 3' and 3' to 5' respectively)

The hybridization of one ssDNA with another is mediated by base pairing but the entire sequence actually influences the process. The most common base pairing occurs between adenine and thymine and between guanine and cytosine as depicted in Figure 1.7. This pattern is called Watson-Crick base pairing. Hydrogen bonds formed between each pair of matched bases (two hydrogen bonds for A-T and three hydrogen bonds for G-C) in conjunction with van der Waals interactions between bases enable hybridization

despite electrostatic repulsion between the negatively-charged phosphate groups along of the backbones. In addition, hydrophobic and pi stacking effects play important roles in mediating duplex formation. Other base pairing schemes also exist including triplex¹¹⁶ and quadruplex¹¹⁷ structures but only under very specific conditions. Hydrogen bond disrupters as well as protonation and deprotonation events from excessive alkali or acidic conditions can inhibit hybridization. Furthermore, under low ionic strength solution conditions, the electrostatic repulsion of the phosphates in the backbone cannot be overcome, and may thus prevent or weaken hybridization events.

Hybridization of two single strands of DNA to form a duplex starts with the formation of critical number of consecutive base pairs (~5), then proceeds in a zipper-like fashion (Fig 1.7) until the duplex either is effectively fully hybridized or falls below the critical number of bases necessary to remain stable.¹¹⁸ In the latter case, the strands dissociate. Though individual base pairs are relatively weak, the time scale for base pair formation is about $10^6 - 10^8$ per second. The association rate of two ssDNA into a duplex reportedly depends on the salt concentration¹¹⁹ but not upon the composition of the sequence. The dissociation rate, on the other hand, varies significantly with the sequence composition.¹²⁰ The measured association rate is $\sim 1.0 \times 10^6 \text{ s}^{-1}\text{M}^{-1}$ based on static fluorescent quenching¹²¹ and nuclear magnetic resonance (NMR)¹¹⁹ experiments.

Some of the most impressive self assembly work with DNA alone has been pioneered by Nadrian Seeman and his group. With carefully chosen DNA sequences, Seeman's group has constructed a rich variety of 2D structures such as tiles and 3D structures such as DNA cubes.¹²² Oriented individual tiles of DNA can be assembled into crystalline 2D DNA arrays.¹²³ DNA nanomechanical walkers and stress gauges have

also been demonstrated.¹²⁴ The rational design of more complex structures mediated by DNA hybridization relies heavily on modeling of DNA hybridization in solution.

1.2.2 Modeling Primary Hybridization in Solution

Early models of DNA hybridization were based on the genomes of organisms involving long and somewhat variable sequences (although still significantly more consistent than a random sequence of A, T, C and G bases). A simple model that only considers the fraction of G-C and A-T base pairs was found to predict the melting temperature of long genomic DNA relatively well, but was not as effective for synthetic sequences.¹²⁵ More complicated statistical mechanics models were also developed but often lacked the critical physical information necessary to make the models predictive.^{126, 127} Despite these limitations, DeVoe and Tinoco used similar models to successfully describe the observed reduction in absorbance of DNA following hybridization, known as the hypochromic effect.¹²⁸ Interactions between neighboring base pairs proved to be a major complicating factor for early models. As one would expect, attempts to numerically model DNA hybridization have been reported, but are not in common usage.^{129, 130}

Nearest neighbor models of oligonucleotide hybridization began with Tinoco in the late 1960's.¹³¹ Turner and coworkers experimentally determined the energy associated with each pair of base pairs for ribonucleic acids (RNA).^{132, 133} Breslauer and Marky applied the methods used earlier for RNA to construct an analogous DNA hybridization model.^{134, 135} Although DNA does not have a sharp melting transition, the

temperature at which half of the total number of DNA strands are in duplex state is considered to be the melting temperature. Santa Lucia and coworkers determined the most complete set of nearest neighbor parameters for DNA including mismatch terms.¹³⁶⁻

139

Santa Lucia's nearest neighbor model has some significant limitation. It is based on a two-state model of hybridization in which ssDNA are treated as either completely hybridized or unhybridized. However, the intermediate states of partially hybridized duplexes probably influence the kinetics of duplex formation significantly.¹⁴⁰ Furthermore, the assumption of no change in specific heat on hybridization had been shown to be incorrect and to have a significant impact on the calculated energetics of DNA hybridization.^{141, 142} In fact, the change in enthalpy on hybridizations has been shown to be smaller than reported in Santa Lucia's work, thus making the entropic contribution and, therefore, temperature more important.¹⁴¹ Despite these limitations, Santa Lucia's nearest neighbor model is still the most complete and accurate model available for predicting the energetics of the hybridization of two ssDNA with a particular alignment of base but there still may be multiple ways of aligning the two DNA strands to produce significant numbers of base pair matches. More recently, Zuker developed an algorithm for calculating the most energetically favorable alignments of strands and, thus, the most likely secondary structures (e.g. self-loops, hairpins, etc.).¹⁴³

1.2.3 Modeling Competitive Hybridization in Solution

Reynaldo et al. presented a model for the displacement of one ssDNA (primary target) hybridization partner by another identical ssDNA (secondary or competitive

target).¹⁴⁴ This model separates competitive (secondary) hybridization events into the displacement and dissociative pathways as shown in Figure 1.8. The displacement pathway of this model is based on both primary and secondary target being bound to the probe strand at the same time. This intermediate state was modeled using Anshelevich's description of DNA hybridization as a gambler's ruin problem in which the number of bases associated with the primary or secondary duplex fluxes until one falls below the critical number of base pairs necessary for stability.¹⁴⁵ The dissociative pathway, on the other hand, occurs through the thermal dissociation of the original duplex prior to hybridization of the secondary duplex. Both of these pathways were considered in Reynaldo's work in order to measure the rate constant associated with secondary duplex formation and was modeled as an exponential rise to maximum.

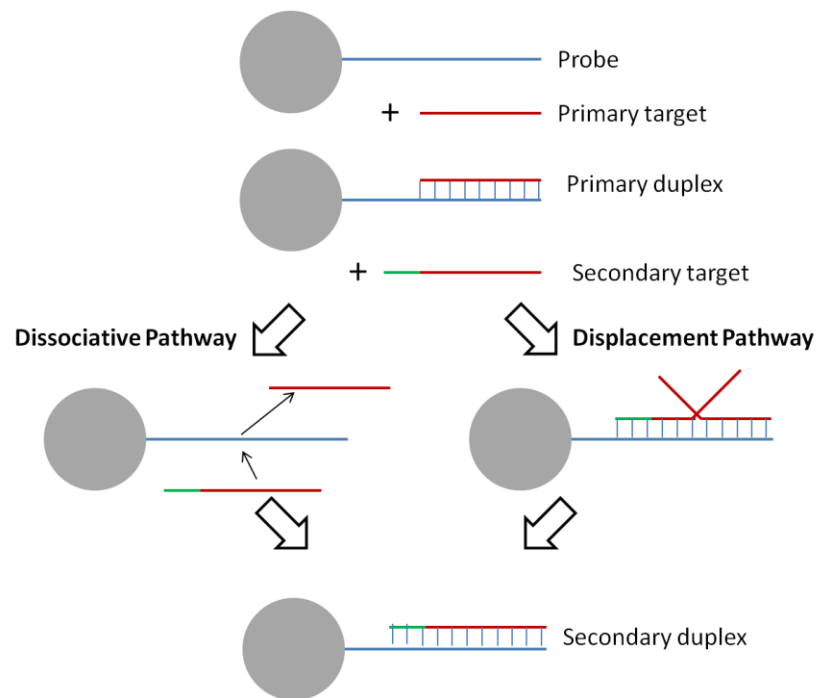


Figure 1.8. Description of the two pathways for secondary duplex formation. The grey circle represents a particle. Objects are not drawn to scale and DNA duplexes are represented as a simple ladder for clarity.

If the primary and secondary target sequences are not identical, the primary and secondary targets will not share the same set of base pair matches with the probe. Bases on the probe strand that do not pair with the primary target but do pair with the secondary target are called toeholds. The secondary target can hybridize to these bases without having to displace the primary target and thus the presence of such bases significantly increases the rate of formation of the intermediate state described above and therefore the rate of competitive displacement as well. Winfree and coworkers have modeled this exchange process for specific sets of sequences and even used DNA hybridization to simulate multiple chemical reaction kinetics.^{146, 147} This toe hold model considers some intermediate states and appears to be predictive over a limited number of short sequences.

1.2.4 Hybridization on Surfaces

Significant differences exist between DNA hybridization at a surface and DNA hybridization in solution. At a surface, one of the DNA strands that make up the helix is immobilized in some manner which limits the conformational and physical space that the strand can explore. These limitations can manifest as shifts in the entropy of the immobilized strand as well as restricted access of a complementary DNA strands to the probe strand. The charge of the surface can also impact the diffusion of charged species like DNA and the stability of immobilized duplexes. The tools for assessing these differences fall into two categories, labeled and unlabeled DNA techniques. Studies using labeled DNA usually use fluorescent molecules or radioactive isotopes to track a particular DNA strand, but the labels themselves may influence the results. Unlabeled

studies typically use spectroscopic techniques to monitor the state of DNA in the system, but the macromolecular mass and electrical properties may also be monitored. Much of the research into DNA hybridization at a surface has involved DNA microarray-based detection of a specific sequence among many different soluble target strands.¹⁴⁸⁻¹⁵⁰ This work will focus on the simpler system consisting of one soluble target strand which is most similar to the systems in DNA-mediated assembly literature.

Georgiadis's group has presented some of the most informative data to date on surface hybridization. They used two photon surface plasmon resonance (SPR) to quantify both unlabeled DNA immobilization and hybridization at a gold surface. Their results show that high probe density reduces the efficiency of hybridization¹⁵¹, an effect which had already been observed by others on microspheres¹⁵² and other surfaces.¹⁵³ They also show that the presence of mismatches slowed the rate of hybridization when the probe density was $\sim 30,000 / \mu\text{m}^2$ but such a slowing was not observed if the probe surface density was $\sim 15,000 / \mu\text{m}^2$. Hybridization to different segments of the probe strand was examined in this same study. At the higher probe surface density, the target that hybridized closest to the surface was inhibited. At the lower probe surface density, hybridization was not affected by the spatial proximity of the complimentary probe segment to the surface. When these results are combined with the strong observed salt concentration dependence of hybridization efficiency it becomes apparent that electrostatic effects play a major role in surface hybridization.

Several others have also observed a reduction in the stability of DNA duplexes at surfaces relative to solution using other techniques. Nasef, Ozalp, Beni and O'Sullivan were able to compare hybridization on gold surfaces and gold nanoparticles by measuring

the quenching of fluorescently-labeled DNA strands by a gold surface.¹⁵⁴ They found that the duplex melting temperature of the DNA strands in solution was higher than for immobilized duplexes on gold nanoparticles, which was in turn higher than the melting temperature on a flat gold surface. After hybridization occurs on a particle surface, the once flexible ssDNA becomes more rigid and extends into the solution. Xu and Craig used this conformational change to generate measureable shifts in hydrodynamic radius of gold nanoparticles as hybridization occurred.¹⁵⁵ They found that hybridization on the surface was generally less favorable than in solution and that this deviation depends on the base length of the target DNA. Notably, using hydrodynamic radii measurements to monitor hybridization did not lend itself to high precision.

There are some reported exceptions to the generally observed lowering of DNA duplex stability at surfaces. Stevens, Henry and Kelso reported that, at temperatures above the melting temperature of the DNA duplex, the duplex is more stable on a surface than in solution but is otherwise generally less stable on a surface than in solution.¹⁵⁶ Vainrub and Pettitt compared the electrostatics of metallic and nonmetallic surface and determined that gold surfaces generally make hybridization more favorable.¹⁵⁷ Marquette, Lawrence, Polychonakos and Lawrence used changes in impedance during hybridization events to both monitor *in situ* hybridization as well as measure melting temperatures.¹⁵⁸ They compared the observed melting temperature value from their experiments with an early solution model and found them approximately equal. Additionally, hybridization activity on small gold nanoparticles was almost identical to hybridization in solution.¹⁵⁹ In a separate study, DNA immobilized on 38 nm latex particles exhibited similar hybridization rates to hybridization in solution.¹⁶⁰

Hybridization on DNA block copolymer micelles are one of the few constructions to demonstrate clearly enhanced binding, especially at low salt concentrations.^{159, 161}

Based on solution studies, the affinity between complementary strands over 10 bases in length should be sufficient to drive hybridization to near completion (>99%) if an excess target concentration is used. The deviations between experiment and theory have been addressed in several drastically different manners. Stevens, Henry, and Kelso use a simple biomolecular reaction with modifications to account for surface reaction volume.¹⁵⁶ Piunno developed a model of surface hybridization that includes contributions from the various charged species (primarily, salt and DNA).¹⁶² Specifically, this model separated the volume containing the immobilized DNA from the bulk and calculates the activity coefficients accordingly. The analysis of Vainrub and Pettitt uses surface charges on nonmetallic surfaces and image charges (phantom charges arising from the mobility of electrons) associated with metallic surface to explain differences in hybridization on these surfaces.¹⁵⁷ These differences in theoretical approaches and their apparently contradicting experimental results point to the need for further investigation of the thermodynamics of DNA hybridization at surfaces.

The kinetics of DNA hybridization at surface has been evaluated with many techniques including quartz crystal microbalance (QCM) and fluorometry. Using QCM, Okahata et al to estimated that a minimum salt concentration of 0.5 M was necessary to drive hybridization to near completion. This relatively high salt concentration (compared to solutions) further supports the idea that hybridization on surfaces is weaker. This group also reported that the hybridization rates increased with target length (yielding rates of $\sim 10^4 \text{M}^{-1} \text{s}^{-1}$).¹⁶³ Since the immobilized probe was increased in base length along

with the soluble target, the probe also extended further into the surrounding solution as the base length increased, which may have played a role in the base length dependence of the rate constant. Glazer and coworkers observed an “overshoot” behavior in DNA hybridization using fluorescently labeled DNA.¹⁶⁴ Notably, this “overshoot” or slight, temporary peak during incubation with absorbates, has been reported previously in protein adsorption studies. They attribute the overshoot to imperfect duplexes that initially form in which single strand of DNA is either incompletely hybridized or bridging between two other strands. Although this intermediate complex is possible on short time scales, the fast rate of base pair formation (on the order of 10^6 s^{-1})¹⁴⁵ should make measurement of such intermediates unlikely. Furthermore, there is little other evidence in literature to support the existence of an overshoot during hybridization at surfaces.

There does not appear to be one universally accepted kinetic model for DNA hybridization at surfaces. Zeng and coworkers suggest that the adsorption is best represented using a second order Langmuir fit based on DNA studies involving an optical nanowire substrate.¹⁶⁵ Chan, Graves, and McKensie apply a reduction-of-dimensionality model, originally used for receptor-ligand binding on cells. In their model, target DNA mobility and hybridization activity on the surface augments the total number of collisions with the probe which, in turn, increases the rate of hybridization.¹⁵³ A similar reduction of dimensionality model is also used by Erickson, Li, and Krull to model hybridization in a flow cell with some success.¹⁶⁶

Milam and coworkers examined sequence dependent effects such as the base length of the complementary segment in DNA strands. For these studies, they used flow

cytometry to quantify the number of fluorescently labeled duplexes on polystyrene microspheres.¹⁶⁷ With regards to primary hybridization, they clearly showed that increasing the base length of a complementary primary target typically increases the extent of hybridization,¹⁶⁸ however, the focus of their work was in the context of a competitive system in which a primary target was initially hybridized to an immobilized probe DNA and is then displaced by a secondary target as shown in Figure 1.8.¹⁶⁸ In other studies, they observed that the position of the recognition sequence within the secondary target has a minimal impact on competitive hybridization activity.¹⁶⁹ The presence of mismatches in the primary duplexes, on the other hand, can promote displacement by perfectly-matched targets.^{169, 170} For the kinetic studies, the form of the displacement of primary targets was fit to an exponential rise to maximum and the effective rate constant was used to quantitatively compare competitive hybridization rates. Longer secondary targets generally led to higher rates of displacements.¹⁷¹ The inclusion mismatches in the primary target led to an increase in the rate of displacement.¹⁶⁹

1.3 DNA-Mediated Colloidal Assembly

1.3.1 Nonspecific Colloidal Forces

The aggregation of colloids is often mediated by nonspecific attractive interactions such as van der Waal, hydrophobic interactions, and depletion interactions. Repulsive interactions such as electrostatic and steric interactions may overcome this attraction between particles and thus prevent aggregation. Derjaguin, Landau, Verway,

and Overbeek (DLVO) developed the classic model for describing the electrostatic and van der Waal forces involved in colloidal interactions, however, it does not apply well to solutions with relatively high salt concentrations (over 10 mM).¹⁷² Zeta potential measurements can provide an approximate electrical potential at the slip plane marking where the bulk fluid flows or slips past the boundary layer around the particle. The Smoluchowski approximation provides a simple conversion between electrophoretic mobility (typically measured using dynamic light scattering) and zeta potential values, but assumes a smooth, round surface and a significantly charged particle. Lietor-Santos and Fernandez-Nieves observed that a polyelectrolyte coating leads to deviation from the Smoluchowski approximation.¹⁷³ In general, particles with small zeta potential values (between -10 and 10 mV) are prone to aggregation. On the other hand, if repulsive forces dominate between uniformly-sized colloidal particles, colloidal crystal formation is favorable. Colloidal crystal structure tends to alternate between fcc and hcp in a random manner. Whether net attractive or repulsive interaction occur between particles, phase diagrams can be constructed as a function of the particle concentration, size ratios, etc. to delineate phase behavior of colloidal suspensions.¹⁷⁴

1.3.2 DNA-mediated Colloidal Assembly

Where many single molecule functionalities can be attached with a single duplex, others, like drug laden particles usually require multiple duplexes to stably bind to the surface. The use of DNA to control the assembly of colloidal particles began with Mirkin and Alivisatos in 1996.¹⁷⁵ Mirkin's system consisted of two populations of ssDNA-functionalized gold nanoparticles that aggregated following the addition of a third ssDNA

which was complementary to the other two, immobilized ssDNA sequences. The aggregation led to a visible change in suspension color. Alivisatos's system was similar except the linker strand was much longer and possessed more than two complementary segments resulting in a longer, linear chain of DNA-linked particles.

Mirkin's group has continued exploring DNA mediated nanoparticle assembly using the basic design schemes depicted in Figure 1.9. The first scheme involves a dsDNA linker strand with unhybridized bases at each end that are complementary to the DNA immobilized on particle surfaces.¹⁷⁵ As hybridization occurs, this linker strand forms a duplex bridge between the particles. The immobilized DNA in the second scheme was oriented in the same manner as the first scheme but now two ssDNA linker strands collectively act as the bridge.¹⁷⁶ Each linker strand in this scheme consists of a portion complementary to the immobilized strand and a portion complementary to the other linker strand. In the third scheme, one population of nanoparticles is coupled to the 5' end of DNA while the other nanoparticle population is coupled to the 3' end of DNA, thus allowing a single ssDNA to link the particles.^{177, 178} The fourth scheme used two populations of particles in which the DNA immobilized on one population of particles is complementary to the DNA immobilized on the other population of particles.¹⁷⁹ Milam et. al. also used this direct hybridization scheme.¹⁶⁷ Kim et. al. added short soluble partner strands to stiffen the immobilized DNA upon hybridization and extend the unoccupied bases at the dangling end away from the particle surface as shown in Figure 1.9 scheme 5.¹⁸⁰ In the fifth scheme, any remaining unpaired bases at the dangling end are hybridized to a linker strand that bridges between particles. In this last scenario, the

orientation of the DNA strands mandates that one end of the linking duplex must fold back as depicted in Figure 1.9.

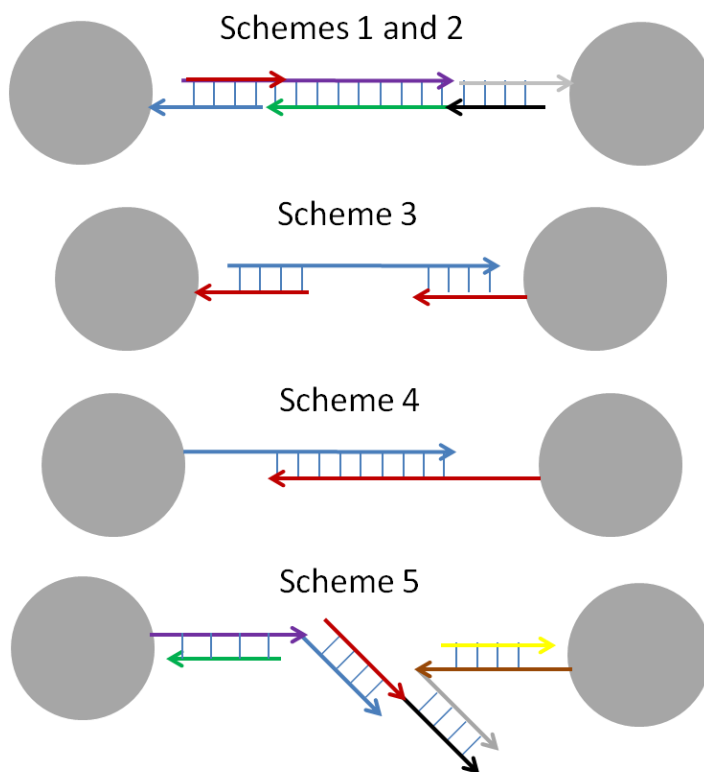


Figure 1.9. Schemes used to induce DNA-mediated particle assembly. Only one set of strands is shown on each particle for clarity. The following color pairs are complementary; red and blue, purple and green, black and gray, brown and yellow.

Mirkin's group also explored the mechanisms driving DNA-mediated colloidal assembly. They found that the melting transition of DNA-functionalized nanoparticles and a surface functionalized with complementary DNA strands occurs at higher temperature and is sharper than the analogous DNA solution.¹⁸¹ DNA-mediated colloidal assembly, however, was found to require higher salt concentrations, possibly due to the enhanced electrosteric repulsions associated with the DNA-functionalized nanoparticles.¹⁷⁷ The mode of aggregation, at least for 60 nm to 80 nm gold

nanoparticles, was found to be reaction limited.¹⁷⁸ Mirkin's group also reported that a single complementary base pair was sufficient to induce aggregation of 150 nm gold nanoparticles at 1 M NaCl.¹⁷⁹ Use of KCl salt permitted a more complicated base pairing interaction. In the presence of KCl, G-quadruplexes were reported to mediate the formation of a core aggregate while standard Watson and Crick pairing was found to mediate the formation of a shell around this core.¹⁸² DNA hybridization between colloidal particles behaves in a manner qualitatively similar to solution hybridization, but there are significant deviations especially in reported cooperativity between hybridization events.

A well known model of this cooperativity, the ion cloud model, states that a major factor mediating the cooperativity observed in DNA-hybridization between particles involves the clouds of duplex-associated counterions overlapping and effectively increasing the local salt concentration around immobilized DNA.^{183, 184} Since higher salt concentrations increases the stability of DNA duplexes, the overlap leads to a collectively stronger binding between DNA-functionalized particles than the sum of the individual duplexes between the particles. Numerical modeling supports this theory^{183, 184} but the primary experimental evidence of cooperativity stems from the increase in the effective melting temperature of DNA-linked particle aggregates and molecules functionalized with multiple DNA strands as well as sharpening of this melting transition relative to unmodified soluble DNA.^{177, 185-187} Considering the Debye length in 150 mM NaCl (a typical salt concentration for such experiments) is about 1 nm, the neighboring DNA duplexes must be in close proximity for significant electrostatic interactions to occur. For this reason, 5 nm is stated as the maximum spacing in which cooperativity still occurs.

However, DNA-mediated aggregation in which immobilized DNA strands have a significantly larger lateral spacing still exhibit an increase in the effective melting temperature as well as a sharpening of the melting transition.¹⁸⁸ In other cases, some surfaces with a supposedly sufficient DNA density for ion cloud overlapping still exhibit lower DNA hybridization efficiency.¹⁵¹ Although there may be some contribution from the overlap of ion clouds, this effect is likely to be much less important than the energetics DNA-hybridization, the entropy loss associated with aggregation, and the collective repulsive electrostatic effects of multiple, closely-spaced DNA strands. Dreyfus and coworkers predict the increase in melting temperature and sharpening of the transition by taking into account the entropy loss of the particles upon binding.¹⁸⁸ Nykypanchuk and coworkers model DNA-mediated colloidal assembly based on geometric and osmotic arguments and derive relatively good fits with their experimental data.¹⁸⁹ Biancaniello and coworkers used a more statistical approach and were able to successfully match their assembly results, but did not explicitly address cooperativity.¹⁹⁰

Milam's group has focused on carboxylated polystyrene (PS) microspheres functionalized with DNA via carbodiimide coupling. The amide bond formed by carbodiimide coupling is more stable than the thiol-gold bonds used to attach DNA to gold surfaces and simpler than the biotin-avidin linkages used in other studies.^{167, 190-192} They investigated both aggregation and the assembly of core-satellite structures using the direct hybridization approach, Scheme 4 in Figure 1.9. A lower surface density of hybridizing DNA on the surfaces of the particles was found to both increase the ability of a competitive strand to redisperse colloidal satellite structures and to achieve better coverage of the colloidal shell around the template particles.¹⁹³ Mismatches and diluent

strands were also found to be useful tools for controlling colloidal assembly.^{170, 194} The number of DNA linkages between attached DNA-functionalized particles was estimated to be less than 5,¹⁹³ which is also consistent with estimations by Valignat and coworkers.¹⁹⁵ Such a low number of duplexes is not unreasonable considering that aggregation can be mediated by DNA strands with just a couple complementary base pairs as discussed earlier for gold nanoparticles.

Milam and coworkers also showed that these structures would redisperse upon addition of competitive DNA without needing to increase the temperature.¹⁶⁸ Previous work used changes in temperature, ionic strength or applied force to break DNA linkages between particles.¹⁷⁷ Hazarika and coworkers, took this reversibility a step further and used a competitive strand to remove the linker stands bridging particles and drive redispersion.¹⁹⁶ Such a system allowed for the cycling between aggregated and dispersed states with alternating additions of the linker and competitive strands.

DNA-functionalized particles have some key advantages *in vivo*. Protein was found to adsorb to the DNA-functionalized gold particles and facilitate their motion across cell membranes, thus, assisting transfection.¹⁹⁷ Furthermore, there is also evidence that immobilized DNA on gold nanoparticles is significantly more resistant to nuclease degradation than soluble DNA.¹⁹⁸ DNA is a relatively biocompatible material whose primary “side effect” could involve unintentional changes in gene expression, which is extremely unlikely. This side effect can be avoided by using sequences with no genomic relevance.

DNA-mediated colloidal crystals were first reported in 2005 by Biancaniello, Kim, and Crocker using PS microspheres in which the concentration of DNA on the

surface was diluted by the presence of PEG.¹⁹⁹ DNA-mediated crystallization of gold nanoparticles was later reported using relatively weak hybridization segments. It has also been shown that the length of spacers between the particle surface and the hybridizing segment can influence whether crystallization will occur and the type of crystal that forms (FCC or BCC).^{200, 201} Dai, Kumar, and Starr simulated DNA crystallization and ultimately found that it follows a two-step crystallization mechanism involving a highly connected amorphous structure as an intermediate state much like proteins and other soft materials.²⁰² This conversion from an amorphous state to crystalline state requires multiple bond breaking and reformation events and is therefore hindered by duplexes with high intrinsic affinity.

Although it was predicted that DNA hybridization should enable the formation of complex structures driven just by the energetics of DNA hybridization, this has yet to be fully realized.²⁰³⁻²⁰⁵ Soto, Srinivasan, and Ratna reported that DNA hybridization could mediate the formation of simple polyhedral structure but differences in the sizes of the particles assembled were not accounted for in their study.²⁰⁶ Heterogeneous deposition of DNA on the surface of the colloids is another route for inducing assembly of complex shape. Bajaj and Laibinis showed that Janus particles with different DNA functionalizations on each side could be fabricated by depositing gold on just one side of a silica particle.²⁰⁷

1.4 References

1. *Cancer of Unknown Primary Origin*, National Cancer Institute Fact Sheet, <http://www.cancer.gov/cancertopics/factsheet/Sites-Types/unknownprimary> (Last Accessed 4/22/2011) 2004.
2. I. Brigger, C. Dubernet and P. Couvreur, *Adv. Drug Delivery Rev.*, 2002, **54**, 631-651.
3. D. Luo, K. Woodrow-Mumford, N. Belcheva and W. M. Saltzman, *Pharm. Res.*, 1999, **16**, 1300-1308.
4. D. H. Jones, S. Corris, S. McDonald, J. C. S. Clegg and G. H. Farrar, *Vaccine*, 1997, **15**, 814-817.
5. J. Panyam, W. Z. Zhou, S. Prabha, S. K. Sahoo and V. Labhasetwar, *FASEB J.*, 2002, **16**, 1217-1226.
6. A. L. Bailey and S. M. Sullivan, *Biochim. Biophys. Acta, Biomembr.*, 2000, **1468**, 239-252.
7. P. Fillion, A. Desjardins, K. Sayasith and J. Lagacé, *Biochim. Biophys. Acta, Biomembr.*, 2001, **1515**, 44-54.
8. H. Lomas, I. Canton, S. MacNeil, J. Du, S. P. Armes, A. J. Ryan, A. L. Lewis and G. Battaglia, *Adv. Mater.*, 2007, **19**, 4238-4243.
9. O. Kreft, R. Georgieva, H. Bäuml, M. Steup, B. Müller-Röber, G. B. Sukhorukov and H. Möhwald, *Macromol. Rapid Commun.*, 2006, **27**, 435-440.
10. K. W. Leong, H. Q. Mao, V. L. Truong-Le, K. Roy, S. M. Walsh and J. T. August, *J. Controlled Release*, 1998, **53**, 183-193.
11. T. Alexakis, D. K. Boadi, D. Quong, A. Groboillot, I. O'Neill, D. Poncelet and R. J. Neufeld, *Appl. Biochem. Biotechnol.*, 1995, **50**, 93-106.
12. C. Weber, C. Coester, J. Kreuter and K. Langer, *Int. J. Pharm.*, 2000, **194**, 91-102.
13. S. C. De Smedt, J. Demeester and W. E. Hennink, *Pharm. Res.*, 2000, **17**, 113-126.
14. F. E. Alemdaroglu, N. C. Alemdaroglu, P. Langguth and A. Herrmann, *Adv. Mater.*, 2008, **20**, 899-902.
15. N. L. Rosi, D. A. Giljohann, C. S. Thaxton, A. K. R. Lytton-Jean, M. S. Han and C. A. Mirkin, *Science*, 2006, **312**, 1027-1030.

16. T. R. Hoare and D. S. Kohane, *Polymer*, 2008, **49**, 1993-2007.
17. W. H. Blackburn, E. B. Dickerson, M. H. Smith, J. F. McDonald and L. A. Lyon, *Bioconjugate Chem.*, 2009, **20**, 960-968.
18. D. J. Quick and K. S. Anseth, *J. Controlled Release*, 2004, **96**, 341-351.
19. A. G. Ward and A. Courts, *The Science and technology of gelatin*, Academic Press, London ; New York, 1977.
20. A. Brunschwig, N. Corbin and C. D. Johnston, *Annals of Surgery*, 1943, **119**, 1058-1063.
21. Y. C. Lee, P. Simamora and S. H. Yalkowsky, *J. Pharm. Sci.*, 1997, **86**, 1361-1364.
22. H. Y. Fan and A. K. Dash, *Int. J. Pharm.*, 2001, **213**, 103-116.
23. Y. Fukunaka, K. Iwanaga, K. Morimoto, M. Kakemi and Y. Tabata, *J. Controlled Release*, 2002, **80**, 333-343.
24. Y. C. Lee, J. W. Millard, G. J. Negvesky, S. I. Butrus and S. H. Yalkowsky, *Int. J. Pharm.*, 1999, **182**, 121-126.
25. *Fed. Regist.*, 1998, **63**, 54082-54089.
26. S. J. Byrne, Y. Williams, A. Davies, S. A. Corr, A. Rakovich, Y. K. Gun'ko, Y. R. Rakovich, J. F. Donegan and Y. Volkov, *Small*, 2007, **3**, 1152-1156.
27. S. Young, M. Wong, Y. Tabata and A. G. Mikos, *J. Controlled Release*, 2005, **109**, 256-274.
28. N. Tanaka, I. Utsumi and S. Takino, *J. Pharm. Sci.*, 1963, **52**, 664-667.
29. Y. Tabata, Y. Ikada, K. Morimoto, H. Katsumata, T. Yabuta, K. Iwanaga and M. Kakemi, *J. Bioact. Compat. Polym.*, 1999, **14**, 371-384.
30. T. Yoshioka, M. Hashida, S. Muranishi and H. Sezaki, *Int. J. Pharm.*, 1981, **8**, 131-141.
31. Y. Tabata and Y. Ikada, *J. Pharm. Pharmacol.*, 1987, **39**, 698-704.
32. J. Allouche, M. Boissiere, C. Helary, J. Livage and T. Coradin, *J. Mater. Chem.*, 2006, **16**, 3120-3125.
33. E. Esposito, R. Cortesi and C. Nastruzzi, *Biomaterials*, 1996, **17**, 2009-2020.
34. K. Iwanaga, T. Yabuta, M. Kakemi, K. Morimoto, Y. Tabata and Y. Ikada, *J. Microencapsulation*, 2003, **20**, 767-776.

35. N. Adhirajan, N. Shanmugasundaram and M. Babu, *J. Microencapsulation*, 2007, **24**, 659-671.
36. I. Akartuna, A. R. Studart, E. Tervoort, U. T. Gonzenbach and L. J. Gauckler, *Langmuir*, 2008, **24**, 7161-7168.
37. R. Narayani and K. P. Rao, *J. Appl. Polym. Sci.*, 1995, **58**, 1761-1769.
38. Y. Lou and M. J. Groves, *J. Pharm. Pharmacol.*, 1995, **47**, 97-102.
39. S. Azarmi, Y. Huang, H. Chen, S. McQuarrie, D. Abrams, W. Roa, W. H. Finlay, G. G. Miller and R. Lobenberg, *J. Pharm. Pharm. Sci.*, 2006, **9**, 124-132.
40. C. J. Coester, K. Langer, H. Von Briesen and J. Kreuter, *J. Microencapsulation*, 2000, **17**, 187-193.
41. R. C. Oppenheim and N. F. Stewart, *Drug Dev. Ind. Pharm.*, 1979, **5**, 563-571.
42. Y. W. Won and Y. H. Kim, *J. Controlled Release*, 2008, **127**, 154-161.
43. C. G. de Kruif, F. Weinbreck and R. de Vries, *Curr. Opin. Colloid Interface Sci.*, 2004, **9**, 340-349.
44. E. Leo, M. A. Vandelli, R. Cameroni and F. Forni, *Int. J. Pharm.*, 1997, **155**, 75-82.
45. J. R. Nixon, S. A. H. Khalil and J. E. Carless, *J. Pharm. Pharmacol.*, 1968, **20**, 528-538.
46. A. Veis and C. Aranyi, *J. Phys. Chem.*, 1960, **64**, 1203-1210.
47. V. L. Truong-Le, S. M. Walsh, E. Schweibert, H. Q. Mao, W. B. Guggino, J. T. August and K. W. Leong, *Arch. Biochem. Biophys.*, 1999, **361**, 47-56.
48. M. L. Bruschi, M. L. C. Cardoso, M. B. Lucchesi and M. P. D. Gremiao, *Int. J. Pharm.*, 2003, **264**, 45-55.
49. Y. Bin Choy, F. Cheng, H. Choi and K. Kim, *Macromol. Biosci.*, 2008, **8**, 758-765.
50. Y. T. Matsunaga, Y. Morimoto and S. Takeuchi, *Adv. Mater.*, 2011, **23**, H90-H94.
51. K. S. Huang, K. Lu, C. S. Yeh, S. R. Chung, C. H. Lin, C. H. Yang and Y. S. Dong, *J. Controlled Release*, 2009, **137**, 15-19.
52. T. Morita, Y. Horikiri, H. Yamahara, T. Suzuki and H. Yoshino, *Pharm. Res.*, 2000, **17**, 1367-1373.

53. T. Morita, Y. Horikiri, T. Suzuki and H. Yoshino, *Int. J. Pharm.*, 2001, **219**, 127-137.
54. M. I. Ugwoke, N. Verbeke and R. Kinget, *Int. J. Pharm.*, 1997, **148**, 23-32.
55. C. Coester, P. Nayyar and J. Samuel, *Eur. J. Pharm. Biopharm.*, 2006, **62**, 306-314.
56. G. Kaul and M. Amiji, *J. Drug Targeting*, 2004, **12**, 585-591.
57. G. Kaul and M. Amiji, *Pharm. Res.*, 2005, **22**, 951-961.
58. S. Kommareddy and M. Amiji, *Nanomedicine*, 2007, **3**, 32-42.
59. A. Bigi, G. Cojazzi, S. Panzavolta, K. Rubini and N. Roveri, *Biomaterials*, 2001, **22**, 763-768.
60. G. Kaul and M. Amiji, *Pharm. Res.*, 2002, **19**, 1061-1067.
61. J. Franz, D. Pokorova, J. Hampl and M. Dittrich, *Int. J. Pharm.*, 1998, **168**, 153-161.
62. R. Nakaoka, Y. Tabata and Y. Ikada, *Vaccine*, 1995, **13**, 653-661.
63. R. Narayani and K. P. Rao, *Int. J. Pharm.*, 1996, **143**, 255-258.
64. A. Hosaka, H. Koyama, T. Kushibiki, Y. Tabata, N. Nishiyama, T. Miyata, H. Shigematsu, T. Takato and H. Nagawa, *Circulation*, 2004, **110**, 3322-3328.
65. W. M. Saltzman, M. L. Radomsky, K. J. Whaley and R. A. Cone, *Biophys. J.*, 1994, **66**, 508-515.
66. K. Zwioerek, C. Bourquin, J. Battiany, G. Winter, S. Endres, G. Hartmann and C. Coester, *Pharm. Res.*, 2008, **25**, 551-562.
67. J. C. Zillies, K. Zwioerek, F. Hoffmann, A. Vollmar, T. J. Anchordoquy, G. Winter and C. Coester, *Eur. J. Pharm. Biopharm.*, 2008, **70**, 514-521.
68. K. D. Yao, Y. J. Yin, M. X. Xu and Y. F. Wang, *Polym. Int.*, 1995, **38**, 77-82.
69. A. J. Kuijpers, G. H. M. Engbers, T. K. L. Meyvis, S. C. De Smedt, J. Demeester, J. Krijgsveld, S. A. J. Zaat, J. Dankert and J. Feijen, *Macromolecules*, 2000, **33**, 3705-3713.
70. J. C. Zillies, K. Zwioerek, G. Winter and C. Coester, *Anal. Chem.*, 2007, **79**, 4574-4580.
71. J. W. McGinity, A. B. Combs and A. N. Martin, *J. Pharm. Sci.*, 1975, **64**, 889-890.

72. C. Coester, J. Kreuter, H. von Briesen and K. Langer, *Int. J. Pharm.*, 2000, **196**, 147-149.
73. G. Decher, J. D. Hong and J. Schmitt, *Thin Solid Films*, 1992, **210**, 831-835.
74. V. Kozlovskaya and S. A. Sukhishvili, *Macromolecules*, 2006, **39**, 5569-5572.
75. Y. Zhang, Y. Guan, S. Yang, J. Xu and C. C. Han, *Adv. Mater.*, 2003, **15**, 832-835.
76. G. K. Such, J. F. Quinn, A. Quinn, E. Tjipto and F. Caruso, *J. Am. Chem. Soc.*, 2006, **128**, 9318-9319.
77. Y. Lvov, G. Decher and H. Mohwald, *Langmuir*, 1993, **9**, 481-486.
78. S. S. Shiratori and M. F. Rubner, *Macromolecules*, 2000, **33**, 4213-4219.
79. E. Kharlampieva, V. Kozlovskaya, O. Zavgorodnya, G. D. Lilly, N. A. Kotov and V. V. Tsukruk, *Soft Matter*, 2010, **6**, 800-807.
80. H. Ai and J. Gao, *J. Mater. Sci.*, 2004, **39**, 1429-1432.
81. H. Ai, S. A. Jones, M. M. de Villiers and Y. M. Lvov, *J. Controlled Release*, 2003, **86**, 59-68.
82. G. B. Sukhorukov, A. Fery, M. Brumen and H. Mohwald, *Phys. Chem. Chem. Phys.*, 2004, **6**, 4078-4089.
83. A. A. Antipov and G. B. Sukhorukov, *Adv. Colloid Interface Sci.*, 2004, **111**, 49-61.
84. X. Yang, X. Han and Y. Zhu, *Colloids Surf., A*, 2005, **264**, 49-54.
85. G. Ibarz, L. Dahne, E. Donath and H. Mohwald, *Chem. Mater.*, 2002, **14**, 4059-4062.
86. S. Ye, C. Wang, X. Liu and Z. Tong, *J. Controlled Release*, 2005, **106**, 319-328.
87. Y. Lvov, A. A. Antipov, A. Mamedov, H. Mohwald and G. B. Sukhorukov, *Nano Lett.*, 2001, **1**, 125-128.
88. T. Serizawa, M. Yamaguchi and M. Akashi, *Biomacromolecules*, 2002, **3**, 724-731.
89. A. Yu, Y. Wang, E. Barlow and F. Caruso, *Adv. Mater.*, 2005, **17**, 1737-1741.
90. J. D. Mendelsohn, S. Y. Yang, J. Hiller, A. I. Hochbaum and M. F. Rubner, *Biomacromolecules*, 2003, **4**, 96-106.

91. S. E. Burke and C. J. Barret, *Langmuir*, 2003, **19**, 3247-3303.
92. B. G. De Geest, C. Dejumat, E. Verhoeven, G. B. Sukhorukov, A. M. Jonas, J. Plain, J. Demeester and S. C. De Smedt, *J. Controlled Release*, 2006, **116**, 159-169.
93. N. Greinert and W. Richtering, *Colloid Polym. Sci.*, 2004, **282**, 1146-1149.
94. F. Caruso, D. Trau, H. Mohwald and R. Renneberg, *Langmuir*, 2000, **16**, 1485-1488.
95. N. G. Balabushevitch, G. B. Sukhorukov, N. A. Moroz, D. V. Volodkin, N. I. Larionova, E. Donath and H. Mohwald, *Biotechnol. Bioeng.*, 2001, **76**, 207-213.
96. C. Picart, P. Lavallo, P. Hubert, F. J. G. Cuisinier, G. Decher, P. Schaaf and J. C. Voegel, *Langmuir*, 2001, **17**, 7414-7424.
97. S. C. Gangloff, G. Ladam, V. Dupray, K. Fukase, K. Brandenburg, M. Guenounou, P. Schaaf, J. C. Voegel and N. Jessel, *Biomaterials*, 2006, **27**, 1771-1777.
98. X. Chen, X. Yan, K. A. Khor and B. K. Tay, *Biosens. Bioelectron.*, 2007, **22**, 3256-3260.
99. E. Donath, G. B. Sukhorukov, F. Caruso, S. A. Davis and H. Mohwald, *Angew. Chem., Int. Ed.*, 1998, **37**, 2201-2205.
100. S. T. Dubas and J. B. Schlenoff, *Macromolecules*, 2001, **34**, 3736-3740.
101. D. L. Elbert, C. B. Herbert and J. A. Hubbell, *Langmuir*, 1999, **15**, 5355-5362.
102. D. O. Grigoriev, T. Bukreeva, H. Mohwald and D. G. Shchukin, *Langmuir*, 2008, **24**, 999-1004.
103. Y. Itoh, M. Matsusaki, T. Kida and M. Akashi, *Chem. Lett.*, 2004, **33**, 1552-1553.
104. A. J. Khopade and F. Caruso, *Chem. Mater.*, 2004, **16**, 2107-2112.
105. F. Caruso, *Chem.--Eur. J.*, 2000, **6**, 413-419.
106. W. C. Mak, J. Bai, X. Y. Chang and D. Trau, *Langmuir*, 2009, **25**, 769-775.
107. Q. Li, J. F. Quin and F. Caruso, *Adv. Mater.*, 2005, **17**, 2058-2062.
108. J. D. Mendelsohn, C. J. Barret, V. V. Chan, A. J. Pal, A. M. Mayes and M. F. Rubner, *Langmuir*, 2000, **16**, 5017-1023.
109. I. Pastoriza-Santos, B. Scholer and F. Caruso, *Adv. Funct. Mater.*, 2001, **11**, 122-128.

110. J. D. Watson and F. H. C. Crick, *Nature*, 1953, **171**, 737-738.
111. C. R. Calladine, H. R. Drew, B. F. Luisi and A. A. Travers, *Understanding DNA*, 3rd edn., Academic Press, London, 2004.
112. J. B. Mills, E. Vacano and P. J. Hagerman, *J. Mol. Biol.*, 1999, **285**, 245-257.
113. C. Rivetti, C. Walker and C. Bustamante, *J. Mol. Biol.*, 1998, **280**, 41-59.
114. T. Lindahl and B. Nyberg, *Biochemistry*, 1972, **11**, 3610-3618.
115. J. T. Lett, E. S. Klucis and C. Sun, *Biophys. J.*, 1970, **10**, 277-&.
116. M. P. Knauert and P. M. Glazer, *Hum. Mol. Genet.*, 2001, **10**, 2243-2251.
117. S. Burge, G. N. Parkinson, P. Hazel, A. K. Todd and S. Neidle, *Nucleic Acids Res.*, 2006, **34**, 5402-5415.
118. M. F. Hagan and A. K. Chakraborty, *J. Chem. Phys.*, 2004, **120**, 4958-4968.
119. W. H. Braunlin and V. A. Bloomfield, *Biochemistry*, 1991, **30**, 754-758.
120. N. Tibanyenda, S. H. Debruin, C. A. G. Haasnoot, G. A. Vandermarel, J. H. Vanboom and C. W. Hilbers, *Eur. J. Biochem.*, 1984, **139**, 19-27.
121. K. M. Parkhurst and L. J. Parkhurst, *Biochemistry*, 1995, **34**, 285-292.
122. N. C. Seeman, *Nature*, 2003, **421**, 427-431.
123. W. Y. Liu, H. Zhong, R. S. Wang and N. C. Seeman, *Angew. Chem., Int. Ed.*, 2011, **50**, 264-267.
124. N. C. Seeman, *Trends Biochem. Sci.*, 2005, **30**, 119-125.
125. J. Marmur and P. Doty, *Nature*, 1959, **183**, 1427-1429.
126. S. Lifson, *Biopolymers*, 1963, **1**, 25-32.
127. D. M. Crothers and B. H. Zimm, *J. Mol. Biol.*, 1964, **9**, 1-9.
128. H. Devoe and I. Tinoco, *J. Mol. Biol.*, 1962, **4**, 500-517.
129. K. Drukker and G. C. Schatz, *J. Phys. Chem. B*, 2000, **104**, 6108-6111.
130. S. Monti, I. Cacelli, A. Ferretti, G. Prampolini and V. Barone, *Mol. BioSyst.*, 2010, **6**, 2230-2240.
131. D. M. Gray and I. Tinoco, *Biopolymers*, 1970, **9**, 223-&.

132. S. M. Freier, N. Sugimoto, A. Sinclair, D. Alkema, T. Neilson, R. Kierzek, M. H. Caruthers and D. H. Turner, *Biochemistry*, 1986, **25**, 3214-3219.
133. S. M. Freier, R. Kierzek, J. A. Jaeger, N. Sugimoto, M. H. Caruthers, T. Neilson and D. H. Turner, *Proc. Natl. Acad. Sci. U. S. A.*, 1986, **83**, 9373-9377.
134. K. J. Breslauer, R. Frank, H. Blocker and L. A. Marky, *Proc. Natl. Acad. Sci. U. S. A.*, 1986, **83**, 3746-3750.
135. L. A. Marky and K. J. Breslauer, *Biopolymers*, 1987, **26**, 1601-1620.
136. J. SantaLucia, Jr., *Proc. Natl. Acad. Sci. U. S. A.*, 1998, **95**, 1460-1465.
137. N. Peyret, A. Seneviratne, H. T. Allawi, and J. SantaLucia, *Biochemistry*, 1999, **38**, 3468-3477.
138. H. T. Allawi and J. SantaLucia, *Biochemistry*, 1997, **36**, 10581-10594.
139. S. Bommarito, N. Peyret and J. SantaLucia, Jr., *Nucleic Acids Res.*, 2000, **28**, 1929-1934.
140. L. E. Morrison and L. M. Stols, *Biochemistry*, 1993, **32**, 3095-3104.
141. T. V. Chalikian, J. Volker, G. E. Plum and K. J. Breslauer, *Proc. Natl. Acad. Sci. U. S. A.*, 1999, **96**, 7853-7858.
142. A. Tikhomirova, N. Taulier and T. V. Chalikian, *J. Am. Chem. Soc.*, 2004, **126**, 16387-16394.
143. M. Zuker, *Nucleic Acids Res.*, 2003, **31**, 3406-3415.
144. L. P. Reynaldo, A. V. Vologodskii, B. P. Neri and V. I. Lyamichev, *J. Mol. Biol.*, 2000, **297**, 511-520.
145. V. V. Anshelevich, A. V. Vologodskii, A. V. Lukashin and M. D. Frank-Kamenetskii, *Biopolymers*, 1984, **23**, 39-58.
146. D. Y. Zhang and E. Winfree, *J. Am. Chem. Soc.*, 2009, **131**, 17303-17314.
147. D. Soloveichik, G. Seelig and E. Winfree, *Proc. Natl. Acad. Sci. U. S. A.*, 2010, **107**, 5393-5398.
148. H. Y. Dai, M. Meyer, S. Stepaniants, M. Ziman and R. Stoughton, *Nucleic Acids Res.*, 2002, **30**.
149. J. Bishop, S. Blair and A. M. Chagovetz, *Biophys. J.*, 2006, **90**, 831-840.
150. M. Jobs, S. Fredriksson, A. J. Brookes and U. Landegren, *Anal. Chem.*, 2002, **74**, 199-202.

151. A. W. Peterson, R. J. Heaton and R. M. Georgiadis, *Nucleic Acids Res.*, 2001, **29**, 5163-5168.
152. M. R. Henry, P. Wilkins Stevens, J. Sun and D. M. Kelso, *Anal. Biochem.*, 1999, **276**, 204-214.
153. V. Chan, D. J. Graves and S. E. McKenzie, *Biophys. J.*, 1995, **69**, 2243-2255.
154. H. Nasef, V. C. Ozalp, V. Beni and C. K. O'Sullivan, *Anal. Biochem.*, 2010, **406**, 34-40.
155. J. Xu and S. L. Craig, *J. Am. Chem. Soc.*, 2005, **127**, 13227-13231.
156. P. W. Stevens, M. R. Henry and D. M. Kelso, *Nucleic Acids Res.*, 1999, **27**, 1719-1727.
157. A. Vainrub and B. M. Pettitt, *Biopolymers*, 2003, **68**, 265-270.
158. C. A. Marquette, I. Lawrence, C. Polychronakos and M. F. Lawrence, *Talanta*, 2002, **56**, 763-768.
159. A. K. R. Lytton-Jean and C. A. Mirkin, *J. Am. Chem. Soc.*, 2005, **127**, 12754-12755.
160. S. F. Wolf, L. Haines, J. Fisch, J. N. Kremsky, J. P. Dougherty and K. Jacobs, *Nucleic Acids Res.*, 1987, **15**, 2911-2926.
161. X. J. Chen, B. L. Sanchez-Gaytan, S. E. N. Hayik, M. Fryd, B. B. Wayland and S. J. Park, *Small*, 2010, **6**, 2256-2260.
162. P. A. E. Piunno, J. Watterson, C. C. Wust and U. J. Krull, *Anal. Chim. Acta*, 1999, **400**, 73-89.
163. Y. Okahata, M. Kawase, K. Niikura, F. Ohtake, H. Furusawa and Y. Ebara, *Anal. Chem.*, 1998, **70**, 1288-1296.
164. M. Glazer, J. A. Fidanza, G. H. McGall, M. O. Trulson, J. E. Forman, A. Suseno and C. W. Frank, *Anal. Biochem.*, 2006, **358**, 225-238.
165. J. Zeng, A. Almadidy, J. Watterson and U. K. Krull, *Sensors and Actuators B-Chemical*, 2003, **90**, 68-75.
166. D. Erickson, D. Q. Li and U. J. Krull, *Anal. Biochem.*, 2003, **317**, 186-200.
167. V. T. Milam, A. L. Hiddessen, J. C. Crocker, D. J. Graves and D. A. Hammer, *Langmuir*, 2003, **19**, 10317-10323.
168. C. K. Tison and V. T. Milam, *Langmuir*, 2007, **23**, 9728-9736.

169. B. A. Baker and V. T. Milam, *Nucleic Acids Res.*, 2011, **30**, doi:10.1093/nar/gkr1293.
170. S. T. Parpart, C. K. Tison and V. T. Milam, *Soft Matter*, 2010, **6**, 3832-3840.
171. C. K. Tison and V. T. Milam, *Soft Matter*, 2010, **6**, 4446-4453.
172. S. H. Behrens, D. I. Christl, R. Emmerzael, P. Schurtenberger and M. Borkovec, *Langmuir*, 2000, **16**, 2566-2575.
173. J. J. Lietor-Santos, A. Fernandez-Nieves and M. Marquez, *Physical Review E*, 2005, **71**.
174. V. J. Anderson and H. N. Lekkerkerker, *Nature*, 2002, **416**, 811-815.
175. C. A. Mirkin, R. L. Letsinger, R. C. Mucic and J. J. Storhoff, *Nature*, 1996, **382**, 607-609.
176. R. J. Macfarlane, B. Lee, H. D. Hill, A. J. Senesi, S. Seifert and C. A. Mirkin, *Proc. Natl. Acad. Sci. U. S. A.*, 2009, **106**, 10493-10498.
177. R. Jin, G. Wu, Z. Li, C. A. Mirkin and G. C. Schatz, *J. Am. Chem. Soc.*, 2003, **125**, 1643-1654.
178. S. Y. Park, J. S. Lee, D. Georganopoulou, C. A. Mirkin and G. C. Schatz, *J. Phys. Chem. B*, 2006, **110**, 12673-12681.
179. S. J. Hurst, H. D. Hill and C. A. Mirkin, *J. Am. Chem. Soc.*, 2008, **130**, 12192-12200.
180. A. J. Kim, P. L. Biancaniello and J. C. Crocker, *Langmuir*, 2006, **22**, 1991-2001.
181. T. A. Taton, C. A. Mirkin and R. L. Letsinger, *Science*, 2000, **289**, 1757-1760.
182. S. J. Hurst, H. D. Hill, R. J. Macfarlane, J. S. Wu, V. P. Dravid and C. A. Mirkin, *Small*, 2009, **5**, 2156-2161.
183. H. Long and G. C. Schatz, *Mater. Res. Soc. Symp. Proc.*, 2003, **735**, C10.11.
184. H. Long, A. Kudlay and G. C. Schatz, *J. Phys. Chem. B*, 2006, **110**, 2918-2926.
185. J. M. Gibbs-Davis, G. C. Schatz and S. T. Nguyen, *J. Am. Chem. Soc.*, 2007, **129**, 15535-15540.
186. I. Eryazici, T. R. Prytkova, G. C. Schatz and S. T. Nguyen, *J. Am. Chem. Soc.*, 2010, **132**, 17068-17070.
187. T. R. Prytkova, I. Eryazici, B. Stepp, S. B. Nguyen and G. C. Schatz, *J. Phys. Chem. B*, 2010, **114**, 2627-2634.

188. R. Dreyfus, M. E. Leunissen, R. Sha, A. Tkachenko, N. C. Seeman, D. J. Pine and P. M. Chaikin, *Phys. Rev. E: Stat., Nonlinear, Soft Matter Phys.*, 2010, **81**.
189. D. Nykypanchuk, M. M. Maye, D. V. Lelie and O. Gang, *Langmuir*, 2007.
190. P. L. Biancaniello, J. C. Crocker, D. A. Hammer and V. T. Milam, *Langmuir*, 2007, **23**, 2688-2693.
191. R. Dreyfus, M. E. Leunissen, R. J. Sha, A. V. Tkachenko, N. C. Seeman, D. J. Pine and P. M. Chaikin, *Phys. Rev. Lett.*, 2009, **102**.
192. M. E. Leunissen, R. Dreyfus, F. C. Cheong, D. G. Grier, R. Sha, N. C. Seeman and P. M. Chaikin, *Nat. Mater.*, 2009, **8**, 590-595.
193. B. A. Baker and V. T. Milam, *Langmuir*, 2010, **26**, 9818-9826.
194. C. K. Tison and V. T. Milam, *Biomacromolecules*, 2008, **9**, 2468-2476.
195. M. P. Valignat, O. Theodoly, J. C. Crocker, W. B. Russel and P. M. Chaikin, *Proc. Natl. Acad. Sci. U. S. A.*, 2005, **102**, 4225-4229.
196. P. Hazarika, B. Ceyhan and C. M. Niemeyer, *Angew. Chem., Int. Ed.*, 2004, **43**, 6469-6471.
197. D. A. Giljohann, D. S. Seferos, P. C. Patel, J. E. Millstone, N. L. Rosi and C. A. Mirkin, *Nano Lett.*, 2007, **7**, 3818-3821.
198. D. S. Seferos, A. E. Prigodich, D. A. Giljohann, P. C. Patel and C. A. Mirkin, *Nano Lett.*, 2009, **9**, 308-311.
199. P. L. Biancaniello, A. J. Kim and J. C. Crocker, *Phys. Rev. Lett.*, 2005, **94**, 058302.
200. D. Nykypanchuk, M. M. Maye, D. Van der Lelie and O. Gang, *Nature*, 2008, **451**, 549-552.
201. S. Y. Park, A. Lytton-Jean, B. Lee, S. Weigand, G. C. Schatz and C. A. Mirkin, *Nature*, 2008, **451**, 553-556.
202. W. Dai, S. K. Kumar and F. W. Starr, *Soft Matter*, 2010, **6**, 6130-6135.
203. D. B. Lukatsky and D. Frenkel, *Phys. Rev. Lett.*, 2004, **92**, 068302.
204. D. B. Lukatsky, B. M. Mulder and D. Frenkel, *J. Phys.: Condens. Matter*, 2006, **18**, S567-S580.
205. A. V. Tkachenko, *Phys. Rev. Lett.*, 2002, **89**.

206. C. M. Soto, A. Srinivasan and B. R. Ratna, *J. Am. Chem. Soc.*, 2002, **124**, 8508-8509.
207. M. G. Bajaj and P. E. Laibinis, *Mater. Res. Soc. Symp. Proc.*, 2004, **EXS-1**, H1.2.1–H1.2.3.

CHAPTER 2

DNA ENCAPSULATION IN GELATIN MICROSPHERES

2.1 Overview

Gelatin was investigated as a matrix for temporarily encapsulating, then releasing active, short oligonucleotide stands. While most previous work has focused on using covalently crosslinked gelatin matrices in which protease digestion triggers release of encapsulated agents, the current study involves uncrosslinked gelatin in order to preserve its relevant temperature sensitivity. First, uniform 150 μ L gelatin blocks loaded with fluorescently-labeled DNA were investigated. Deposition of poly(allylamine)-poly(acrylic acid) bilayers on the gel hindered DNA release at room temperature, but promoted at least 5-fold greater release at 37 °C relative to the room temperature samples. Next, a polydisperse population of DNA-loaded gelatin microspheres was prepared and coated with a polyelectrolyte bilayer. The gelatin microsphere system exhibited a similar temperature dependence as the block system, however, the total amount of DNA released was greater due, mostly likely, to the higher surface area to volume ratio of the microspheres. In both systems, any active DNA released from the gelatin matrices was quantified through subsequent hybridization events with polystyrene particles functionalized with the complementary partner sequence. Overall, our studies indicate that these DNA-loaded, uncrosslinked gelatin carriers represent a promising system for triggered release of encapsulated oligonucleotides for a variety of bio-related applications.¹

2.2 Materials and Methods

2.1.1 Materials

Three sequences of DNA, probe **A20** (5'-TTT TTT GGA TTG CGG CTG AT-3'); complementary target **P14** (3'-CCT AAC GCC GAC TA-5'); and noncomplementary target **NC** (3'-GGA TTG CGG CTG AT-5') were purchased from Integrated DNA Technologies (Coralville, IA). Fluorescein or amine functionalization (including a (CH₂)₆ spacer) of the 5' end of the DNA strands and HPLC purification of the DNA strands were performed by the supplier. MES hydrate, Tris/EDTA pH 7.4 and Tris/EDTA pH 8.0 buffers were purchased from Fisher Scientific (Pittsburg, PA). PBS, NaCl, Type A gelatin from porcine skin (300 Bloom and pI ~ 8.0), acetone, isooctane, Span 80, Tween 80, Procline®, 1-ethyl-3-[3-dimethylaminopropyl]-carbodiimide hydrochloride (EDC), and Grade 1 filter paper were purchased from Sigma Aldrich (St. Louis, MO). The polyelectrolytes used for the LbL film were sodium polyacrylate (M_w ~ 85 kDa) and poly(allylamine hydrochloride) (M_w ~ 56 kDa) purchased from Polysciences (Warrington, PA) and Sigma Aldrich respectively. Carboxylated 1.1 μm diameter polystyrene latex particles and MESF flow cytometry standards were purchased from Bangs Laboratories, Inc (Fishers, IN).

2.2.2 Preparation of DNA-Gelatin Blocks

The gelatin block experiments are represented in Figure 2.1. A liquid gelatin-DNA mixture was prepared by adding 0.2 g, 0.5 g, or 1.3 g of Type A gelatin to 2 mL of 2 μM or 10 μM fluorescently-labeled **P14** (designated as **P14-**

F) in nanopure water at 40 °C to yield 10, 20, and 40 wt% gelatin solutions. The resulting solution was lightly vortexed and allowed to mix until clear. Any remaining air bubbles were removed using sonication. 150 µL aliquots of the gelatin solution were carefully dispensed into microwells of a 96 microwell plate. The tip of the micropipetter was warmed above 40 °C prior to each aliquot to ensure good flow. Contact between the sides of the wells and the micropipetter tip was carefully avoided. Afterwards, the wells were covered with Parafilm® to prevent the gel from drying out. The gels were allowed to solidify in a refrigerator at ~6 °C overnight.

To deposit LbL films on the surface of each block, 250 µL of a 1 mg/mL PAH (150 mM NaCl and pH 7.0) solution was added on top of each DNA-gelatin block and allowed to incubate for 10 min. After 10 min, the PAH solution was removed and the gel was rinsed 3 times with saline solution (150 mM NaCl). A 250 µL volume of a 1 mg/mL PAA solution (150 mM NaCl and pH 7.0) was then added and allowed to incubate for 10 min. Washing was performed as described above and the PAH and PAA adsorption steps were alternated until the intended number of bilayers were added. Once the intended number of layers were added to one well, 250 µL of saline solution was gently added to the top of the DNA-gelatin block. Any remaining solution (not absorbed by the gelatin matrix) was replaced with 230 µL of PBS and the samples were incubated at room temperature or 37 °C for 4 h prior to supernatant analysis.

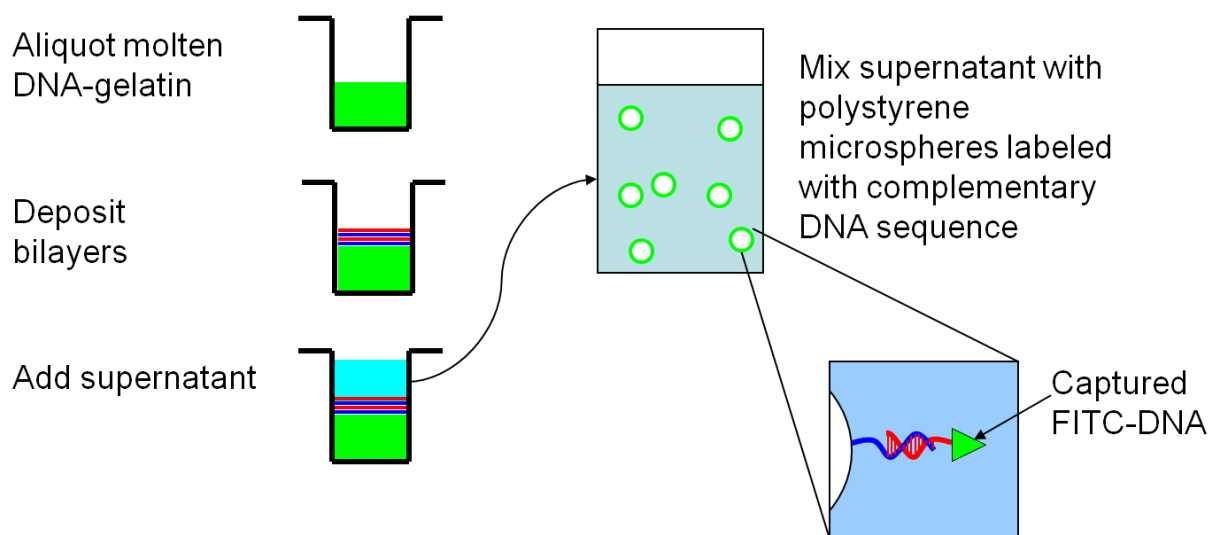


Figure 2.1. Graphical description of the study involving DNA release from gelatin blocks. A gelatin-DNA mixture is aliquoted into a microwell and allowed to gel. A polyelectrolyte film was then deposited using LbL deposition. The gelatin block was then incubated at room temperature or 37 °C with a layer of fresh PBS solution on top of the gelatin-DNA block. The released active DNA was collected from the supernatant by polystyrene microsphere labeled with complementary DNA. The concentration of released DNA was then be measured using flow cytometry.

2.2.3 Preparation and DNA Loading of Gelatin Microspheres (GMS)

Gelatin microspheres were first prepared using a water in oil emulsion technique as depicted in Figure 2.2. The oil phase consisted of 10 mL of isooctane, 250 μ L of Tween 80, and 250 μ L of Span 80 at 40 °C. A solution of 20 wt% gelatin was prepared by adding 2.5 g of gelatin to 10 mL of nanopure water at 40 °C. The solution was allowed to mix for 30 min. A 0.5 mL volume of the gelatin solution was added to the oil phase and strongly vortexed for 10 min while cooling to room temperature. The cooled emulsion was added drop-wise to 60 mL of acetone under magnetic stirring. The acetone and GMS suspension was then passed through grade 1 filter papers under light agitation to remove large particles.

The material that passed through the filters was centrifuged at 10,000 rpm for 10 min. The supernatant was removed and the particles were washed 3 times in acetone to remove remaining surfactant and isooctane and, finally, resuspended in 1 mL of acetone.

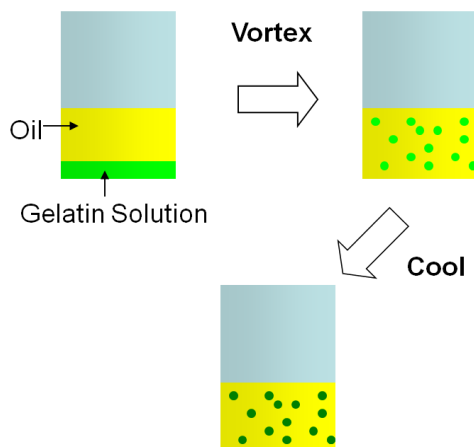


Figure 2.2. W/O emulsion synthesis of GMS. The molten gelatin is mixed with oil to form oil droplets. These droplets are then cooled to solidify them.

Suspensions of GMS were then infiltrated with soluble **P14-F** using the following approach. A 50 μL aliquot of GMS suspended in acetone was centrifuged at 2300 rpm for 1 min. The supernatant was then removed and replaced with a pH \sim 4.5 solution of 150 mM NaCl and 10 μM **P14-F**. Since the isoelectric point of Type A gelatin is typically at a pH of 7 - 9, the gelatin should possess a net positive charge at pH 4.5 and thereby electrostatically attract the negatively-charged DNA. The GMS suspensions were incubated with the DNA for 30 min while rotated end-over-end. Following DNA infiltration, the samples were centrifuged for 1 min at 2300 rpm, and the supernatant was replaced with 100 μL

of saline. Centrifugation and supernatant replacement was repeated before the GMS were resuspended by vortexing and sonication in the PAH solution described earlier. The samples were then incubated for 10 min while rotating end over end. Afterwards, the samples were centrifuged and the supernatant was replaced two times as described above. The GMS samples were then resuspended in the PAA solution for 10 minutes followed by centrifugation and supernatant replacement, as described above. Select samples were resuspended in saline instead of polyelectrolyte, however, the total number of washes was consistent for all samples.

2.2.4 Zeta Potential Measurements of GMS

Zeta potential measurements were performed on a Zetasizer NS (Malvern Instruments, Worcestershire, UK) using a dip cell. GMS were prepared as described earlier except that GMS were washed in a pH 7.0, 10 mM NaCl solution for the final two resuspension steps to prepare a 1 mL suspension.

2.2.5 Release of Encapsulated DNA Strands

The gelatin blocks and GMS were incubated in a hybridizing oven at 37 °C or at room temperature for 4 h. The gelatin blocks were also incubated for 1, 2, and 3 h to observe release over time. Each well containing a gelatin block was covered with Parafilm to minimize evaporation during the incubation. Prior to the incubation, the saline solution above the blocks was replaced with 230 µM of PBS. GMS samples were prepared as described above and then each sample was

split in half. Half of these GMS samples were then incubated at 37 °C while the others were left at room temperature. After the appropriate incubation time had elapsed, the gelatin blocks and GMS samples were placed in the refrigerator for 10 min to stabilize the gelatin phase against mixing with the supernatant before collecting the supernatant. GMS samples were centrifuged at 10,200 rpm for 5 min and the supernatant saved to remove potential remnants of GMS.

2.2.6 Preparation and Hybridization of DNA-Functionalized Polystyrene Microspheres

A more detailed description of the preparation and characterization of DNA-functionalized polystyrene microspheres is provided in Chapter 3.² Briefly, aminated **A20** strands were coupled to 1 μm carboxylated polystyrene particles and resuspended to a final particle concentration of 1 v%. Hybridization was performed by resuspending 5 μL of the coupled polystyrene particles in 100 μL of a PBS/Tween buffer. 100 μL of either a DNA solution of known concentration (for calibration purposes) or a supernatant solution of unknown DNA concentration was then added to the suspension for an overnight incubation. The samples were then washed 3 times and resuspended in 100 μL of the PBS/Tween buffer.

2.2.7 Flow Cytometry

The surface density of **A20:P14-F** duplexes on the polystyrene microspheres was analyzed with a BD-LSR II flow cytometer (Becton, Dickinson and Company, Franklin Lakes, NJ). The singlet population was gated using the

forward and side scattering plots to then determine the mean fluorescence value per microsphere. A FITC calibration standard was used to convert the mean fluorescence per microsphere into an average number of fluorescent moieties per microsphere. (Note: negative controls using the fluorescently-labeled noncomplementary target, **NC-F**, revealed that nonspecific associations between DNA released from gelatin matrices and the **A20**-functionalized lattices were negligible). **A20**-functionalized microspheres were incubated with either the extracted supernatant from the gelatin-based samples or with a prepared **P14-F** solution of known concentration (for calibration purposes). The average surface density of **A20:P14-F** duplexes on the microspheres was determined through linear interpolation between nearest known concentrations to derive the final **P14-F** concentration in the original supernatant. The average concentration is reported for all cases except one - the average value of 2 samples is reported for the uncoated gelatin blocks with the highest DNA loading conditions (10 μ M) studied.

2.2.8 Determination of GMS Concentration

To determine the GMS concentration used for the release studies, a sample of GMS was washed in saline solution using the handling conditions described earlier. The particles were then resuspended in Isoton II solution through vortexing and sonication. A second set of samples was directly resuspended in Isoton II solution without undergoing any prior washing steps. Samples were analyzed using a BD Multisizer III Coulter Counter (Becton, Dickinson and Company, Franklin Lakes, NJ) with a 50 μ m diameter aperture. Three measurements were

taken for each 0.5 mL sample. The results were tabulated by organizing raw data into bins of different particle diameter ranges. The counts in each bin were converted into a volumetric dispersion of the GMS and normalized to the bin size.

2.2.9 Microscopy

Samples were viewed on a Zeiss Axiovert 200 inverted fluorescence microscope (Carl Zeiss AG, Oberkochen, Germany). Images were captured on a Sony Handicam (3.0 Megapixels) with the auto-focus feature disabled in order to preserve the object sizes in the images. 15 μ L of each sample was added to microscope wells from VWR International (West Chester, PA). GMS images were taken in phase contrast and fluorescence modes. Fluorescence micrographs were taken after a 5 s illumination time.

2.3 Results and Discussion

2.3.1 Oligonucleotide Release from Gelatin Blocks

The release of active DNA from gelatin was first studied in a model system using gelatin blocks with known, equivalent amounts of loaded DNA. The first experiments tested the ability of gelatin alone (i.e. no polyelectrolyte coating) at various gelatin concentrations to initially trap DNA in the gel state at room temperature and then release DNA when heated to 37 °C. As shown in Figure 2.3, increasing the gelatin concentration reduces the amount of DNA released in all cases, however, a significant temperature dependence on release behavior was

only observed at the highest gelatin concentration of 40 wt%. This gradual decrease in the DNA release with gelatin concentration implies that the effective pore size of the solid gelatin is approaching the size of the encapsulated DNA strands and restricting the diffusion of the DNA to a tortuous path through pores

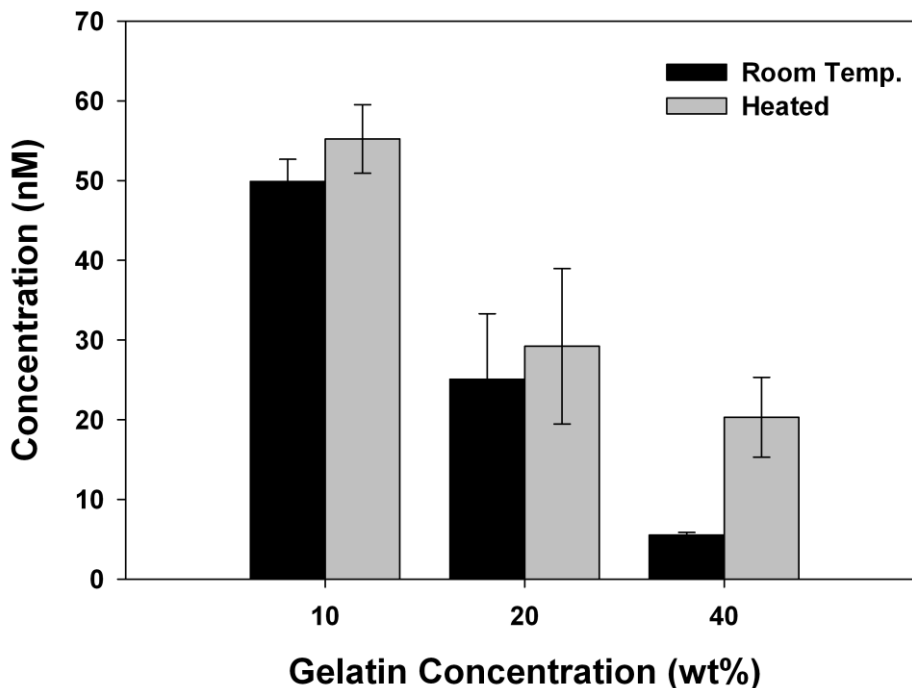


Figure 2.3. Concentration of **P14-F** DNA released from uncoated gelatin-DNA blocks of varying gelatin concentration at either ~ 22 °C (room temperature) or 37 °C (heated). Taken from reference 1.

of sufficient size. The pore size of the gelatin can be estimated using the reported 10 nm pore size for 10 wt% gelatin at room temperature.³ If the effective pore size, a_{pore} , scales with gelatin concentration, [gelatin], as follows: $a_{pore} \sim [\text{gelatin}]^{0.5}$, then 20 wt% and 40 wt% gelatin samples have estimated pore sizes of ~ 7 nm and ~ 5 nm, respectively.³ Using the worm-like chain model and a persistence length of 1.3 nm for single-stranded DNA⁴ yields a root-mean-squared,

end-to-end distance of ~4 nm for the 14 base-long encapsulated DNA strands, a size just below the estimated pore size of 40 wt% gelatin at room temperature. The transition from gel to viscous fluid that occurs on raising the temperature also shifts the mode of diffusion from tortuous motion through a pore structure to simple diffusion through a viscous fluid where the viscosity is dependent on the gelatin concentration. Although 40 wt% gelatin was the only concentration to show significant temperature dependence for DNA release, the relatively high viscosity of the liquid gelatin and excessive swelling of the gelled blocks made mixing and handling steps less reliable than the two other lower gelatin concentrations explored. Thus, 20 wt% gelatin was chosen for all subsequent studies involving polyelectrolyte adsorption.

Due to the experimental difficulty of measuring the surface potential of these semi-permeable gelatin blocks, zeta potential measurements of GMS were taken after incubation with PAH and PAA to confirm the adsorption of polyelectrolytes on the gelatin matrices. The zeta potential values of GMS with DNA infiltrated was found to be weakly negative at -5.0 mV as expected since type A gelatin typically has an isoelectric point of pH 7.0 - 9.0. Subsequent incubation of GMS with the polycation PAH yields particles with a positive zeta potential value of +12.8 mV. Subsequent incubation with the polyanion PAA yields a zeta potential of -14.8 mV, a value more negative than the uncoated GMS. For GMS with no infiltrated DNA, the analogous zeta potential values at the various processing stages are -4.2, +8.1, and -15.4 mV respectively. The sign alternation and magnification of the zeta potential following each incubation stage

strongly point to sequential absorption of the polyelectrolytes as opposed to displacement of an underlying polyelectrolyte layer. After successfully confirming deposition of the bilayer on DNA-infiltrated GMS with zeta potential measurements, the gelatin block system was then revisited to test the efficacy of the polyelectrolyte layers as a temperature-dependent diffusion barrier.

Following the deposition of up to 3 PAH/PAA bilayers, DNA-loaded gelatin blocks were incubated for 4 h at room temperature or 37 °C. The results of subsequent supernatant analysis are shown in Figure 2.4 and demonstrate that little DNA release occurs at room temperature if any bilayers are present. In fact, compared to the uncoated gelatin blocks, the addition of just one bilayer reduced the quantity of DNA released at room temperature by ~98%. Additional bilayers further reduce the quantity of DNA released at room temperature. If warmed to 37 °C, however, a notable increase (at least ~5-fold) in released DNA occurs for coated samples. Thus, the polyelectrolyte capsule appears to effectively trap, then release active DNA from the gelatin matrices as they are warmed from room temperature to 37 °C. The release was also examined over time as shown in Figure 2.5 by taking samples at 1 h intervals (separate gels were used for each time point). These results showed that the release was not pulsed and that the release would continue beyond the 4 h of the experiment (no plateau value was reached) however, little could be drawn from these time studies to help further elucidate the nature of the release.

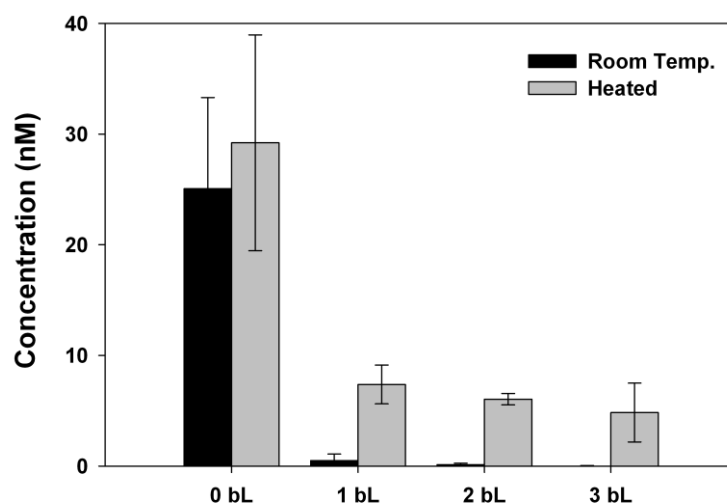


Figure 2.4. Concentration of P14-F DNA released from gelatin-DNA blocks coated with varying numbers of PAH/PAA bilayers (bL) after a 4 h incubation at $\sim 22^{\circ}\text{C}$ (room temperature) and at 37°C (heated). The gelatin concentration is 20 wt%. Taken from reference 1.

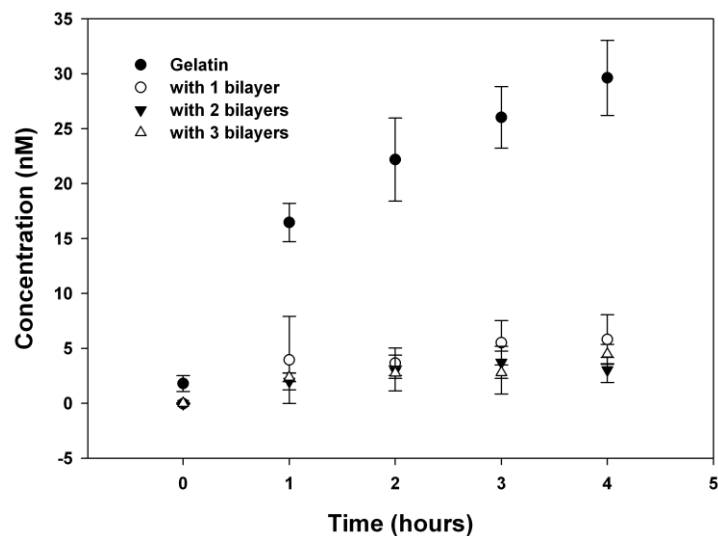


Figure 2.5. Release of DNA from 20 wt% gelatin blocks coated with 1 to 3 bilayers after 1 to 4 hours of incubation at 37°C .

In order to better understand the effects of the oligonucleotide loading in these release studies, the initial solution concentration of DNA (prior to mixing with gelatin) was increased from 2 μM to 10 μM . As shown in Figure 2.6, bare or uncoated gelatin-DNA blocks prepared using the higher concentration of DNA yield an ~ 5 -fold increase in DNA release at 37 $^{\circ}\text{C}$. The gels covered with one bilayer, on the other hand, show only a modest difference in released DNA (~ 1.3 -fold increase) at 37 $^{\circ}\text{C}$ for the two DNA loading conditions. One possible reason for the minimal increase in the latter case may be that the higher concentration of encapsulated DNA influences the subsequent formation of the polyelectrolyte bilayer on the gelatin. A change in bilayer construction and the associated diffusion coefficient through this barrier may explain why DNA release is not enhanced for the blocks prepared using the solution with the higher DNA concentration. Exposing gels with 1 bL to an EDC crosslinking process, similar to the coupling procedure in Section 2.2.6, arrested diffusion at both room temperature and elevated temperature. The lack of DNA release from crosslinked gels implies that their release is affected by a reorganization of the molecules at the interface. Although there are many unknown details of the interface, pinpointing the exact conformation of composition of the bilayer, however, is beyond the scope of the current work.

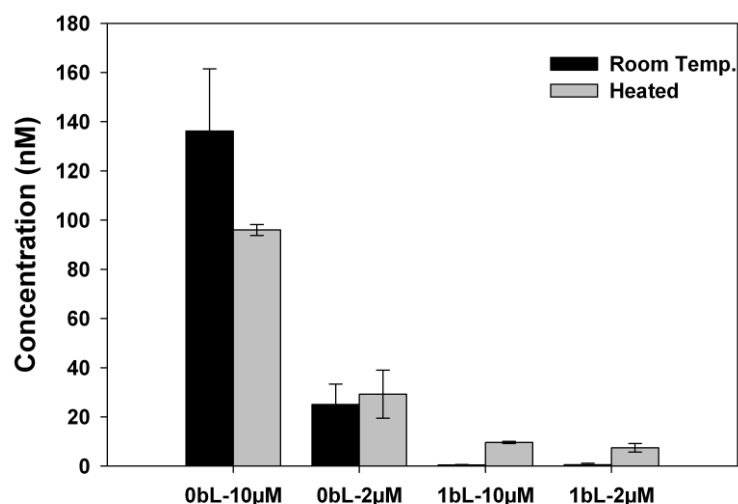


Figure 2.6. Concentration of **P14-F** DNA released from uncoated (0 bL) and coated (1 bL) gelatin-DNA blocks loaded with either 2 μ M or 10 μ M solution of DNA. The gelatin concentration is 20 wt%. Taken from reference 1.

The large variability in the amount of released DNA in Figures 2.4, 2.5, and 2.6 could be due to several factors. Gelatin is known to have wide variability in its physical properties depending on its processing history.⁵ Though care was taken to replicate the same procedure every time, slight changes in handling, such as the rate the gelatin was dispensed into the microwells, may serve as a source of variability in the results. Another significant source of error is the partial or complete lift off or disruption of the LbL barrier during the release of DNA. The release of trapped air bubbles as the gelatin melts at 37 °C is the most likely cause of this disruption. Lift off of the LbL barrier was visually observed in preliminary work on a similar system as a very thin rolled up film floating in the supernatant. This lift off could lead to a jump in the DNA released from unprotected areas in the gelatin. Such jumps in DNA released were only occasionally observed in the

current study (<10% of samples). The experimental setup used in the current release studies, however, do not permit direct observation of the lift off. Since lift off could not be confirmed directly, no data points were excluded from the Figures presented.

2.3.2 Oligonucleotide Gelatin Microspheres

Although gelatin blocks are a convenient model system, GMS have broader applications as injectable therapeutic carriers.⁶ A broad range of variables were explored before the final W/O emulsion technique was settled upon. Low gelatin concentrations (10 wt%) and fast cooling of the emulsion were found to produce mechanically unstable particles with poor edge definition. Mineral oil emulsions led to relatively poor yields while olive oil emulsions had better yields but less spherical particles. Type B bovine gelatin did not appear to take up as much DNA as Type A porcine gelatin. This is most likely because of a weak but negative charge of the Type B gelatin under the infiltration conditions. Lower surfactant concentration led to poor yields but higher surfactant concentrations made little difference. Processing differences also had significant effects. Adding acetone to the emulsion instead of the emulsion to acetone caused a large precipitate to form and few microspheres. Splitting the acetone-emulsion mixture in two and filtering each portion separately helped overcome clogging of the filters. Increase in the total volume of the acetone bath also appear to increase yield. Conditioning the gelatin at 40 °C for 30 min may have reduced internal bubbles in the product GMS. Due to the many variables in this process, the processing approach used in

this work may be further optimized in the future but it has clearly demonstrated the capacity to produce the desired temperature-dependent semipermeable properties and was thus suitable for the purposes of exploring GMS as a controlled release reservoir for DNA.

The size distribution of the GMS population is depicted in Figure 2.7. The chemical composition of the Isoton II solution differs from that of the saline and PBS solutions used in zeta potential and release studies. Thus, while modest swelling or deswelling of the gelatin particles is possible in these different solutions, the data in Figure 2.7 agrees well with visual observations of the GMS. The final volume fractions of GMS in the sample before and after the washing steps were 0.037 v% and 0.007 v%, respectively. Although the GMS are polydisperse in size, they do appear to have a consistent spherical shape in saline solution with negligible autofluorescence prior to DNA infiltration as shown in

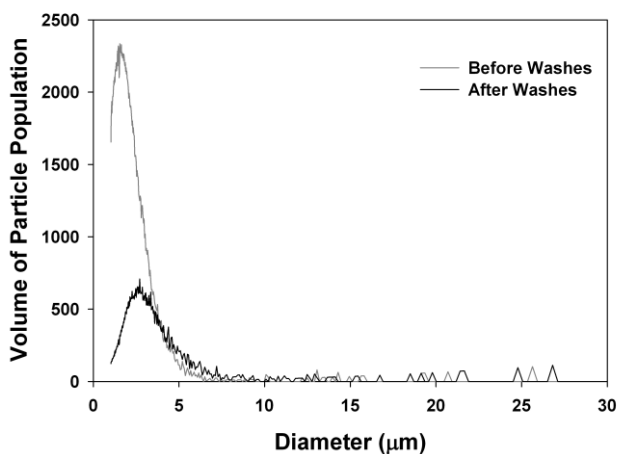


Figure 2.7. Histogram of GMS diameters before and after washing steps taken to precipitate and resuspend GMS. Data was normalized for data bin size. Taken from reference 1.

Figure 2.8(a). Incubation with fluorescently-labeled DNA results in the green fluorescent GMS shown in Figure 2.8(b). The fluorescence also appears to be uniform across the particle indicating successful infiltration of DNA inside the GMS as opposed to exclusive surface adsorption which should yield a fluorescent ring. Following exposure to PAH, the fluorescence of the particles shown in Figure 2.8(c) looks very similar to that of Figure 2.8(b) though the background fluorescence of the solution has diminished in intensity. The particles that were exposed to PAH then PAA also exhibit significant fluorescence with minimal background fluorescence as shown in Figure 2.8(d). These particles, however, acquire a rough surface topography as shown in the higher magnification micrographs in Figure 2.9. The roughness is more prominent than expected from just irregular deposition of the polyelectrolytes. Furthermore, incubation in PAA following incubation in PAH appears to induce the surface roughness without any accompanying change in size. Multiple pH (6.0 to 7.0), polyelectrolyte concentrations (0.1 to 2.0 mg/mL), and ionic strengths (75 mM to 300 mM) of the deposition solution were tried to reduce this roughness but the differences were generally minimal. Crosslinking the GMS with EDC prior to LbL deposition did lead to a smooth surface after a complete bilayer but this also incurs all of the the problems with crosslinking that were discussed in Chapter 1. Since polyelectrolytes reportedly weaken gelatin gels by interfering in the triple helical structure,⁷ the extensive surface roughness following bilayer deposition may stem from an erosion or contraction of the underlying gelatin matrix. Based on these results, the PAA and PAH may not exclusively deposit on the surface but may

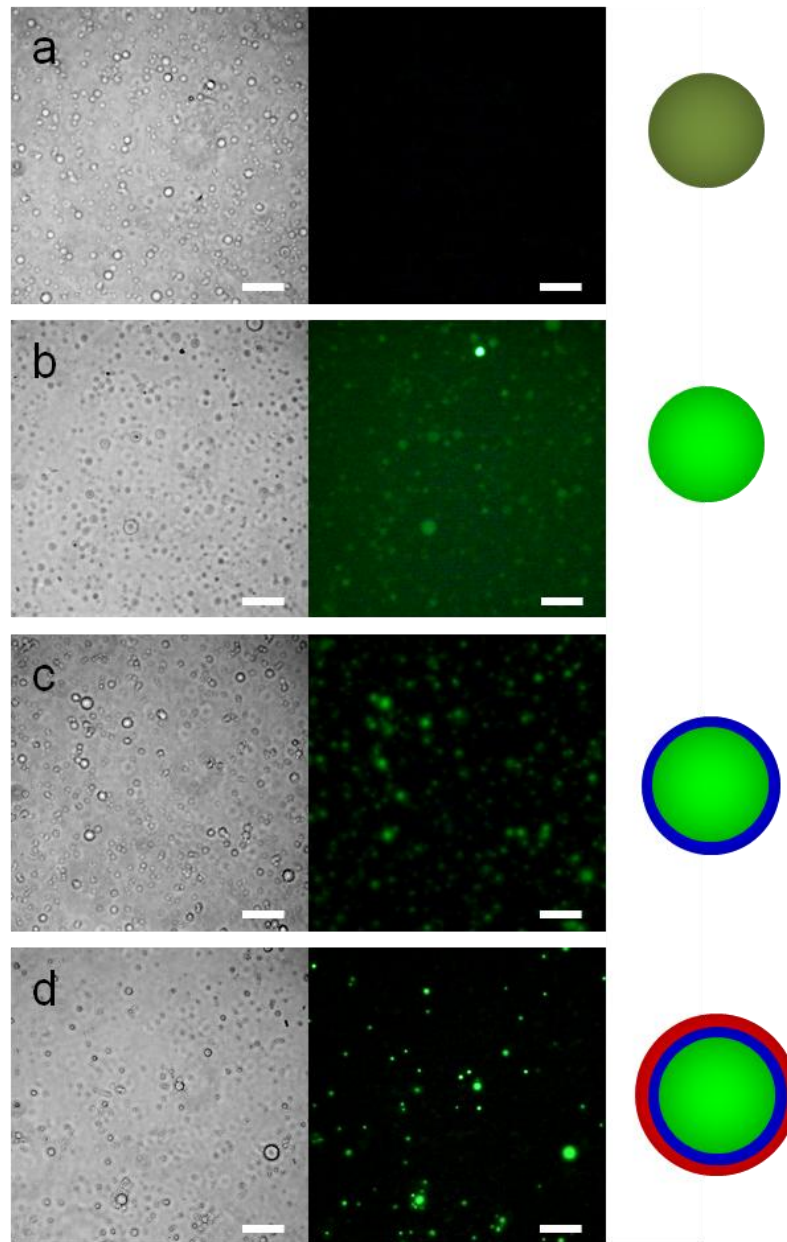


Figure 2.8. Phase contrast (left) and fluorescence (right) micrographs showing GMS suspensions at various processing stages. Following emulsion-based preparation, GMS were (a) resuspended in saline; (b) infiltrated with fluorescently-labeled DNA, **P14-F**; (c) exposed to PAH polycation solution, washed, and then (d) exposed to PAA polyanion solution to form a complete bilayer. The scale bar is 50 μm . Adapted from reference 1.

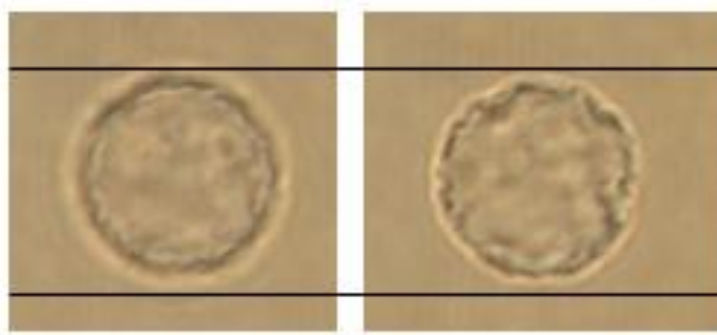


Figure 2.9. Phase contrast micrographs of an individual GMS that was initially incubated in the PAH solution, washed, and then resuspended in the PAA solution. The left micrograph was taken immediately after resuspension in the PAA solution and the right micrograph was taken 10 min later. Taken from reference 1.

penetrate to a limited degree into the GMS, however, deep penetration into the GMS by these long polyelectrolyte chains is probably sterically hindered by the gelatin matrix itself.

Figure 2.10 shows the amount of DNA released following key stages of GMS preparation. Bare GMS with no infiltrated DNA (denoted **G**) do not result in fluorescence-based detection events while those loaded with dye-labeled **P14-F** DNA, (denoted **D**) show significant release of active DNA. In the absence of any bilayers, this DNA release is relatively independent of temperature conditions. Once incubated with PAH (denoted **H**), the DNA-loaded GMS exhibit a much stronger temperature dependence with minimal release at room temperature and significant release at elevated temperature. Compared to the uncoated (**D**) heated samples, the slight reduction in hybridizing DNA in the PAH-coated GMS (**H**) may be due to some DNA complexation with positively-charged PAH as the DNA attempts to escape from the gelatine matrix and encounters the polyelectrolyte layer. Interestingly, the samples exposed to PAH and PAA (denoted **H+A**) to form

a bilayer show greater DNA release both at room and elevated temperatures than the samples exposed to just PAH (**H**). This increase in DNA release may be due to the oppositely-charged polyelectrolytes complexing with each other in the bilayer and thereby minimizing subsequent complexation with mobile DNA strands as they diffuse through the bilayer when the gelatin matrix melts. The diffusion of DNA at 37 °C is most likely controlled by the bilayer since the time it would take for a DNA a chain to diffuse through the gelatin would be on the order of seconds (for a viscosity of gelatin of 200 cP and a DNA hydrodynamic radius of 4 nm). Notably, control samples infiltrated with noncomplementary **NC-F** and coated with a bilayer indicate that nonspecific association between released DNA and **A20**-functionalized polystyrene particles (used in our flow cytometry-based detection platform) are negligible. The concentration of hybridizing **P14-F** DNA that is ultimately released from these bilayer-coated samples does exceed the minimum 100 nM DNA we found necessary for effective competitive redispersion of a DNA-linked colloidal satellite assemblies.⁸ In fact, since the concentration of the GMS was measured to be 0.007 v%, the estimated concentration of encapsulated DNA in the fully processed GMS (DNA-loaded GMS with one bilayer) was ~140 μM, much higher than the estimated 2 μM DNA in the gelatin blocks. Significant sequestering of the DNA into the GMS must have occurred because the DNA infiltration solution was only 10 μM. The low pH infiltration conditions may help promote effective DNA loading into these particles. In addition, the high surface area to volume ratio may facilitate both infiltration and release, particularly since the GMS appear to completely melt after 4 h of heating.

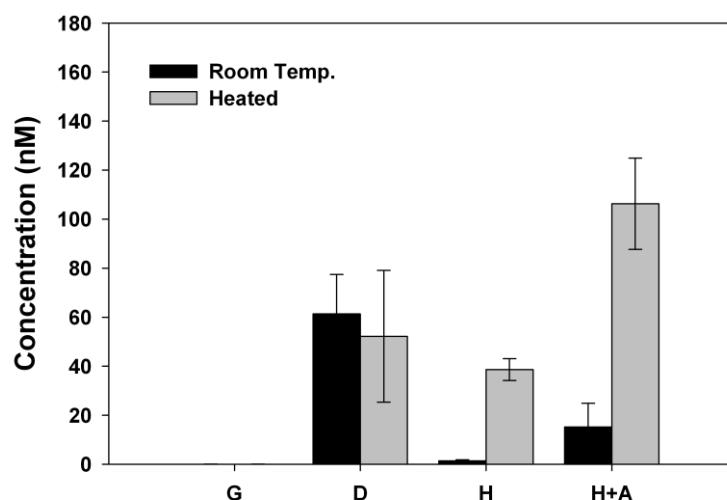


Figure 2.10. Concentration of **P14-F** DNA released from GMS at the following four sequential processing stages: GMS resuspended in saline solution (G); infiltrated with DNA (D); exposed to PAH polycation (H); and finally exposed to PAA polyanion to form a complete bilayer (H+A). Samples were incubated at either ~22 °C (room temperature) or 37 °C (heated) for 4 h. Taken from reference 1.

There appears to be a concern in literature that uncrosslinked GMS are not stable. To investigate this concern, GMS were incubated in water for up to 2 months and then infiltrated with **P14-F** and coated with one bilayer. The results clearly show that GMS survive such incubation conditions at room temperature as shown in Figure 2.11. Coated GMS also remain intact at 37 °C for at least 12 h. These two observations strongly imply that uncrosslinked GMS are stable enough warrant further investigation.

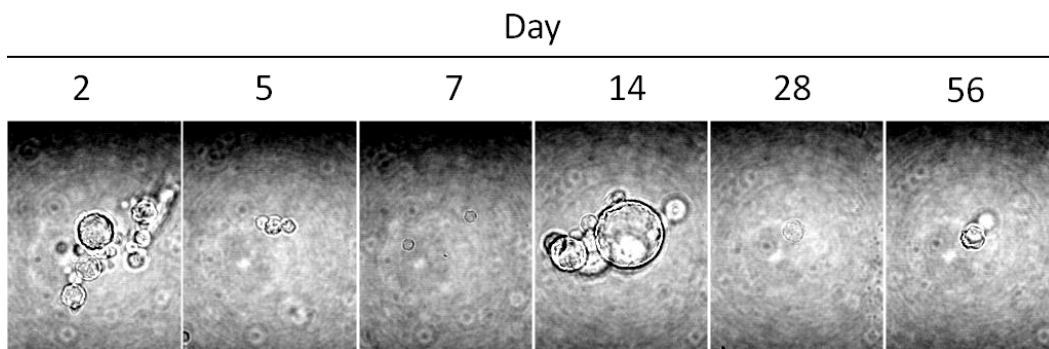


Figure 2.11. Impact of incubation at room temperature on GMS. Microspheres are present in all micrographs but are not clearly visible in the 7 and 28 day samples.

2.4 Conclusions

In this chapter we demonstrated the successful preparation and oligonucleotide loading of uncrosslinked gelatin matrices. Adsorption of PAH and PAA on either gelatin blocks or GMS was first shown to effectively hinder DNA release at room temperature, then permit release of active DNA once warmed to 37 °C. This on/off release character occurs in a temperature range relevant for medical applications such as gene therapy or as a potential encapsulant for a release agent designed to disperse DNA-linked colloid assemblies while simultaneously allowing for storage under room temperature conditions. Furthermore, the order of magnitude increase in the effective concentration of encapsulated DNA in the GMS (compared to the initial infiltration solution) supports the use of gelatin as a cost-effective vehicle for achieving high oligonucleotide loading without compromising its subsequent hybridization activity following release.

2.5 References

1. J. O. Hardin and V. T. Milam, *Soft Matter*, 2011, **7**, 2674-2681.
2. C. K. Tison and V. T. Milam, *Langmuir*, 2007, **23**, 9728-9736.
3. W. M. Saltzman, M. L. Radomsky, K. J. Whaley and R. A. Cone, *Biophys. J.*, 1994, **66**, 508-515.
4. C. Rivetti, C. Walker and C. Bustamante, *J. Mol. Biol.*, 1998, **280**, 41-59.
5. A. G. Ward and A. Courts, *The Science and technology of gelatin*, Academic Press, London ; New York, 1977.
6. T. Yoshioka, M. Hashida, S. Muranishi and H. Sezaki, *Int. J. Pharm.*, 1981, **8**, 131-141.
7. J. R. Gillmor, R. W. Connelly, R. H. Colby and J. S. Tan, *J. Polym. Sci., Part B: Polym. Phys.*, 1999, **37**, 2287-2295.
8. C. K. Tison and V. T. Milam, *Soft Matter*, 2010, **6**, 4446-4453.

CHAPTER 3

INVESTIGATING DNA HYBRIDIZATION AT SURFACES

3.1 Overview

In order to better utilize the oligonucleotide release system described in Chapter 2, we investigated DNA hybridization at surfaces. This chapter covers flow cytometry experiments used to observe the kinetics and thermodynamics of primary and secondary hybridization on colloidal surfaces. In addition to the typical flow cytometric measurements which are made after washing samples, in this work we sampled the reaction volume directly to remove the possibility of duplex dissociation during washing steps. Hybridization involving perfectly matched target DNA strands as well as strands with center mismatches was examined. The primary hybridization results indicate that hybridization on the surfaces of carboxylated polystyrene microspheres is less favorable than predicted by models of solution hybridization. The kinetics of competitive hybridization also deviate from expectations based on the calculated solution thermodynamics but are consistent with the kinetic effects from toehold regions or differences in branch migration. The post washing and *in situ* flow cytometry results were similar in trends although more displacement was observed in the post washing experiments thus implying that there is some dissociation occurring during washing steps for the sequences used in this work.

3.2 Materials and Methods

3.2.1 DNA Sequences

DNA sequences from Integrated DNA Technologies (Coralville, IA), shown in Table 3.1, were selected based on previous work to minimize self-complementarity.^{1, 2} DNA was stored at 100 μ M in Tris/EDTA buffer at pH 7.4 (TE 7.4) in the unlabeled and aminated cases and at pH 8.0 (TE 8.0) for fluorescently labeled strands. Immobilization on polystyrene microspheres was carried out based on a previously described procedure.³ Briefly, aminated DNA was coupled to 1.1 μ m or 5 μ m carboxylated polystyrene microspheres, from Bangs Laboratories (Fishers, IN) and Molecular Probes (Eugene, OR) respectively, in a solution of 5.3 μ M aminated **A20** probe, 5.3 mM Tris, 0.53 mM EDTA, 86 mM EDC (1-ethyl-3-(3-dimethylaminopropyl) carbodiimide), 23 mM MES (2-(*N*-morpholino)ethanesulfonic acid) and 0.023 v% Proclin. DNA-functionalized microspheres were then washed three times in PBS-Tween (PBS and 0.2 v% Tween 20) to remove nonspecifically adsorbed strands and stored in the same solution (1 wt% particles).

3.2.2 Post washing Hybridization Experiments

For measurements involving sample washes as part of preparation for flow cytometry, both primary hybridization³ and secondary hybridization¹ were carried out as described previously. Briefly, 100 μ L of 0.025 v% **A20**-functionalized 5 μ m microspheres were mixed with 100 μ L of a 10 μ M solution of primary target DNA in TE 7.4 or TE 8.0 and

Table 3.1. List of the function and nomenclature for all DNA sequences employed. The theoretical change in Gibb's free energy of hybridization, ΔG_{hyb} , between **A20** probes and various target strands in 150 mM NaCl were determined using Zuker's M-fold server⁴. Mismatches are indicated in bold, underlined text.

Function	Sequence	ΔG_{hyb} (kcal/mol)
Immobilized probe	A20 = 5'-TTT TTT GGA TTG CGG CTG AT-3'	NA
Perfectly-matched primary targets	P7 = 3'-CC GAC TA-5'	-8.0
	P9 = 3'-C GCC GAC TA-5'	-13.0
	P11 = 3'-AAC GCC GAC TA-5'	-15.3
	P13 = 3'-CT AAC GCC GAC TA-5'	-17.9
	P15 = 3'-A CCT AAC GCC GAC TA-5'	-20.9
Mismatch primary targets	M11 = 3'-AAC <u>GCG</u> GAC TA-5'	-13.3
	M13 = 3'-CT AAC <u>GGC</u> GAC TA-5'	-13.9
	M15 = 3'-A CCT AAC <u>CCC</u> GAC TA-5'	-14.2
Perfectly-matched secondary targets	P15 = 3'-A CCT AAC GCC GAC TA-5'	-20.9
Noncomplementary targets	NC = 3'-GGA TTG CGG CTG AT-5'	-4.4

incubated overnight. Following the incubation, the samples were washed three times with 100 μ L of PBS-Tween and stored, as needed, in the same solution until preparation for secondary hybridization. Unlabeled **P15** secondary target was added to a suspension of 5 μ m polystyrene microspheres (0.06 v%) with fluorescently labeled primary duplexes to bring the concentrations to 10 nM, 100 nM, 1,000 nM and 10,000 nM **P15** and allowed to incubate at room temperature. An aliquot of the suspension was taken at 1, 7, 15, and

30 min, and 1, 8, and 24 h. The sample was quickly centrifuged and resuspended in PBS/Tween three times and stored at 4 °C. The primary targets used to form the fluorescently labeled duplexes on the surface of the particles were the perfectly matched **P11-F**, **P13-F**, and **P15-F** and strands containing center mismatches, **M11-F**, **M13-F** and **M15-F**. The average fluorescence of the particle population was measured using a BD-LSR II flow cytometer (Becton, Dickinson and Company, San Jose, CA). The fluorescent values were converted to a surface density value of fluorescently-labeled primary duplexes using MESF standards from Bangs Laboratories (Fishers, IN).

3.2.3 *In situ* Hybridization Experiments

In contrast to the post washing hybridization experiments described in the above section, the *in situ* hybridization studies did not involve washing following target incubation. *In situ* primary hybridization experiments were carried out by adding 2.5 µL of 1.0 v% **A20**-labeled 1.1 µm microspheres to 1 mL of a 1 µM solution of primary targets (**M11-F**, **M13-F**, **M15-F** and **P15-F**), vortexing and immediately sampling the suspension with the flow cytometer. Once a reliable signal was attained (approximately 30 s from vortexing), three measurements (10,000 particles each) were taken. Subsequent measurements were then taken every minute for 30 min. Each measurement took less than 10 s. *In situ* secondary hybridization experiments were performed by resuspending **M11-F:A20**-labeled microspheres (which had been washed three times after primary hybridization) in PBS/tween solutions of 0, 10, 100, and 1,000 nM of **P15** secondary target and then taking flow cytometry measurements as described for the *in*

3.2.4 Analysis of Competitive Displacement Activity

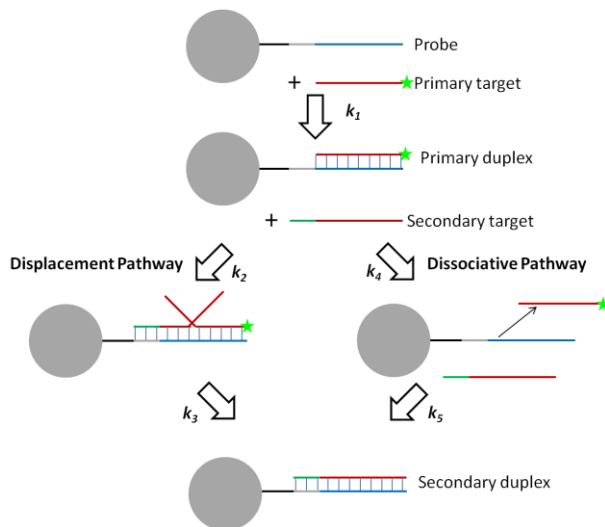


Figure 3.1. Schematic diagram of the hybridization reactions and pathways examined in this work. Although each particle possess many immobilized probe strands, for clarity only one immobilized probe and relevant target species are shown here. The green segment denotes bases of the secondary target that can bind to the gray single-stranded segment or toehold region, on the probe. The rate constant for primary hybridization between probes and primary targets is k_1 . Following addition of secondary targets, two pathways for secondary duplex formation are indicated. In the displacement pathway, k_2 is the rate constant for formation of a complex between the probe and both primary and secondary targets. Following the formation of this complex, the base pairs between the primary target and the probe are replaced by base pairs with the secondary target until the primary target is fully displaced with a rate constant of k_3 . In the dissociative pathway, k_4 is the rate constant for the dissociation of the primary duplex and k_5 is the rate constant for duplex formation between the now unoccupied probe and secondary target. Due to the experimental conditions involving weaker primary targets and stronger secondary targets in excess concentration, all reaction presented in both pathways are assumed to be biased in the forward directions as indicated by the arrows. Similar to prior approaches^{1, 5, 6}, the first step in each pathways is assumed to be the rate limiting step (i.e. $k_2 \ll k_3$ and $k_4 \ll k_5$). Given this assumption, k_2 is denoted as the displacement rate constant and k_4 is denoted as the dissociation rate constant in the text.

situ primary hybridization experiments.

The surface density of fluorescently-labeled primary duplexes on the microspheres, σ , was measured under various conditions over time and normalized by the initial duplex density, σ_0 , to yield the fraction of primary duplexes, f_{pd} , as shown in equation 3.1. The fraction of primary targets released from these duplexes in the presence of complementary secondary targets, f_r , or noncomplementary secondary targets, $f_{r,NC}$, are calculated using equation 3.2. Importantly, both the dissociative and displacement pathways shown in Figure 3.1 potentially contribute to f_r , but only the dissociative pathway contributes to $f_{r,NC}$. Thus to delineate the effect of the displacement alone, the fraction of primary target displaced, f_d , is determined using equation 3.3 which effectively subtracts out dissociative effects. To calculate f_d , $f_{r,nc}$ was first calculated from three runs and then this value was used in equation 3.3 to calculate f_d for each of the three runs in the presence of a complementary competitive DNA. These three calculated f_d were then used to generate the mean and standard deviation of f_d . Each of the three runs used in the above calculations were from separately coupled population of **A20**-functionalized microspheres. Further discussion of this treatment can be found in Appendix A.3.

$$f_{pd} = \sigma/\sigma_0 \quad (3.1)$$

$$f_r = 1 - f_{pd} \quad (3.2)$$

$$f_d = (f_r - f_{r,nc})/(1 - f_{r,nc}) \quad (3.3)$$

Since the *in situ* competitive hybridization studies involving weak partner strands, which may dissociate during even mild processing, do not permit the measurement of a true initial data point, σ_0 values for the *in situ* studies were determined via linear extrapolation through the first three time points. The average value and error bars from at least three runs are reported for each concentration of secondary target. For the *in situ* measurements, the fraction of primary target released due to thermal dissociation was determined in the absence of any secondary target.

The rate constant for primary hybridization, k_1 , was determined by fitting the time dependent primary duplex density data to equation 3.4. Similarly, the rate constant for displacement, k_2 , was determined by fitting the time dependent fraction of primary target displaced data to equation 3.5. This analytical approach is consistent with previous reports^{1, 5-7}. The fitting parameters, σ_∞ , k_1 , f_∞ and k_2 , were determined using Sigma Plot (SysStat Software Inc., San Jose CA). Rate constants with a p-value above 0.05 are not reported.

$$\sigma = \sigma_\infty(1 - \exp(-k_1 t)) \quad (3.4)$$

$$f_d = f_\infty(1 - \exp(-k_2 t)) \quad (3.5)$$

3.3 Results and Discussion

3.3.1 *In situ* Primary Kinetics

To investigate *in situ* primary duplex formation between immobilized probes and various targets, suspensions of A20-functionalized microspheres were interrogated with

flow cytometry immediately following introduction to **NC-F**, **M11-F**, **M13-F**, **M15-F** or **P15-F** primary targets at 1 μM concentrations. Importantly, these *in situ* measurements were made in the absence of any conventional wash steps (to remove unassociated target). As shown in Figure 3.2, all five target cases reached a plateau value in duplex density within 30 min following introduction to target and thus indicating that equilibrium was reached within the experimental timeframe. Incubation with the noncomplementary **NC-F** strand showed a low fluorescence values at all time points. This important control indicates that both adsorption to the microsphere surface as well as nonspecific association between noncomplementary targets and immobilized probes was minimal, even in the absence of washing steps. The kinetics of primary hybridization were further evaluated by fitting the data to equation 3.4 as indicated by the dotted lines in Figure 3.2. As shown in Table 3.2, the values for the primary hybridization rate constants, k_I , were nearly identical for all of the complementary and nearly complementary target strands. This lack of sequence dependence for k_I is consistent with prior reports⁸⁻¹⁰. If we assume the classic two state model discussed in Chapter 1, in which target concentration, $[T]$, is effectively constant and dissociation rate of primary duplexes is negligible, then $k_I = k_a[T] + k_r \sim k_a[T]$ where k_a is the association rate constant for primary duplex formation and k_r is the rate constant for the reverse reaction. This analysis yields k_a values of $\sim 2 \times 10^6 \text{ M}^{-1} \text{ s}^{-1}$ which is about two orders of magnitude faster than values reported between soluble targets and probes immobilized on a flat surface¹¹ but similar to k_a values reported for analogous hybridization experiments on high curvature surfaces¹² as well as oligonucleotide solutions^{9, 13, 14}. The lower

plateau values of mismatch strands implies that the k_r is at least of the same order of magnitude as $k_d[T]$, however the expected sequence dependence associated with such a large k_r is not observed in the k_f values in Table 2. This would further support the assertion that hybridization at surfaces is more complicated than in solution.

Table 3.2. Observed rate of primary duplex formation, k_f , determined from *in situ* experiments between **A20**-functionalized microspheres and the primary targets listed.

Primary Target	$k_f(s^{-1})$
M11-F	2.3
M13-F	2.6
M15-F	1.5
P15-F	2.0

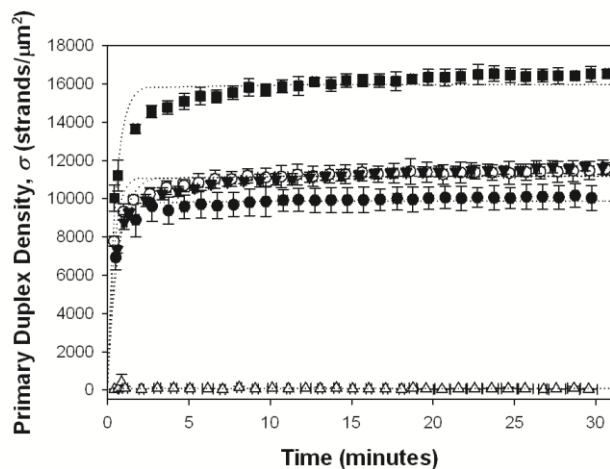


Figure 3.2. *In situ* measurements of primary duplex formation between **A20**-functionalized microspheres and fluorescently-labeled **P15-F** (closed squares), **M15-F** (closed triangles), **M13-F** (open circles), **M11-F** (closed circles) or **NC-F** (open triangles). Dotted lines represent fits to equation 3.4. Error bars for both surface density and time values are shown.

In addition to providing insight into hybridization kinetics at colloidal surfaces, we can also qualitatively infer some thermodynamic effects on primary duplex formation from these results. We are limited to relative comparisons of probe occupation since experimental determination of the true single-stranded density is complicated by (1) possible undesired coupling between carboxyl group on a fluoroscein label and the amine group on the 5' end of the probes (should we try to fluorescently label the probe strands as we have labeled the target strands) and (2) reports of adsorption of DNA to the micropipette tips (should we try to measure the concentration of remaining probe DNA after coupling)¹⁵. The near equivalence of the all three mismatch strands in Figure 3.2 is unexpected even with relatively small energetic differences tabulated in Table 3.1. As a reference, a 0.5 kcal/mol difference in ΔG value should theoretically correlate to a 2.3 fold increase in the equilibrium concentration of unhybridized probe (based on simple manipulation of the equilibrium constant). Assuming that the plateau values reached in each target case is indicative of equilibrium, the three mismatch strands appear to have effectively identical ΔG of hybridization according to our results and this ΔG is much higher (less favorable) than predicted by solution theory (otherwise they would hybridize effectively to the same degree as the perfectly matched target). The difference between the solution based ΔG_{hyb} (which are sequence dependent) and the observed energetics of the mismatches (which are sequence independent), implies a sequence dependent effect of immobilizing the probe on the microsphere surface that is not accounted for by ΔG_{hyb} in solution (which includes base interactions, phosphate back bone repulsion between strands, entropic loss on hybridization and counter ions). Electrostatic repulsion between

the particle surface and the soluble DNA is consistent in trend (longer strands incur greater repulsion and greater change in ΔG) and relatively small in magnitude (thus **P15-F** still hybridizes to a greater degree than **M11-F**) but would require considerable further investigation of the ionic strength and base length effects to confirm. Entropic differences due to immobilization are also strand length dependent and further discussed in Appendix A.1.

3.3.2 Investigation of Electrostatics of Hybridization

In order to investigate the electrostatic effects on DNA hybridization, primary hybridization was performed in multiple primary hybridization solutions of differing salt concentrations. The hybridization solutions were sampled by flow cytometry following overnight incubation. The effect of salt concentration on the fluorescent molecule was accounted for by preparing the MESF standards in matching salt solutions. Salt induced aggregation was also a concern as it may bias the singlet population toward strongly charged microspheres (those with more duplexes and/or probe functionalization). Such a bias would lead to an increase in the average fluorescence of the singlet population that is not representative of an increase in the fluorescence of the whole particle population. Aggregation was minimized by incubating the **A20**-functionalized microspheres in 1 M NaCl then separating off any aggregates using centrifugation. This processing step resulted in significantly more stable particles as evidenced by a higher and more consistent (across salt concentration) percentage of singlets. The low density of the

microspheres (~1.05 g/cc) limited the maximum salt concentration because higher salt concentrations increase the density of the fluid.

As shown in Figure 3.3, higher salt concentrations led to higher surface densities of primary duplexes. In general, longer perfect targets have higher surface densities than shorter ones and mismatches have lower surface densities than their analogous perfect strands. Microspheres incubated with noncomplementary DNA exhibited minimal fluorescence, indicating minimal nonspecific adsorption. However, the lack of a plateau value in primary duplex density in Figure 3.3 again implies that hybridization may not be complete and further supports the idea that duplex formation on the surface of microspheres is less favorable than in solution.

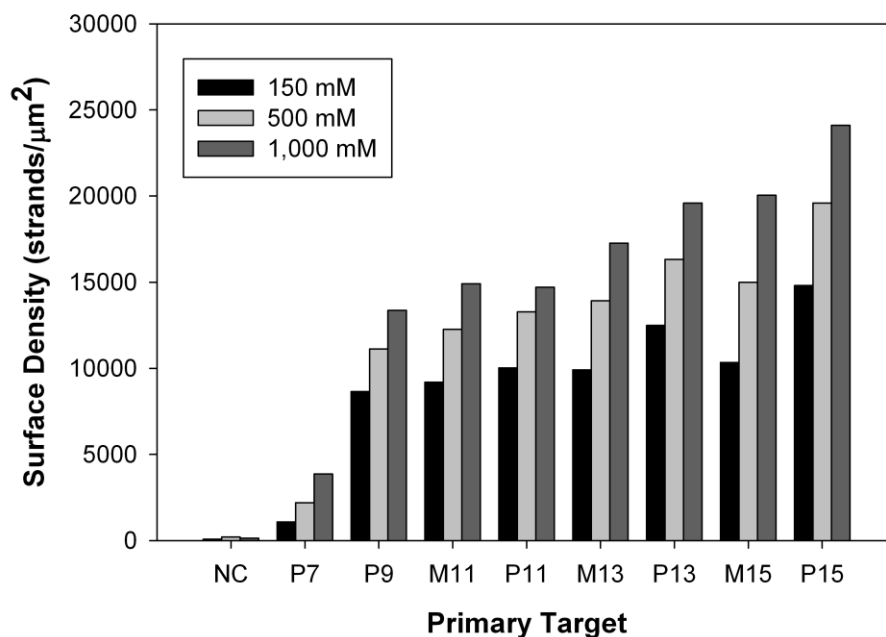


Figure 3.3. Surface density of fluorescently labeled primary targets on the surface of A20-functionalize microspheres at 150, 500, and 1,000 mM NaCl.

In order to better understand the cause of inhibited hybridization activity on surfaces, the energetics of hybridization were investigated. The region around the microspheres occupied by the DNA strands, extending ~6.8 nm (0.34 nm per base progression of a duplex X 20 bases in **A20**) from the surface, was assumed to be the system of interest. The bulk solution then behaves similar to a temperature, pressure, and target concentration reservoir. It is then assumed that the reaction is at equilibrium following incubation overnight in order to derive an effective equilibrium constant from the hybridization data set based on the effective local concentrations of the probe, target and duplexes in a shell surrounding each microsphere. The target concentration is at least two orders of magnitude in excess and is, therefore, effectively constant at 1 μM . The localized duplex concentration can be calculated from the measured surface density assuming a fully extended duplex as the height shell and that the highest surface density measured represents nearly full occupancy of the probe strands, (assumed probe density is 25,000 strands/ μm^2 , slightly above the highest value measured). Considering the increase in surface duplex density on increasing the salt concentration from 500 mM to 1,000 mM NaCl, it is quite possible that the probe density is actually significantly larger than 25,000 strands/ μm^2 . While any underestimation of the probe density will yield greater deviation from solution hybridization kinetics than is presented below, the assumptions made provide at least qualitative indication of any differences between surface and solution hybridization activity.

The values calculated for the observed ΔG_{obs} were significantly higher than those calculated from solution hybridization theory, ΔG_{hyb} . Hybridization of **A20** with every

primary target but **NC** and **B7** appeared to be very similar energetically. This reduced differentiation was also seen between salt concentrations. In the solution model, the impact of salt concentration on ΔG_{hyb} are constant with respect to sequence. One possible cause of this salt insensitivity is the counterion cloud around the microsphere. If this cloud envelopes the DNA duplex, then increasing the salt concentration in the bulk solution will have a smaller change on the counterion concentration near the surface of the microsphere. The width of such a counterion cloud is approximated by the Debye length (less than 1 nm in all cases in this work) for flat surfaces, which renders this explanation less likely. In an attempt to separate out the various contributions to this deviation, the change in ΔG between the observed and calculated solution values was plotted in Figure 3.4.

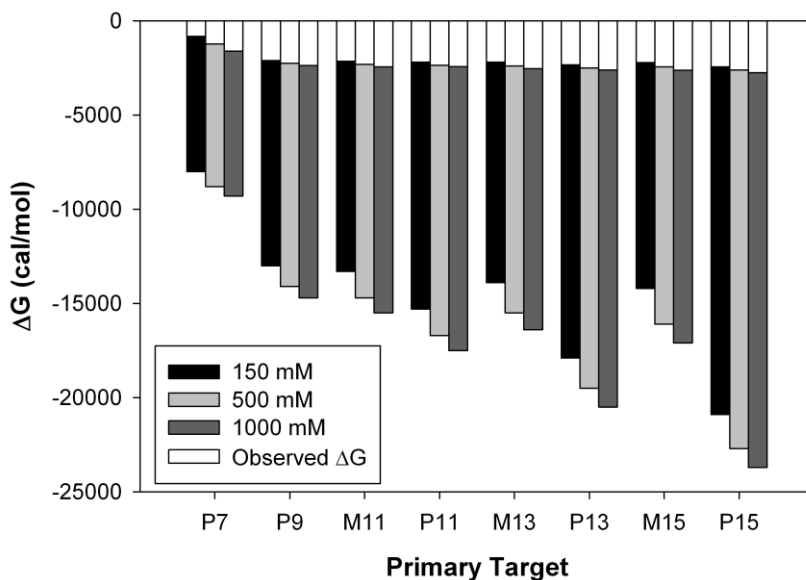


Figure 3.4. Comparison between the calculated solution-based and experimentally observed (white bars) ΔG values for hybridization for different primary targets and at various salt concentrations.

There are two key observations, increases in base length yield larger deviations from theoretical solution behavior and mismatch strands follow a different trajectory than perfectly matched primary targets as shown in Figure 3.5. The increase in deviation with base length could be due to steric effects such as penetration into a DNA brush layer or electrostatic effects such as the repulsion of the negatively charged target DNA by the negatively charge microsphere. However, purely length dependent explanations do not account for the different between the perfectly match and mismatched results. The deviation between the perfect matched and mismatch trajectories may be more a consequence of surface density than mismatches directly as perfectly matched targets form more duplexes on the surface and therefore lead to greater electrostatic repulsion to new strands. The increased deviation with salt concentration contradicts expectations if electrostatic interactions between the probe functionalized surface and the targets were the dominant cause of this deviation. The trend in $\Delta\Delta G$, defined in equation 3.6, follows the same trend as the observed duplex density as well as the ΔG_{hyb} for a given salt concentration.

$$\Delta\Delta G = \Delta G_{obs} - \Delta G_{hyb} \quad (3.6)$$

3.3.3 Secondary Post Washing Hybridization Experiments

We next examined the effect of primary target base length and mismatch inclusion on competitive displacement kinetics by perfectly-matched **P15** secondary

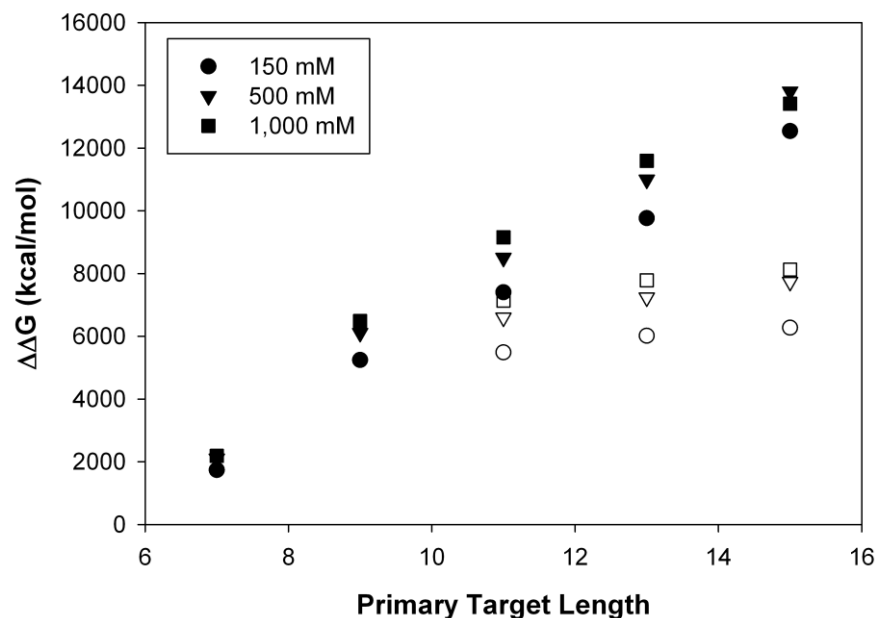


Figure 3.5. The difference between observed and calculated energetics as a function of number of bases in primary target. The perfectly matched targets are represented with closed symbols and the mismatched targets are represented with open symbols.

targets. In order to directly compare results with our previous system¹, 5 μm microspheres were employed and suspensions were washed following various incubation times with secondary targets. After washing, flow cytometry was used to quantify the density of fluorescently-labeled primary duplexes remaining on the microspheres. To facilitate comparison of displacement between different primary duplex systems with various surface density values these surface densities were converted to fraction of primary target displaced and analyzed as described in the previous section. The fractions displaced and fits to equation 3.5 can be seen in Figure 3.6. The resulting displacement rate constants, k_2 , that pass the p-test are listed in Table 3.3 and plotted in Figure 3.7. While considerably lower than primary hybridization rate constants shown in Table 3.2,

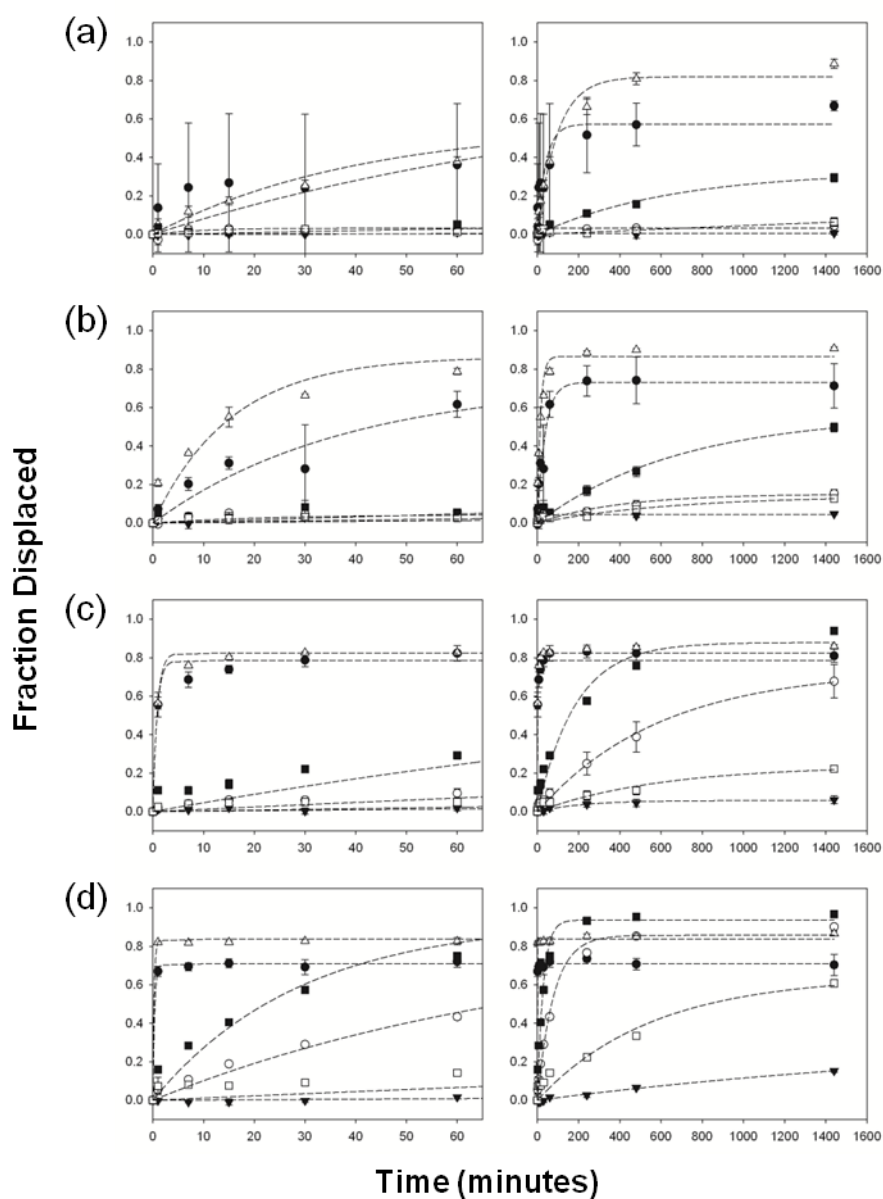


Figure 3.6. Fraction of various primary targets displaced by (a) 10 nM, (b) 100 nM, (c) 1,000 nM, and (d) 10,000 nM **P15** secondary target strand for the first hour (left) and first day (right) following washing steps. The primary targets serving as the original hybridization partner to **A20**-functionalized microspheres are the perfectly-matched **P11** (solid circles), **P13** (open circles), and **P15** (solid triangles) and the center mismatched **M11** (open triangles), **M13** (solid squares), and **M15** (open squares). Dashed lines represent curve fits for each data set to equation 3.5.

Table 3.3. Measured displacement rates, k_2 , for the primary targets incubated in different concentration of competitive DNA, **P15**. The displacement rates from *in situ* experiments are shown for **M11-F** (*in situ*). Only values from fits passing the p-test are shown.

Concentration of P15 Secondary Target (<i>in situ</i>)	$k_2(\text{s}^{-1})$ for Primary Targets Listed					
	M11-F	M11-F	P11-F	M13-F	P13-F	M15-F
0.01 μM	5.88E-04	1.74E-04	—	2.61E-05	—	—
0.1 μM	1.05E-03	1.09E-03	4.45E-04	2.42E-05	—	—
1.0 μM	3.03E-03	1.92E-02	2.04E-02	9.01E-05	2.79E-05	—
10.0 μM	—	6.55E-02	4.80E-02	5.74E-04	2.11E-04	3.01E-05

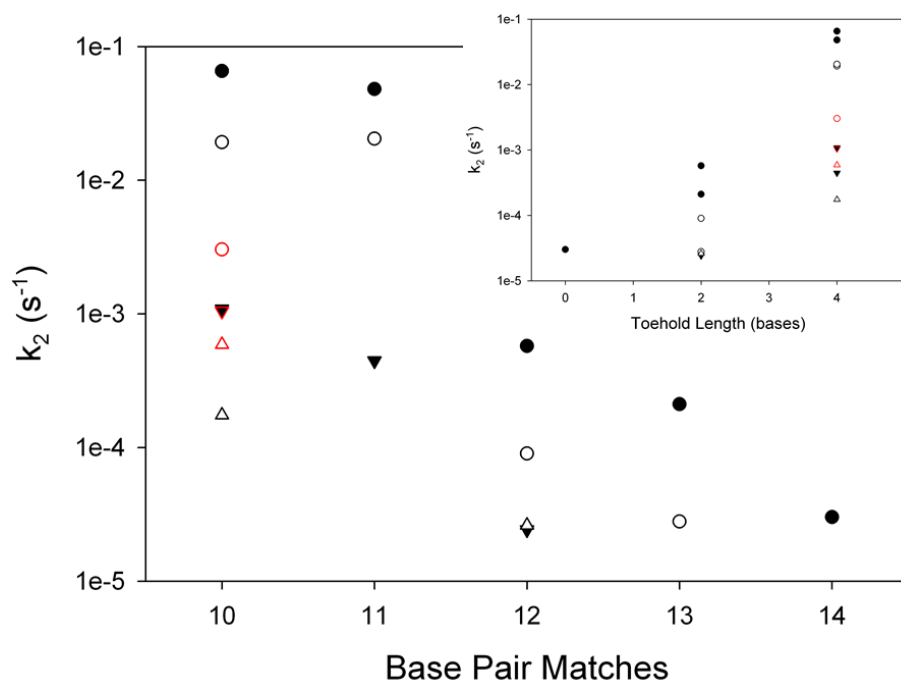


Figure 3.7. Observed displacement rates as a function of total number of base-pair matches between **A20** probes and various center-mismatched and perfectly-matched primary targets at concentrations of 10 nM (open triangles), 100 nM (solid triangles), 1,000 nM (open circles) and 10,000 nM (solid circles) secondary target, **P15**. Red symbols mark values from *in situ* hybridization experiments with secondary target. Black symbols are used for values determined from the displacement studies involving washing steps prior to measurements.

these k_2 values are comparable to the rate constants reported for a related ¹ and unrelated ⁶ DNA-functionalized colloidal systems involving the exchange of one partner for a stronger partner strand. Under comparable temperature and secondary target concentrations, however, the rate constants for displacement in the current work are actually about 2 orders of magnitude higher than rates reported for oligonucleotide solutions by Reynaldo and coworkers for identical primary and secondary targets ⁵. Though hybridization events are typically faster in oligonucleotide solutions, the slower reported displacement⁵ likely stems from the lack of an affinity difference between the original and secondary partner strands. Reynaldo and coworkers also reported a linear dependence of the rate constant on target concentration. Although this work does observe an increase in displacement rate with target concentration it is not linear and neither are the results from our previous work on a similar system ¹. Such a deviation from theory and solution studies implies another significant difference between solution-based and immobilized studies of DNA hybridization. Aside from general comparisons to prior work, we can also examine common trends within the family of related sequences studied here. Overall, for a given secondary target concentration, the largest differences in displacement rates occurred with changes in base length (e.g. **M11-F** vs. **M15-F** or **P11-F** vs. **P13-F**). Smaller differences in displacement rate occurred from one base changes in sequence composition through mismatch inclusion (e.g. **P11-F** vs. **M11-F** or **P13-F** vs. **M13-F**). Figure 3.7 shows that displacement rate generally falls with an increasing number of primary base matches. It is important to point out, however, that this chart plots activity for both mismatched and perfectly-matched targets. In fact, based

on ΔG_{hyb} values shown in Table 3.1, one might expect displacement rates for all the mismatched targets to exceed those of any perfectly-matched targets. This lack of correlation between ΔG_{hyb} values and displacement rates suggests that solution-based thermodynamics does not completely account for the observed behavior for immobilized oligonucleotides and we should look into alternative explanations such as toehold regions where secondary duplexes are likely to nucleate.

As described in Figure 3.1, toehold regions or single-stranded segments in the original duplex that are complementary to secondary target exist in every case except for the **M15-F** and **P15-F** primary targets. In solution studies involving primary duplexes of 7 or fewer base pairs, Zhang and Winfree reported a 10^n -fold increase in displacement rates for secondary target capable of forming toeholds on n bases long¹⁵. Although the number of base pairs in the primary duplex, m , is greater than 7 in the current work they may be more energetically similar due to immobilization effects as discussed earlier. This model predicts an ~ 100 -fold difference in displacement rate for every two base length extension of the toehold region (e.g. **P13-F** vs. **P11-F** or **M13-F** vs. **M11-F**). Displacement rates from our previous data¹ as well as current data shown in Table 3.3 and Figure 3.7 exhibit a good match to the model's predictions.

After the secondary target partially hybridizes to the probe through the toehold segment, the next step in secondary duplex formation is the sequential displacement of the primary target. This second phase involves what is called branch migration in which one partner strand is exchanged for another one base pair at a time. Although this step is assumed to occur relatively quickly in solution, molecular crowding or other surface

effects may slow this step for immobilized sequences. Branch migration can be modeled as a random walk since there is approximately equal chance for the branch to move forward (displacing the primary target) or backward (displacing the secondary target). This reversible migration process happens on an m^2 time frame. Mismatch targets should not be treated as simply $m-1$ base pairs because, once the mismatched base in the primary target strand is replaced by a matched base in the secondary target, the energetic difference between the mismatched and match base pairings makes subsequent replacement of the matched base pair by the mismatched one very unlikely. If mismatched duplexes are treated simply as two $(m-1)/2$ segments, displacement by a perfectly-matched strand can be estimated to occur on a $(m-1)^2/2$ time frame¹⁶. By this analysis, a given secondary target would require greater than twice as much time to displace a perfectly-matched target than a mismatched target of equal base length. This doubling of displacement time was evident in comparing pairs of perfectly match and mismatch primary target in the current work such as **P13-F** and **M13-F** or **P11-F** and **M11-F**.

The results from the post washing competitive hybridization experiments also indicate a deviation from predicted behavior based on solution thermodynamics. The significant differences in the theoretical ΔG_{hyb} values between primary duplexes and secondary **A20:P15** duplexes (~ 7 kcal/mol for the **M13-F** being displaced by **P15**) suggest that displacement by **P15** strands is energetically favorable for each of the shorter and/or mismatched primary target. Furthermore, if primary hybridization partners were all displaced, their concentration would remain much lower (<10 nM) than the

concentration of competitive **P15** (5 μM) introduced to the suspension. Despite these factors favoring an exchange of one partner strand for another stronger partner strand, displacement activity is significant but does not go to completion for any of the sequence combinations studied. This deviation from expected behavior suggests that immobilizing strands on microspheres may effectively reduce the differences in ΔG of hybridization between primary and secondary duplexes resulting in a reduction in overall displacement activity similar to the reduction in hybridization affinity observed in the previous section. It is important to realize that relevant factors such as substrate interference with hybridization and the collective electrostatic effects of the DNA brush on the microspheres are not taken into account in solution-based ΔG_{hyb} . The apparent equilibrium concentration also appears to be strongly dependent on the concentration of competitive strand despite being in significant excess in most cases and further supports a weak thermodynamic driving force.

3.3.4 *In situ* Secondary Displacement Studies

In contrast to the previous section involving washing steps prior to measurement, our *in situ* displacement studies were conducted by directly sampling the suspension at various times during incubation with **P15** secondary targets. As with the *in situ* primary studies, 1.1 μm microspheres were used instead of the 5.0 μm microspheres to increase the count rate (but not the microsphere concentration) and thus reduce the time it took for each sampling (10,000 particles) to occur. Although both the 1.1 μm and the 5.0 μm microspheres are carboxylated polystyrene, the two microsphere populations may also

differ in their surface structure. For example, the difference in measured surface density of primary duplexes ($\sim 10^4$ strands/ μm^2 for 1.1 μm particles as opposed to $\sim 10^3$ strands/ μm^2 for 5.0 μm particles) implies a difference in the surface density of the carboxyl groups involved in covalent conjugation to aminated **A20** sequences. Since the observation time window was only 30 min for the *in situ* measurements, **M11-F** was selected as the primary target based on its relatively quick displacement behavior in the post washing studies discussed earlier.

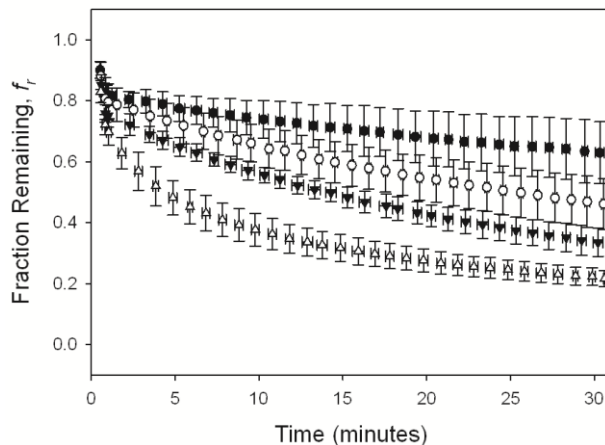


Figure 3.8. *In situ* measurements of the fraction of fluorescently labeled primary target, **M11-F**, remaining hybridized to immobilized **A20** strands in the presence of **P15** secondary targets at concentrations of 0 nM (closed circles), 10 nM (open circles), 100 nM (closed triangles) and 1,000 nM (open triangles). Error bars for fraction remaining and time are shown.

Figure 3.8 shows the results of *in situ* measurements of primary targets remaining hybridized over time at varying concentration of secondary target. Although the fraction of primary target remaining hybridized diminished with increasing concentrations of competitive **P15**, there was also an almost 40% loss of **M11-F** in the absence of **P15**. This significant loss of **M11-F** in the absence of competitive DNA prevented reliable

measurement of the initial primary duplex density for these *in situ* measurements. Prior studies ⁶ indicated a significant loss of 17% in a single wash for a weak primary target. Based on these previous results and the results in Figure 3.8, washing clearly has a significant impact on the surface density of primary duplexes despite the strong duplex stability predicted by solution theory. As shown in a prior report ⁶, some fraction of weaker primary hybridization partners are likely to be released during each wash step to restore equilibrium. In fact the higher probe DNA concentration near the microspheres surface relative to the bulk solution may promote dissociation of weaker duplexes allowing release or displaced primary target to diffuse into the bulk solution thereby reducing its contribution to the local equilibrium of immobilized oligonucleotides. The solution equilibrium constant of the primary hybridization can be modified by a term arising from the dilution of the concentration of free primary target ⁶ as it diffuses away from the smaller volume occupied by the immobilized DNA probes to the total volume of the bulk solution. In this equation, α is equal to the ratio of these two volumes and leads to significant changes in the apparent stability of the duplex as described by equation 3.8. For $\alpha \ll 1$, the result of the correction is a less stable duplex. A value of α in the current work can be estimate from the diameter of the particles, d , volume fraction of particles, f , and height of the layer containing the immobilized probes, h , using equation 3.8 to be 7.5×10^{-6} (using $d = 10^{-6}$ m, $f = 1.25 \times 10^{-4}$ and $h = 10$ nm). The effective change to ΔG of hybridization due to this dilution effect is then 7 kcal/mol, thus making dissociation considerably more likely. This effect is further discussed in Appendix A.2.

$$K_{corrected} = \frac{[PT]}{[P]\alpha^{-1}[T]} = e^{-\Delta G/RT} e^{\ln \alpha} \quad (3.7)$$

$$\alpha = \frac{6fh}{(1-f)d} \quad (3.8)$$

Despite difference between the *in situ* and post washing experiments, the overall trends in the fraction of primary target displaced over time are very similar as shown in Figure 3.9. The values of k_2 from the post washing and *in situ* data are similar at secondary target concentrations of 10 nM and 100 nM. At 1,000 nM secondary concentration, however, k_2 values differ by a factor of ~10. If the higher surface density of **A20:M11-F** duplexes on the 1.1 μm microspheres was making duplexes less stable, then faster release in all solutions would be expected. This effect, however, was not observed. There is also a larger reaction volume in the *in situ* experiments than the post washing experiment thus reducing the ratio of probe strands to secondary target strands, therefore, yielding a more stable secondary target concentration as the hybridization reaction progresses. This shift should only be relevant at the lowest concentrations of secondary target and would partially explain a higher rate of displacement of at a secondary target concentration of 0.01 μM in the *in situ* experiments samples but this is also not observed. Although there is a difference in surface curvature, surface curvature effects are unlikely to be relevant considering the large relative sizes of the particles compared to the DNA strand. In general, the *in situ* results show that the trends in the previous work are probably accurate but there may be considerable uncertainty in the actual rate of displacement.

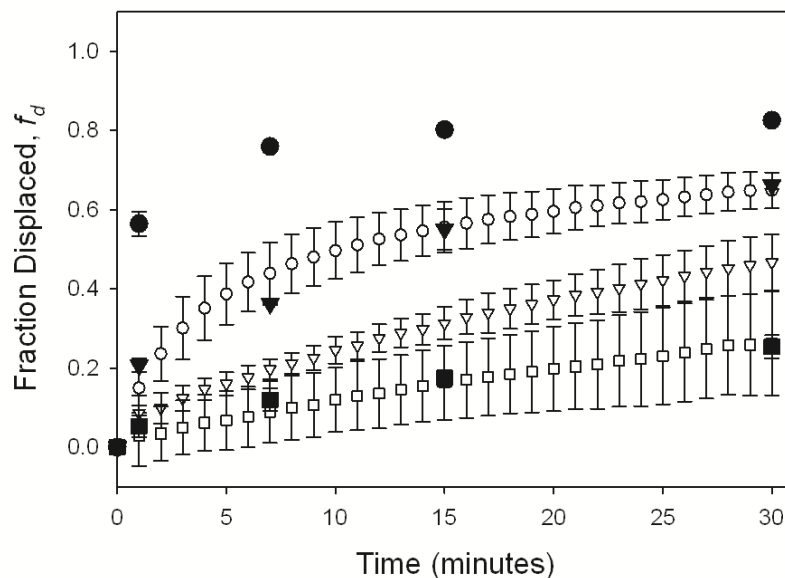


Figure 3.9. Fraction of primary target, **M11-F**, displaced by **P15** secondary targets at concentrations of 10 nM (open squares), 100 nM (open triangles) and 1,000 nM (open circles). Open symbols indicate *in situ* hybridization experiments while closed symbols indicate measurements taken after washing step to remove excess unassociated **P15** strands.

To determine if fluorescent labeling affected hybridization, two comparative control experiments were run using fluorescently-labeled DNA and unlabeled DNA with identical sequences. One experiment used fluorescently labeled DNA as the primary target and unlabeled DNA as the competitive target. Although unlabeled DNA will hybridize with unhybridized probe first, these events are not observable in this experiment. In the other control experiment, unlabeled DNA is used as the primary target and fluorescently-labeled DNA is used as the competitive target. In this case the hybridization of the now fluorescent competitive strands to unoccupied probes can be observed but it occurs much faster than the competitive reaction. Since it is likely that there will be hybridization of competitive target to unoccupied probe in the early

moments of the experiments, the latter time points of the experiment are more likely to result from the less favorable competitive displacement reaction. The results of these experiments are displayed in Figure 3.10. Each point represents one measurement. Linear interpolation between nearest points was used to project the surface densities of one control experiment to the time points of the other and the results were then summed to produce the essentially flat progression in Figure 3.10. Such a result strongly implies that the unlabeled and labeled strands have the comparable hybridization rates over the course of this experiment.

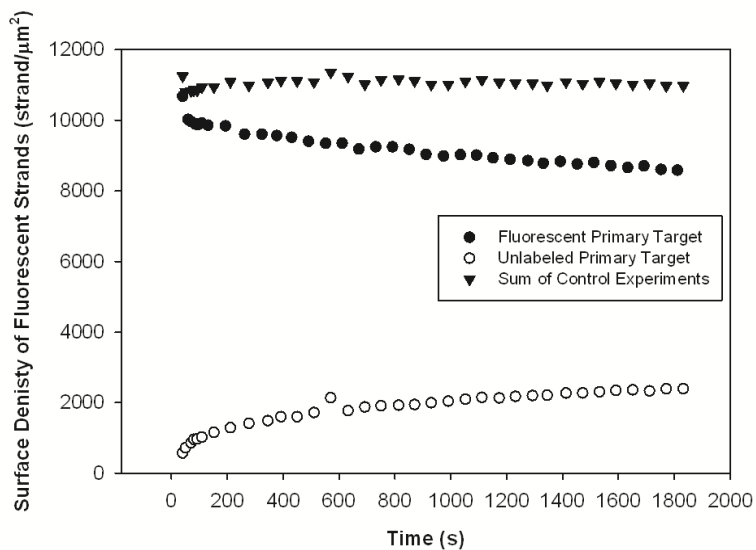


Figure 3.10. Investigation of the effect of the fluorescent label on hybridization. The surface density of fluorescently-labeled DNA on microspheres functionalized with fluorescently labeled primary duplexes (solid circles) or unlabeled primary duplexes (open circles) that are then incubated with unlabeled (solid circles) or fluorescently labeled (open circles) competitive DNA respectively. The solid triangles indicate the sum of the results of these two control experiments.

3.4 Conclusions

In situ hybridization studies were found to be capable of capturing the relevant time scales for both primary and secondary hybridization at colloidal surfaces. Although hybridization at surfaces is related to solution thermodynamics, the different environment of the surface relative to the bulk leads to significant sequence specific effects on the extent and efficiency of hybridization. Based on post washing studies, toehold regions appear to have a strong effect on the kinetics of competitive displacement and explain the largest differences in displacement rates. Branch migration differences between perfectly matched and mismatched primary targets may also be relevant factors in comparing displacement rates. Finally, the results of *in situ* studies indicate that washing steps cause some significant changes in the measured reaction rates though the overall trends in time-dependent displacement behavior were still consistent between the post-wash and *in situ* protocols.

3.5 References

1. C. K. Tison and V. T. Milam, *Soft Matter*, 2010, **6**, 4446-4453.
2. S. T. Parpart, C. K. Tison and V. T. Milam, *Soft Matter*, 2010, **6**, 3832-3840.
3. C. K. Tison and V. T. Milam, *Langmuir*, 2007, **23**, 9728-9736.
4. *The DINAmelt Web Server*, <http://mfold.rna.albany.edu/?q=DINAMelt/Two-state-melting> (Last Accessed 11/17/2010)
5. L. P. Reynaldo, A. V. Vologodskii, B. P. Neri and V. I. Lyamichev, *J. Mol. Biol.*, 2000, **297**, 511-520.
6. B. A. Baker and V. T. Milam, *Nucleic Acids Res.*, 2011, **30**, doi:10.1093/nar/gkr1293.
7. V. V. Koval, O. V. Gnedenko, Y. D. Ivanov, O. S. Fedorova, A. I. Archakov and D. G. Knorre, *IUBMB Life*, 1999, **48**, 317-320.
8. N. Tibanyenda, S. H. Debruin, C. A. G. Haasnoot, G. A. Vandermarel, J. H. Vanboom and C. W. Hilbers, *Eur. J. Biochem.*, 1984, **139**, 19-27.
9. D. Porschke and M. Eigen, *J. Mol. Biol.*, 1971, **62**, 361-&.
10. M. A. Livshits and A. D. Mirzabekov, *Biophys. J.*, 1996, **71**, 2795-2801.
11. K. Tawa, D. F. Yao and W. Knoll, *Biosens. Bioelectron.*, 2005, **21**, 322-329.
12. J. Zeng, A. Almadidy, J. Watterson and U. K. Krull, *Sensors and Actuators B-Chemical*, 2003, **90**, 68-75.
13. D. Porschke, Uhlenbec.Oc and F. H. Martin, *Biopolymers*, 1973, **12**, 1313-1335.
14. K. M. Parkhurst and L. J. Parkhurst, *Biochemistry*, 1995, **34**, 285-292.
15. D. Y. Zhang and E. Winfree, *J. Am. Chem. Soc.*, 2009, **131**, 17303-17314.
16. C. Green and C. Tibbetts, *Nucleic Acids Res.*, 1981, **9**, 1905-1918.

CHAPTER 4

TRIGGERED CHANGES IN SURFACE FUNCTIONALITY OF GMS-BASED COLLOIDAL ASSEMBLIES

4.1 Overview

In Chapter 2 it was shown that encapsulated DNA released from a polydisperse population of GMS could undergo subsequent hybridization to complementary DNA. In this chapter, microspheres functionalized with DNA duplexes were adsorbed onto microfluidically-fabricated monodisperse GMS containing encapsulated DNA to yield a colloidal assembly with a DNA functionalized surface. Release of competitive DNA from the GMS core at 37 °C was then shown to drive displacement of the primary hybridization partner on the satellite particles thus changing the surface functionality of the colloidal assembly. This chapter also covers the optimization of the DNA sequences for this application using techniques developed during the work in Chapter 3 as well as the microfluidic production of monodisperse GMS.

4.2 Materials and Methods

4.2.1 Materials

DNA was purchased from Integrated DNA technologies (Coralville, IA). The sequences used in this work, function, and ΔG of hybridization can be found in Table 3.1. Span 80, Span 20, type A gelatin from porcine skin (300 bloom, $pI \approx 8.0$), Procline, 1-ethyl-3-[3-dimethylaminopropyl]-carbodiimide hydrochloride (EDC), PBS, poly(allylamine hydrochloride) ($M_w \approx 56$ kDa), isooctane, octadecyltrimethoxysilane

(hydrophobic coating) and sodium chloride were purchased from Sigma Aldrich (St, Louis, MO). Poly(acrylic acid sodium salt) ($M_w \approx 85$ kDa) was purchased from Polysciences (Warrington, PA). Mineral oil (viscosity of 34.5-150.0 mm^2s^{-1}) and acetone was purchased from VWR international (Arlington Heights, IL). 1.1 μm carboxylated polystyrene microspheres were purchased from Bangs Laboratories (Fishers, IN). 200 nm Nile Red nanoparticles were purchased from Molecular Probes (Eugene, OR). Ethanol, Tris/EDTA buffers (pH 7.4 and 8.0) were purchased from Fischer Scientific (Pittsburg, PA). Two types of epoxy were used, 5-minute epoxy (Devcon, Danvers, MA) and 30-minute Permaoxy epoxy (Permatex, Solon, OH).

4.2.2 Construction of Device

The capillary microfluidic device was constructed as described in literature¹ from concentric glass capillaries to yield a device as shown in Figure 4.1. A square capillary was cut to an appropriate size and attached to a glass slide using 5- minute epoxy. Round capillaries were pulled to appropriate shape on a micropipette puller (Sutter Instruments, Navato, CA) and cut to exact dimensions for the outlet and gelatin needles using a microforge (Narishige, Tokyo, Japan). The cut needles were dipped in the hydrophobic coating solution and allowed to adsorb for 2 minutes before being rinsed with ethanol. After coating, the round capillaries were then placed into the square capillary from opposite ends and their axes were aligned. Syringe needles were cut to fit over the junctions between the round and square capillaries and another was cut to fit over the end of the capillary that would supply the gelatin. A purge outlet is added under the gelatin inlet needle to permit quick exchange of the material in the gelatin inlet needle and thus

reduce the time necessary for loading the device. The device was then sealed using a minimal amount of 5-minute epoxy. Finally, 30-minute epoxy was applied and cured twice at 45 °C to further seal the device.

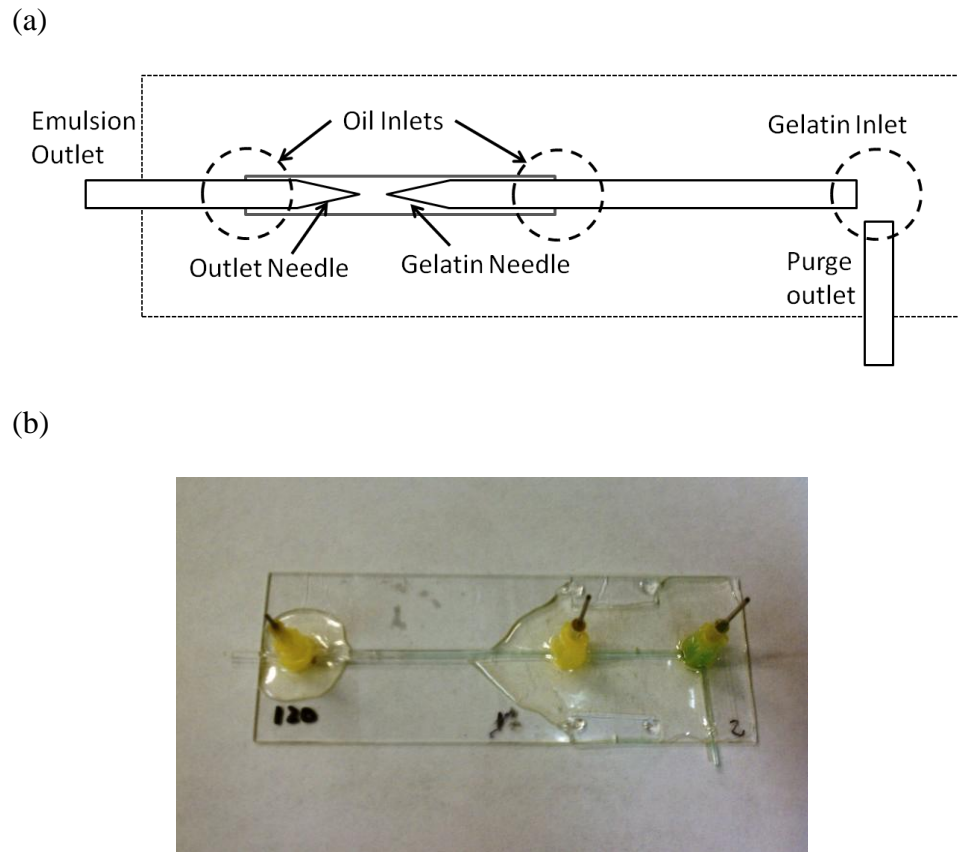


Figure 4.1. (a) Top view schematic and (b) photograph of microfluidic device used to form uncrosslinked gelatin microspheres. Dashed circles represent locations of attached needles (oriented at 90° angle to the capillary device) where gelatin solution and oil are introduced. The diagram is not to scale. The gelatin and outlet needles have inner diameters of 12 and 260 μm respectively.

4.2.3 Generation of Microspheres

The microfluidic apparatus was complicated by the need to keep the gelatin warm throughout the fabrication process as shown in Figure 4.2. The required heating was

accomplished by using a heated syringe for the gelatin (syringe from SGE Analytical Science (Australia) wrapped in Nichrome heating wire), a heated tube containing the gelatin line (plastic tubing with Nichrome wire running inside), and a small hot box that enclosed the microfluidic device and fit on the microscope stage. The hot box consisted of a lower section that fit in the microscope stage and an upper section that guided the hot air, but did not interfere with the microscope optics. The hot air was introduced to the hot box by a hair dryer (Conair Midsize Turbo Dryer) but the other heated elements were controlled by two variable AC transformers linked in series. The temperature inside the hot box was $\sim 50\text{ }^{\circ}\text{C}$ and the positive air pressure in the hot box also led to heating of the interface between heating tube and the hotbox (as the hot air escaped) thus maintaining more consistent heating throughout the gelatin phase. A small wedge was placed at the



Figure 4.2. Arrangement of microfluidic GMS production apparatus.

exit to the hot box to deflect the hot air up while the sample leaving the device traversed down for collection.

Prior to placing the device on the microscope stage, the microfluidic device was flushed with ethanol to remove dust and other debris and then the gelatin line was filled with water containing a green dye from the purge outlet. Afterwards, the device was attached to the lower section of the hot box and placed on the microscope stage. The oil phase consisted of heavy mineral oil with 6 v% Span 80. The gelatin phase consisted of 20 wt% gelatin in 150 mM NaCl water. The gelatin was pumped from a heated syringe through a heated tube to the gelatin line and into the microfluidic device. The green water in the gelatin inlet was allowed to leave the gelatin inlet through the purge outlet and then the purge outlet was closed, thus the only remaining dyed water was in the gelatin needle. The upper section of the hot box was placed on top of the lower section and hot air was passed through the box using a hair dryer. Syringe pumps (KD Scientific, Holliston, MA) were used to pump fluids through the device. The alcohol remaining in the device was first displaced by the oil and then the dyed water was displaced by the gelatin solution in order to avoid precipitation of the gelatin by the alcohol. At this point the final flow rates were set on the syringe pumps and gelatin microspheres were generated. The emulsion produced by the device was collected in a 50 mL tube in an ice bath (to induce gelation of the gelatin droplets) and particle production was monitored using a Phantom v9.1 high speed camera (Vision Research, Wayne, NJ). The GMS were then extracted into octane and then into acetone via centrifugation and resuspension by vortexing and sonication. Three acetone washes were used to clean the particles of

residual octane, mineral oil, and surfactant. The size of these particles upon resuspension in water was measured using a stage micrometer on an inverted microscope. Still images were captured on the inverted microscope using a Sony Handicam camera.

4.2.4 GMS Processing

DNA was infiltrated into GMS and a bilayer of PAA/PAH was added in a manner identical to previous work discussed in Chapter 2.² Briefly, GMS in acetone were resuspended in a DNA solution and allowed to incubated for 30 minutes. The solution was then exchanged with saline twice to remove excess DNA and then the particles were resuspended in a PAH solution for 10 minutes. The excess PAH was removed by centrifugation and replacing the supernatant with saline twice. The GMS were finally resuspended in a PAA solution for 10 minutes and then washed four times in saline.

4.2.5 Preparation of PS Microspheres

Aminated DNA was coupled to 1.1 μm carboxylated polystyrene particles following the procedure based on the Polylink coupling kit from Bangs Laboratories and previous studies.³ Briefly, the microspheres were washed and resuspended in 150 μL of a coupling buffer (aqueous solution of 50 mM MES and 0.05 v% Proclin and adjusted to pH 5.1). 200 μL of 10 μM DNA in TE 7.4 and 25 μL of 1.28 M EDC were then added to the suspension and incubated for 2 h. Another batch of microspheres was also coupled by this method except that the concentration of DNA was two orders of magnitude smaller. Three washes were done to remove free **A20**. 10 μL these **A20**-functionalized microspheres were added to 90 μL of PBS/Tween and 200 μL of primary target in TE 8.0

and incubated at 37 °C for 30 min and then washed three times (bringing the particle back to 37 °C between each wash) to reduce thermal dissociation at later steps.

4.2.6 Optimization of DNA Hybridization

To determine what hybridization conditions were best for detecting competitive hybridization on the satellite particles of the assembly, DNA-functionalized microspheres were processed in a way to mimic the assembly steps and testing protocol described below. After the particles were prepared as described above, they were incubated at 37 °C in solutions of 10 nM or 100 nM of **P15** or **NC** overnight in order to simulate release of low concentrations of DNA from the GMS. After the incubation, the samples were sonicated and prepared for flow cytometry.

4.2.7 Assembly on GMS

Polydisperse GMS were prepared as described previously² and used to check for assembly of the polystyrene microspheres on GMS because they are significantly easier to manufacture. Bare, **A20**-functionalized, **A20:P13**-functionalized and **A20:P13-F**-functionalized polystyrene microspheres were prepared following the procedure above. One bilayer of PAH/PAA was added to polydisperse **P15**-loaded GMS. The processed GMS were resuspended in 50 µL of saline and added to 100 µL of the various PS microsphere sample prepared earlier, vortexed and incubated for 2 hours. After incubation, the suspension was centrifuged at 500 g for 1 min and the supernatant was removed and replaced with PBS/Tween four times to remove the majority of singlets. A 20 µL suspension was then prepared for microscopy. Electrophoretic mobility was

measured on all of these particles using a Zetasizer NS (Malvern Instruments, Worcestershire, UK) and converted to zeta potential using the Smoluchowski approximation.

4.2.8 Release of Competitive DNA

To investigate the release of DNA from core-satellite structures built around nearly monodisperse GMS produced using microfluidics, assemblies were prepared as described above for polydisperse GMS. Colloidal satellite structures (in microcentrifuge tubes and on slides) were then incubated overnight at 37 °C. After incubation, the samples were cooled in a 4 °C refrigerator for 10 min. After cooling to solidify the gelatin microspheres, the samples were sonicated for ~10 s to desorb the satellite polystyrene particles from the core GMS. Centrifugation at 500 g for 1 minute was used to remove the GMS templates and remaining assemblies, leaving mostly singlets. 100 µL of supernatant was removed and prepared for flow cytometry.

4.3 Results and Discussion

4.3.1 GMS Synthesis

A progression of the device types constructed is described in Figure 4.3 culminating in the design in Figure 4.1. The first device, Figure 4.3 (a), constructed by CW Ye in the Martinez group at Purdue University, uses relatively large needles in an arrangement similar to Figure 4.1 (a). The large needles were not capable of producing

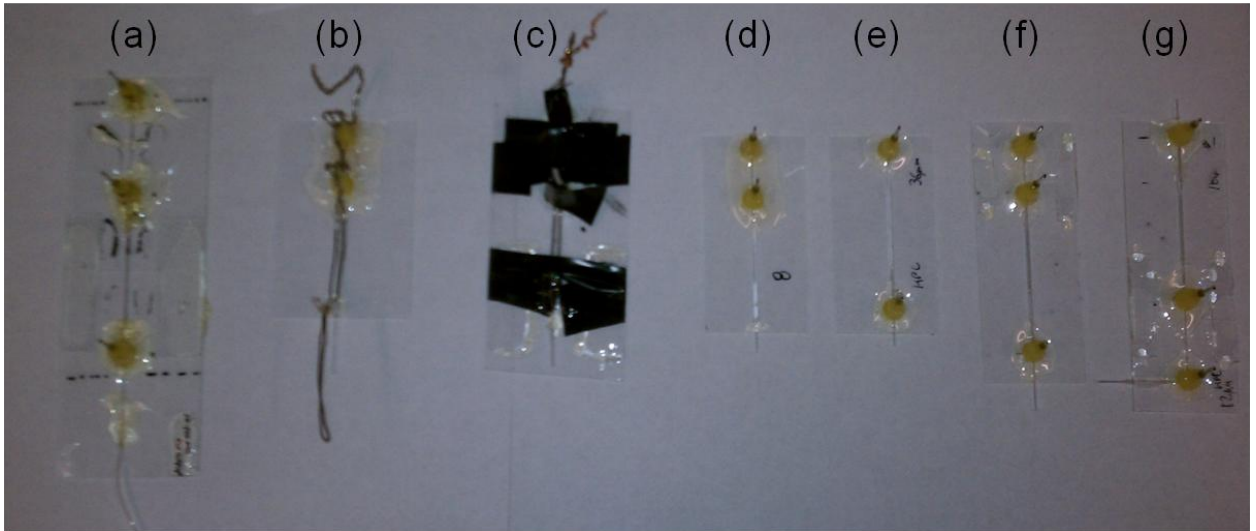


Figure 4.3. Picture of the various device types investigated in this project. (a) CW Ye from the Martinez Lab at Purdue made the first device but it was originally deemed unnecessarily complex and the tip diameters were too large to produce particles in the size range of interest. (b) A simple coflow device was tried next with NiChrom heating wire glued to it. (c) To better control the ambient air flow, electrical tape was wrapped around the heating wire and the needles in the next embodiment. After replacing the directly attached heating wire with a surrounding hot box (d) coflow and (e) flow focusing arrangements were tried again. (f) Following failed attempts with both of these devices, a modified coflow arrangement was made that is similar to (a) but with a much larger ratio between the gelatin needle and outlet needle diameters. (g) The final design was identical to (f) but with a purge outlet added to decrease setup time.

particles of small enough size and the two needles were initially judged to be unnecessarily complex. The next generation of devices, Figure 4.3 (b) and (c) were simple coflow and flow focusing designs as depicted in Figure 4.4 with heating wire directly attached to the devices. The heating wire proved unable to keep the device at a stable temperature due to the significant ambient air flow. The next designs, Figure 4.3 (d) and (e), depended on a hot box instead of direct heating wires for temperature control but were still simple coflow and flow focusing arrangements. Since the hot box effectively removed instabilities in the gelatin flow from temperature changes, issues with the flow arrangement could finally be addressed. Coflow devices were capable of

particle production but required such high flow rates of the continuous phase that the resulting low particle concentration and low total number of particles before device failure made subsequent work unfeasible. Gelatin needles down to 5 μm in inner diameter were attempted but below 10 μm , debris in the gelatin phase would quickly and irreversibly clog the device. Flow focusing devices as depicted in Figure 4.4 were also attempted but instabilities in the interface never resolved themselves enough to produce uniform particles. The modified coflow system described in Figures 4.3 (f) and 4.4 locally increases the speed of the fluid at the gelatin tip and thus could produce smaller particles with less dilution of the particles than the simple coflow arrangement. For these

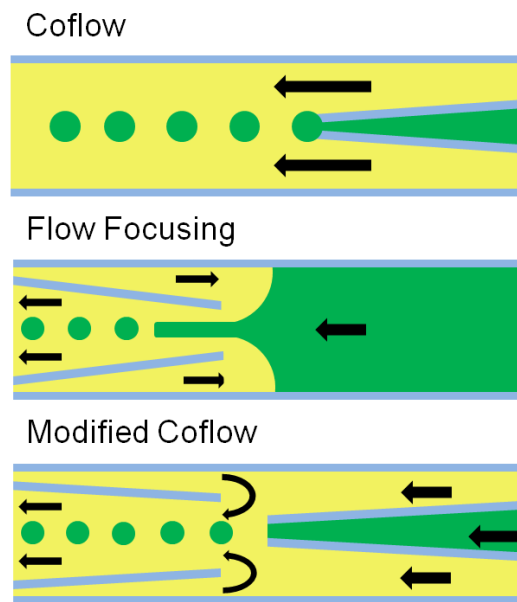


Figure 4.4. The three flow arrangements mentioned in this work for making gelatin (green) droplets in a continuous oil (yellow) phase. Capillary walls are denoted by blue lines. The coflow arrangement (top) is where droplet is pushed off the tip by another fluid flowing the same direction. The flow focusing arrangement (middle) is where the gelatin is pulled into a thin stream and then breaks up to form droplets. The modified coflow arrangement (bottom) used in this work is where the restricted exit flow leads to a local increase in fluid speed at the tip carrying the gelatin.

reasons, the modified coflow arrangement was used to produce the particles for most of the work presented in this chapter. To decrease the amount of time necessary to clear the green water from the device, a purge outlet was added to the devices shown in Figures 4.1 and 4.3 (g) and thus the final design was settled upon.

The microfluidic synthesis successfully produced particles of 35 μm in diameter with a standard deviation of 1 μm (based on 8 particles) and with good spherical shape in saline, as seen in Figure 4.5. These are significantly smaller than GMS produced using microfluidics elsewhere in literature in addition to being higher in gelatin concentration. Furthermore, they are mechanically stable in aqueous solution at room temperature over the course of these experiments without covalent crosslinking. Although the particles are significantly more prevalent from the modified coflow device than the simple coflow devices, a very limited number were produced before the device failed.

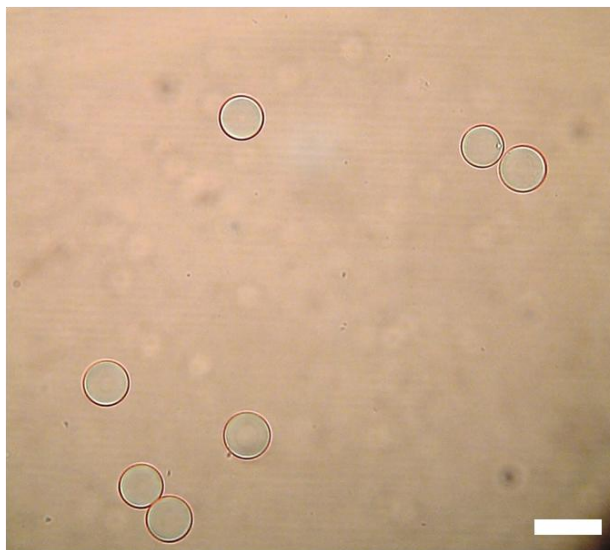


Figure 4.5. Phase contrast micrograph showing the uniform gelatin microspheres (GMS) fabricated with microfluidic device. Scale bar represents 50 μm .

4.3.2 Investigation of Competition at Elevated Temperature

To find the best competitive DNA hybridization system, two DNA coupling conditions and four primary target sequences were investigated. Microspheres with fluorescently-labeled primary duplexes were exposed to 10 or 100 nM of **P15** or **NC** and the remaining surface density of fluorescently-labeled duplexes was measured using flow cytometry. The surface density of the primary target was much higher on the particles exposed to a higher concentration of probe DNA during coupling than those exposed to lower concentrations of probe DNA as shown in Figure 4.6. This result is most likely due to higher surface densities of probe DNA on these microspheres, therefore, these particles will subsequently be referred to as high and low density particles. Although higher surface densities generally yield clearer fluorescence peaks, it is the difference between the samples incubated with **NC** and **P15** competitive DNA that is indicative of strand displacement. The higher density particles, Figure 4.6 (a), show virtually no evidence of competitive displacement while the lower density particles, Figure 4.6 (b), show strong evidence of competitive displacement by **P15**. In contrast to the results in Figure 4.6 (a), competitive hybridization at room temperature was observed on high density microspheres in Chapter 3 as well as in literature on a very similar system.^{3,4} The cause of the negligible difference between the **NC** and **B15** samples in Figure 4.6 (a) may be due to the large number of thermal dissociation events that occurred at 37 °C (compared to the ~22 °C conditions used in Chapter 3). Furthermore, assuming that the fraction of unhybridized probe DNA is constant between the particle populations, the higher probe density particles should numerically have more unhybridized probe DNA that can hybridize with competitive target DNA before subsequent displacement events

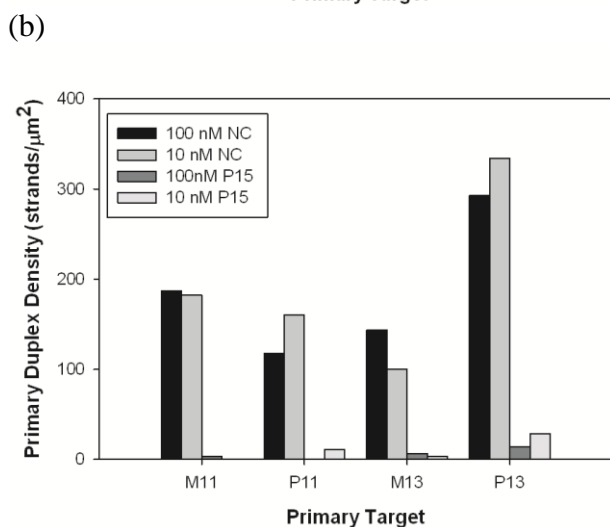
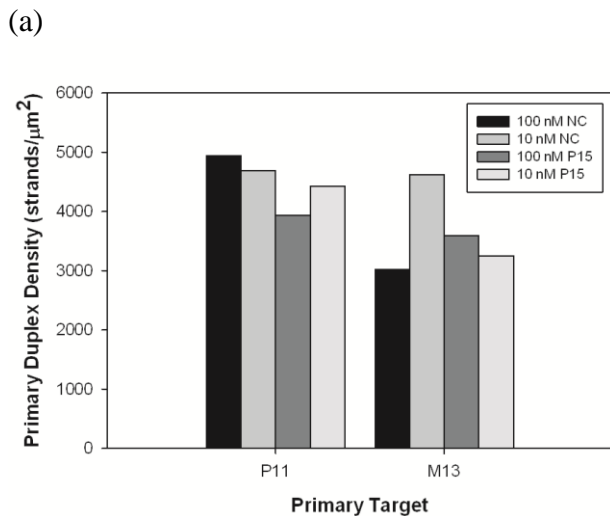


Figure 4.6. Bar graphs of primary targets remaining hybridized to (a) high density and (b) low density (of immobilized probe DNA) polystyrene microspheres following incubation with noncomplementary (NC) and complementary (P15) secondary targets at 37 °C. Each point represents the average of 2 samples.

are likely to occur. It has also been observed that probe density has a strong effect on primary hybridization efficiency,⁵ thus the higher density particles may also have a higher fraction of unhybridized probes than the lower density particles. In either scenario, the secondary targets are likely to seek unoccupied probes first for hybridization. Based on the results of the competitive hybridization experiments, the best

balance between differentiation between **P15-F** and **NC** secondary targets and significant surface density of primary target occurred with the **P13-F** primary target.

4.3.3 Assembly

The PS satellite particles appeared to form a largely complete monolayer shell around the core GMS that remained after multiple cycles of centrifugation and vortexing as shown in Figure 4.7 (a) and (b). This result was also observed on the polydisperse GMS with all four of the cases investigated in Section 4.2.7. The nearly identical assembly on the polydisperse GMS using all four of the satellite particle types implies that neither the fluorescent label nor the DNA is sole mediator of assembly. In the absence of specific recognition between the satellite particles and the GMS core, nonspecific forces such as van der Waals or electrostatic force must be responsible. The zeta potentials in 10 mM NaCl are -36.0, -34.6, -43.1, -40.6 mV for the bare, **A20**-functionalized, **A20:P13**-functionalized, and **A20:P13-F**-functionalized polystyrene microspheres, respectively. The GMS were previously shown in Chapter 1 to be weakly negative at -14.8 mV. Since the assembly takes place in 150 mM NaCl, the zeta potential of the particles in the assembly solution should be even smaller in magnitude. The smaller particles are observed to be relatively stable at 150 mM NaCl but the GMS should spontaneously aggregate with such a weak zeta potential. With the small particles in significant excess concentration during assembly suspensions, they appear to adsorb to the surfaces of the GMS before the “bare” GMS aggregate with each other, thus stabilizing the assembly.

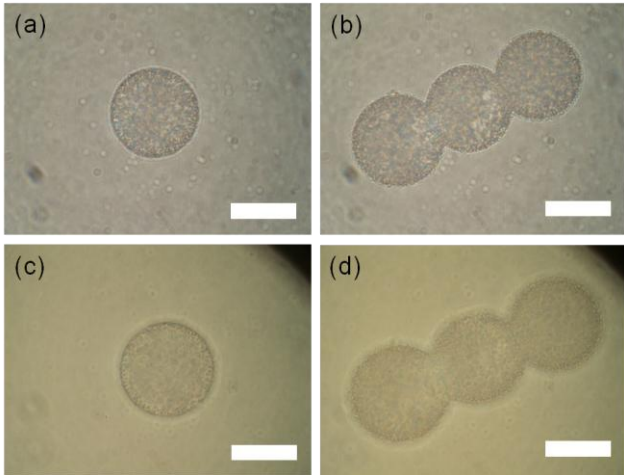


Figure 4.7. Phase contrast micrographs of the colloidal satellite assemblies comprised of a layer of DNA-functionalized microspheres (1.1 μm diameter) adsorbed on gelatin microspheres at (a, b) room temperature and (c, d) following incubation at 37 $^{\circ}\text{C}$ overnight. Scale bars represent 25 μm .

The satellite particles are fluorescent as one would expect due to the **P13-F** hybridized on their surfaces. Only a few assemblies were visible in the sample taken prior to incubation at 37 $^{\circ}\text{C}$. This observation indicates that either very few assemblies survived processing, they are sticking to the vessel walls or they are forming aggregates that settle before they can be collected. The impact of heating on the morphology of the particles was investigated by heating the microscope slide with the well containing a sample of the assemblies. As seen in Figure 4.7 (c) and (d), the GMS cores are still covered to approximately the same degree even after heating. Furthermore, minimal swelling is evident in the micrographs and the particles are still $\sim 35 \mu\text{m}$ in diameter. Figure 5.7 (b) and (d) show that neighboring particles do not coalesce or significantly change shape, thus supporting the assertion that the particles are mechanically stable.

Since the satellite particles adsorbed to the surface of the GMS are of primary interest in this work, the influence of remaining unabsorbed microspheres needs to be

accounted for. Total removal of the unadsorbed microspheres would require roughly twice as many washes and would also remove most of the few remaining assemblies. Conservatively assuming that each resuspension performed in this work reduces the concentration of singlets by 90%, the final number of singlets in the whole sample should be on the order of 1000 particles, much less than the ~10,000 singlet detected in a fraction of the sample by the flow cytometer after sonicating the assemblies. The structural stability of the assemblies demonstrated in Figures 4.7 also implies that minimal release of particles occurs during the heating process. Cumulatively, these observations strongly support that the vast majority PS particles remain adsorbed to the surface of the GMS throughout the 37 °C incubation and thus and observed changes in the functionalization of the microspheres are indicative of changes in the functionalization of the assembly.

The template GMS of the assemblies were either loaded with **NC** of **P15**. After incubating overnight at 37 °C, many of the satellite particles were intentionally desorbed via sonication. The samples with **P15**-loaded GMS were found to have a lower surface density of **P13-F** than those incubated with **NC**-loaded GMS as shown in Figure 4.8. This implies that **P15** strands are inducing competitive displacement of the **P13-F**. Previous work demonstrated that light sonication was not enough to affect full release of DNA from PAH/PAA coated GMS,² thus these results represent a change of the surface functionalization of a colloidal assembly induced by release of competitive oligonucleotides from a source intrinsic to the colloidal assembly. This work also demonstrates that the encapsulation and release of DNA by GMS is not mediated by the fluorescent moiety attached to the DNA in previous release studies.

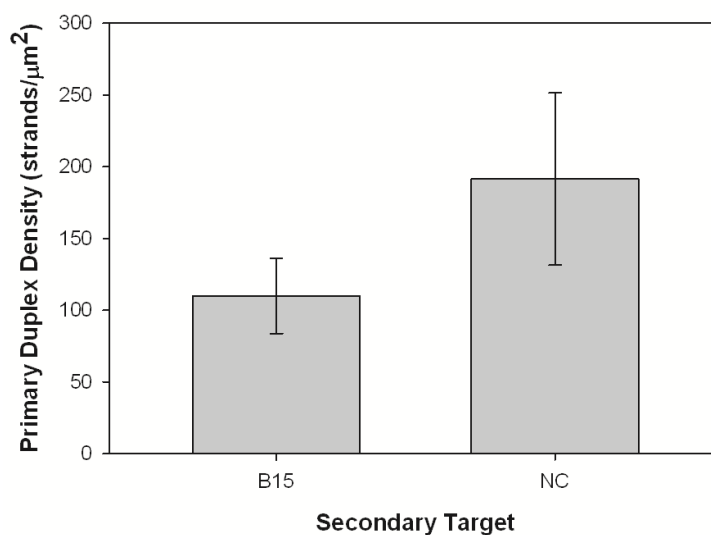


Figure 4.8. Evidence of intrinsic DNA-mediated change in surface functionalization. Surface density of **A20:P13-F** primary duplexes remaining on polystyrene (PS) microspheres was measured following overnight 37 °C incubation of GMS-PS core-satellite assemblies with GMS templates loaded with either complementary **P15** of noncomplementary **NC** secondary targets.

Using DNA to mediate the disassembly of the colloidal assemblies was also attempted by incubating assemblies like those describe above with fluorescent 200 nm particles functionalized with DNA complementary to the 1.1 μm particles already on the surface. No change in the number particles around the GMS was evident after heating the suspension to release intrinsic competitive DNA or the direct addition of competitive DNA (10 μM **P15**) to the suspension, however the resulting micrographs do clearly show the structure of these assemblies and those previously described. The series in Figure 4.9 (a) shows the effect of infiltrating fluorescently-labeled DNA and coating (3 bilayers in this case) on a 65 μm microsphere. The outer ring of green (fluorescein) fluorescence indicates trapping of DNA in the bilayer while the consistent fluorescence across the microsphere indicates good penetration of the DNA into the microsphere. The series in

Figure 4.9 (b) shows a strongly fluorescent ring of 200 nm red (Nile red) fluorescent particles attached to the assembly. The weaker red glow in the center is a product of out of plane particles still attached to the surface of the assembly. Strong green fluorescence in Figure 4.9 (b) also indicated a large amount of trapped DNA. Despite the lack of disassembly, these experiments do demonstrate the ability to attach multiple particles to the same template in a stable manner.

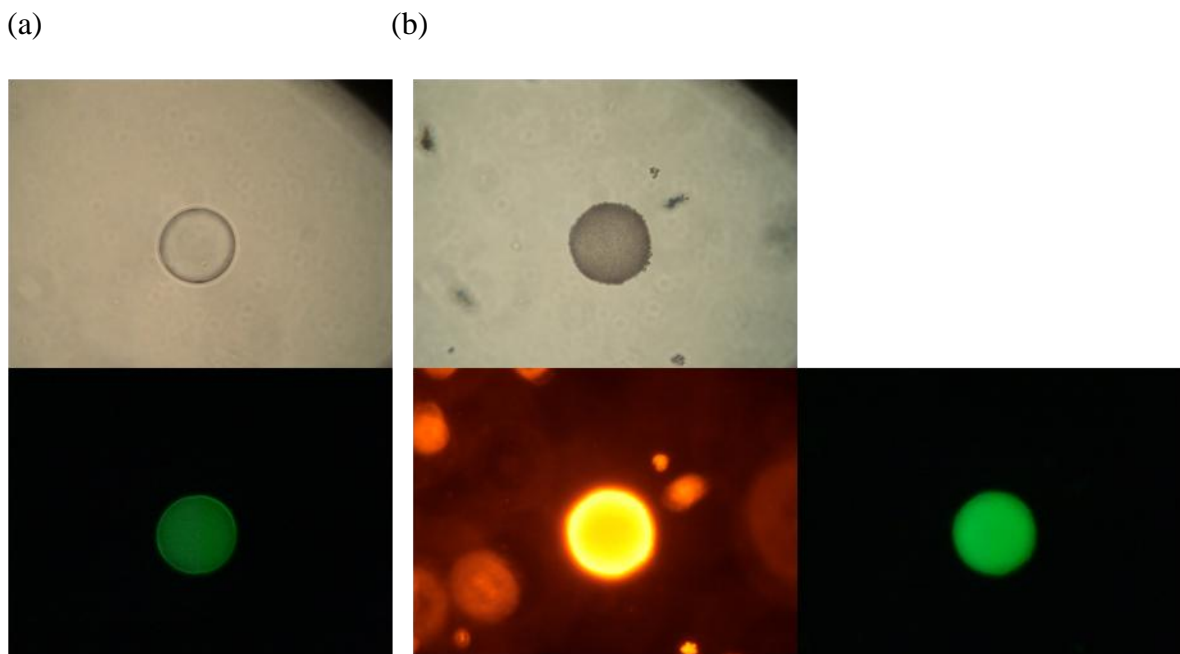


Figure 4.9. A series of micrographs depicting the structure of the assemblies used in an attempt to induce DNA-mediated disassembly. (a) The GMS were first incubated with fluorescent DNA (green) and coated with polyelectrolytes (yielding the outer ring). (b) Nonfluorescent DNA-functionalized 1.1 μm microspheres were then deposited on the surface of the microspheres nonspecifically followed by DNA-mediated deposition of 200 nm fluorescent particles (red). The microspheres in these images were microfluidically produced and are of $\sim 65 \mu\text{m}$ in diameter. The top row are phase contrast micrographs while the bottom row are fluorescent micrographs.

4.4 Conclusions

In this work we demonstrated the microfluidic production of GMS smaller than those described by others in literature. The GMS were also of higher gelatin concentration and stable over the course of this experiment without chemical crosslinking. We further demonstrated the adsorption of a monolayer of colloidal DNA duplex-functionalized PS microspheres. Finally we showed that, after incubation of these assemblies at 37 °C, competitive displacement occurred on the surface of the GMS thus changing the surface functionalization of the assemblies via a release agent (i.e. competitive DNA targets) encapsulated in the colloidal assembly. Such a system with switchable surface functionality may have application to drug delivery. For example, a stealth coating could be attached to the assembly via a DNA duplex and shed at a later time through the action of released competitive DNA. Although inducing colloidal disassembly via this intrinsic mechanism was not observed, the results in this chapter represent a major step toward this objective.

4.5 References

1. R. K. Shah, H. C. Shum, A. C. Rowat, D. Lee, J. J. Agresti, A. S. Utada, L.-Y. Chu, J.-W. Kim, A. Fernandez-Nieves, C. J. Martinez and D. A. Weitz, *Materials Today*, 2008, **11**, 18-27.
2. J. O. Hardin and V. T. Milam, *Soft Matter*, **7**, 2674-2681.
3. C. K. Tison and V. T. Milam, *Langmuir*, 2007, **23**, 9728-9736.
4. S. T. Parpart, C. K. Tison and V. T. Milam, *Soft Matter*, 2010, **6**, 3832-3840.
5. A. W. Peterson, R. J. Heaton and R. M. Georgiadis, *Nucleic Acids Res.*, 2001, **29**, 5163-5168.

CHAPTER 5

CONCLUSIONS AND FUTURE WORK

Although the research presented in previous chapters demonstrates significant progress toward the goal of a multifunctional drug delivery vehicle with an intrinsic DNA-based release mechanism, many challenges remain and many unexpected observations could benefit from further exploration. DNA was successfully trapped in polydisperse GMS at room temperature and released on heating to 37 °C. Uniform GMS were fabricated using microfluidics. These GMS particles were smaller than other microfluidically produced GMS in literature and stable without crosslinking. These uniform GMS were then used as semipermeable templates for colloidal assemblies, and DNA released from these assemblies was capable of changing the surface functionalization of the assemblies. Although colloidal disassembly was not induced by the released DNA in preliminary tests, changing of the surface functionalization may enable medically relevant materials with shedable stealth coatings. Throughout these GMS studies, exploration of DNA hybridization at surfaces was also explored to enable more rational choices of the DNA sequences used. This exploration resulted in the development of an *in situ* hybridization flow cytometry protocol which more directly assesses hybridization than previous post washing studies and potentially allows for more precise investigation of the kinetics and thermodynamics of hybridization at surfaces. The remaining steps in developing an intravenous drug delivery vehicle include demonstrating the capacity for colloidal disassembly, reducing the size of the assembly, and testing with living cells and animals.

Both the behavior of the GMS and DNA hybridization at surfaces proved to be more complicated than was initially expected. Deposition of PAH/PAA bilayer on a gelatin interface yielded significant roughening of the surface but did not appear to inhibit the temperature controlled release properties as one would generally expect for surface degradation. The interaction between the gelatin matrix and the other three polyelectrolytes (PAH, PAA, and DNA) in the system is mostly likely complex but ultimately critical to the controlled release of DNA. Although considerable work was put into optimizing both the emulsion and microfluidic synthesis protocols, both systems could also benefit significantly from further investigation. Finally, DNA hybridization at surface was clearly less favorable than in solution and this deviation also appeared to have a dependence on strand length. Electrostatics, local concentration effects, branch migration changes, and entropic penalties of immobilization were proposed as possible causes of this deviation. Although electrostatics and local concentration effects almost certainly have a significant impact, more investigation is necessary to model these effects and determine the contribution of other components. The rest of this chapter covers some possible future directions based on the work already presented.

5.1 Gelatin Microsphere Synthesis

The two methods for producing GMS face different challenges moving forward. W/O emulsion based fabrication produces significantly smaller particles than the microfluidic approach as shown in Chapters 2 and 4, but ideally these particles need to be below 200 nm in diameter. For the W/O emulsion synthesis, the production of smaller particles may just be a matter of using sonication to break up the droplets during the emulsification and cooling steps and adding more surfactant to keep the droplets stable. It is hard to predict how this will affect

the polydispersity but using appropriate filters may enable greater uniformity in the final product. Microfluidic synthesis has very few issues with polydispersity but significantly greater limitations regarding reducing particle sizes and increasing particle concentration and production rates. The most direct way to increase the production of particles is through improvements in device construction techniques, specifically, making a device capable of working at higher pressures under heat without leaking. Making gelatin particles under 200 nm using microfluidics is a considerable challenge. Standard flow focusing microfluidics is limited to producing particles that are approximately half the tip diameter. Such small tips have severe issues with clogging and pressures necessary to produce significant volumes of particles would make the device vulnerable to leaking. Electrically driven microfluidic jets look and behave much like electrospun nanofibers. Thus they can generate jets that are small enough to break into nanoparticles. At the moment such jets are limited to charged fluids and there are issues with collecting the particles produced but future progress may make this a viable option.

5.2 Gelatin-Polyelectrolyte Interface

Gelatin matrices are unlikely to produce a smooth surface on the scale of hydrodynamic radius of the polyelectrolytes or DNA strands used in this work. This implies that the soluble polyelectrolytes can interact not only with charged groups on the outer surface of the gel or microsphere but may also be able to penetrate significant distances into the gel. Such interactions are probably the cause of the increase in roughness of the GMS surfaces after incubation with PAH and then PAA. Variable pressure SEM may provide some useful insight as to the physical structure of this interface without the drying or destruction of the surface that traditional SEM would require. Additionally, removal of some of the polyelectrolyte material

through exposure to high salt concentrations should enable investigation of the gelatin supporting the polyelectrolyte bilayer. The use of fluorescently labeled polyelectrolytes during adsorption and removal of the polyelectrolyte will permit the estimation of the quantity deposited on the GMS. From this information one may be able to better understand the mechanism for the controlled release for GMS coated with PAH/PAA and which could also have application of other hydrogel systems.

5.3 Intrinsic Colloidal Disassembly

Although assembly of the first particle layer on the GMS cores appears to be mediated by nonspecific forces in Chapter 4, and assembly of a second layer of particles functionalized with complementary DNA appears to be reticent to disassembly even in the presence of high concentration of competitive DNA, thus, specific control of colloidal assembly and disassembly is an ongoing goal. The likely cause of the lack of responsiveness of the second particle layer to competitive DNA is the release of soluble PAH or gelatin that then adsorbs to the surface of the microspheres and induces aggregation. A possible solution to this problem is the addition of more polyelectrolyte bilayers to more securely trap the gelatin. Ensuring that the particles attaching via DNA-hybridization are highly charged (same sign) also increases the odds of specific assembly that is then reversible. In general, stronger charges of the satellite particles in the two layers increase the likelihood of specific assembly and disassembly. The change of the surface functionalization of colloidal assemblies after release of competitive DNA from the core particle demonstrated in Chapter 4 strongly suggests that colloidal disassembly via the same mechanism is possible but will require the changes described above and sequences specifically chosen for this purpose.

5.4 Surface Hybridization

Understanding hybridization at surfaces is critical for both the surface functionalization changes demonstrated in Chapter 4 as well as any DNA-detection technologies where the probe DNA is immobilized on a surface. Both careful characterization of the surface and analysis of the thermodynamics of hybridization at surfaces are currently lacking. Surface roughness, charge, and curvature can all impact the hybridization of the immobilized DNA. While surface curvature is relatively simple to characterize, the surface charge is complicated by interaction with the solution and the nature of the surface (metallic or nonmetallic). Although zeta potential is often used to characterize the electrostatic surface potential for colloidal species, it is challenging to convert from electrophoretic mobility (the measured quantity) to zeta potential for complicated surfaces such as a DNA-polymer brush affixed to polymeric surface.

The *in situ* hybridization protocol permits a more in depth investigation into the thermodynamics and kinetics of hybridization on colloidal surfaces. Colloidal surfaces behave differently than flat surfaces because the boundary layer of effectively still liquid next to the surface is significantly smaller at colloidal surfaces thus reducing or removing the kinetics effect of such a diffusive barrier. By changing the composition of the DNA sequences used but not the lengths, it is possible to shift the energetics of the hybridization event while leaving all other variables essentially constant. Changing the spatial location of the hybridizing region on the probe DNA allows exploration of the effect of distance from the surface. Ionic strength and probe concentration can also be varied to gain further insight into the electrostatics and the relative proportion of entropy and enthalpy.

Experimentally, a very carefully collection of sequences must be selected in a manner similar to Santa Lucia but including surface specific variables.¹ The thermodynamics of the specific sequences used should be directly assessed in relevant solution conditions using DNA melting experiments rather than relying on existing nearest models. Furthermore, although Santa Lucia's simpler model for calculating the thermodynamics of solution hybridization may be most common in literature,² this work may benefit from the more accurate models accounting for the changes in the specific heat on hybridization.^{3,4} The measured solution thermodynamics can then be directly compared to hybridization at surfaces to assess the effect of immobilization.

5.5 Alternate Applications

The coated GMS can be used as a controlled release reservoir for more than just DNA. In theory, it should work for any molecule that does not interact strongly with the gelatin matrix. This could be pharmaceuticals or cells for tissue engineering. Cells encapsulated in gelatin are effectively delivered in a matrix very similar to the collagen that is common in most extracellular matrix. Even if oligonucleotides are the payload, the oligonucleotides could be therapeutic on their own instead of controlling the release of other therapeutics. For example, the encapsulated DNA could be used for gene transfection or gene knockdown therapies. Gelatin is well known for its food applications. Gelatin microspheres may also have application as stable containers for flavoring molecules or nutrients that only release their payload on increase in temperature even in aqueous environments.

Although nano- and micro- particles are becoming more prevalent in modern technology, there is still limited understanding of interactions between colloidal particles with polymer brushes. DNA-functionalized colloidal particles represent a unique tool for studying

fundamental colloidal science since the interactions can be tuned and the DNA chains can be produced with low polydispersity. Changing ssDNA length can be used to tailor the electrostatics while inclusion of double strand segments can force the DNA to extend further into the solution, thus increasing the thickness of the polymer brush. In summary, the applications of the research presented in this work significantly exceed those which originally motivated it.

5.6 References

1. H. T. Allawi and J. SantaLucia, *Biochemistry*, 1997, **36**, 10581-10594.
2. J. SantaLucia and D. Hicks, *Annu. Rev. Biophys. Biomol. Struct.*, 2004, **33**, 415-440.
3. A. Tikhomirova, N. Taulier and T. V. Chalikian, *J. Am. Chem. Soc.*, 2004, **126**, 16387-16394.
4. T. V. Chalikian, J. Volker, G. E. Plum and K. J. Breslauer, *Proc. Natl. Acad. Sci. U. S. A.*, 1999, **96**, 7853-7858.

APPENDIX A

FURTHER DISCUSSION OF KINETICS AND ENERGETICS OF HYBRIDIZATION

A.1 ΔS Changes Due to Immobilization

The most obvious difference between solution and surface hybridization as described in this work is the immobilization of one of strands intended for duplex formation. Conjugation to a surface alters the entropy of the immobilized strand since the number of states it can attain becomes severely restricted. For this discussion, entropy will be divided into its translational, rotational, and conformational components. All of the subsequent arguments are based on simple state counting and thus assume that all states counted are approximately equal in probability. To begin evaluating the translational and rotational components of the change in entropy of hybridization, ssDNA and dsDNA are both assumed to behave as rigid rods. Notably, this rigid rod structure more appropriately represents for dsDNA (persistence length of ~50nm) than ssDNA (persistence length of ~1 nm). If the number of rotational states that a particular soluble strand of DNA can attain are Ω_{rot} , the rotational entropy of two strands is then $k_B \ln / (\Omega_{rot})^2 /$ or $2 k_B \ln / \Omega_{rot} /$ prior to hybridization and $k_B \ln / \Omega_{rot} /$ following hybridization in solution where k_B is the Boltzmann constant. The change in rotational entropy on hybridization in solution is then $- k_B \ln / \Omega_{rot} /$. Although restricted by the surface, immobilized DNA still has some rotational freedom. Assuming a sufficiently low surface density of probes such that probe strands act essentially independently ($2/\kappa$ and $2l$ are less than the spacing of probe strands on surface where l/κ and l are the Debye length and length of the DNA, respectively) and weak

electrostatic forces near the surface, the residual rotation of the immobilized probe prior to hybridization and after hybridization with the target should be the same. Under this collection of assumptions the change in rotational entropy for hybridization at a surface is identical to in solution, however, these assumptions are not necessarily valid for our system. Interacting immobilized duplexes and probe DNA at the surface can yield changes in rotational freedom following hybridization because dsDNA, which are more charged, may incur electrostatic hindrance to rotation. In the real system, the dsDNA also has a larger end to end distance than ssDNA due to dsDNA's higher rigidity and thus may also incur more steric restrictions in addition to the electrostatic ones. We will assume a two-fold decrease in rotational freedom upon hybridization (the strand can only rotate half as much). This will yield an approximate change in rotational entropy per mole of $N_A k_B \ln/2$ or 1.37 cal/mol/K where N_A is the ideal gas constant. At 23 °C, this yields a change in the free energy of hybridization of 407 cal/mol relative to solution hybridization, thus making hybridization less favorable. Translational entropy can be treated similarly with a similar possible contribution to the free energy as neighboring strands begin interacting. In the case of translational entropy, one considers the motion of the center of mass. As the strand rotates, its center of mass follows the surface of a sphere. Restrictions in rotation therefore yield identical restriction in translation.

Conformational entropy is significantly harder to account for since the ssDNA can no longer be treated as rigid rod. Prior to hybridization the entropy of the two ssDNA in solution can be described by equation A.1 in which Ω_{ssDNA} is the total number of possible conformational states of a ssDNA strand. Upon hybridization in solution to form a duplex the change in configurational entropy can be described by equation A.2, in which Ω_{dsDNA} is the number of conformational states of a dsDNA. Since the ssDNA is more flexible than dsDNA, the

conditions represented by equation A.3 are applicable and allow simplification of equation A.2 to equation A.4.

$$S_{conformational,solution} = 2 k_B \ln|\Omega_{ssDNA}| \quad (A.1)$$

$$\Delta S_{conformational,solution} = k_B \ln|\Omega_{dsDNA}| - 2 k_B \ln|\Omega_{ssDNA}| \quad (A.2)$$

$$\Omega_{dsDNA} \ll \Omega_{ssDNA} \quad (A.3)$$

$$\Delta S_{conformational,solution} \sim - 2 k_B \ln|\Omega_{ssDNA}| \quad (A.4)$$

In the simple case of an oligonucleotide attached at one end to a flat surface, the number of available states can be approximated using as a random walk approach in which the first segment (one persistence length) extends perpendicular to the surface and following segments each change the total height of the oligonucleotide by a random value less than or equal to the length of a segment in magnitude. Such a model was constructed and the fraction of stands not impacting the surface (out of 500) are displayed in Figure A.1. Different initial heights were also investigated. Such a treatment neglects restrictions from collision of the chain with itself and does not explicitly take into account the mechanical properties of the macromolecule. Based on Figure A.1, for ~10 statistical segments (12 nm contour length / 1.3 nm persistence length) and a starting height of 1 statistical segment, this model predicts that immobilization on a flat surface alone reduces number of possible conformations by a faction of two as shown in equation A.5.

$$\Delta S_{conformational,surface} \sim - k_B \ln|\Omega_{ssDNA}/2| - k_B \ln|\Omega_{ssDNA}| \quad (A.5)$$

It is clear from equation A.5 that the difference in entropy between the solution and immobilized cases is $k_B \ln|2|$, thus making hybridization more favorable in solution but of the same order of magnitude as the rotational and translational entropy. Restrictions from interaction with neighboring probe stands could significantly widen the difference in these entropic contributions. Based on the analysis above, the difference in free energy of hybridization between solution and surface hybridization due to entropic consideration is on the order of -0.5 kcal/mol which is a small but not insignificant reduction in the stability of immobilized strands.

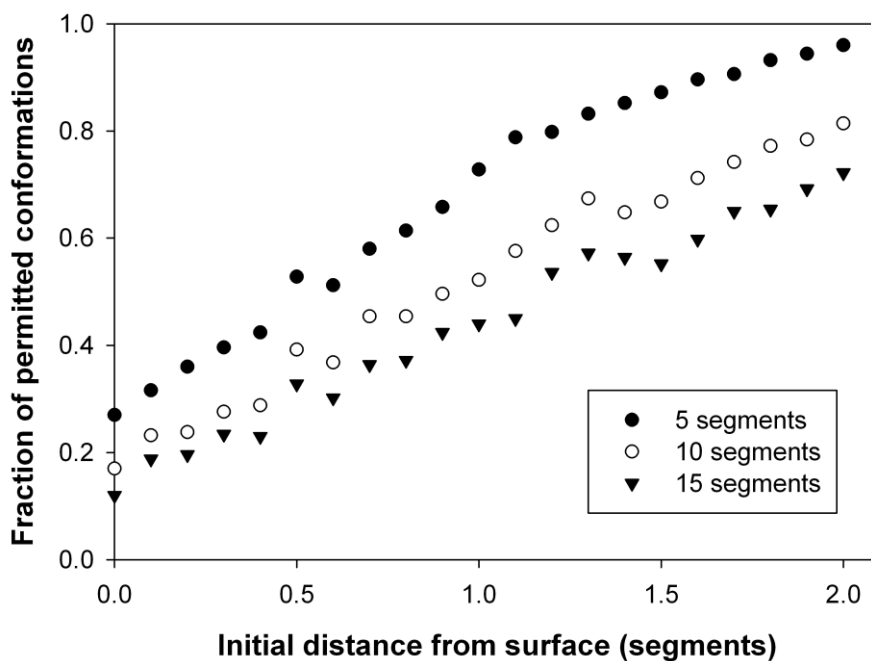


Figure A.1. Fraction of allowed conformations as a function of the initial height above the surface for 5, 10 and 15 statistical segments based on an average of 500 runs of the random process described in the text.

There are many deviations from the various simplifying assumptions used above. While these are beyond the scope of this work to fully address, a select subset of these deviations will

be briefly discussed. Surface roughness can impact all the factors above. Roughness on a size scale that is significantly larger or smaller than the DNA strand can be ignored; however roughness on a similar size scale as to the DNA strands can alter how strands are confined and accessed by soluble species. Electrostatic effects from charged surfaces as well as local and bulk ionic strength are also likely to significantly alter the distribution of available states.

A.2 Reaction at the Surface

Although primary hybridization in solution is well characterized by prior work and described by equation A.6,¹ some modifications still need to be made to account for the size of the reaction volume near a surface. Since the hybridization reaction is limited to within a DNA macromolecule's length of the surface, the concentrations used should be based on this effective reaction volume. When hybridizing to an excess bulk concentration of target DNA, probe-target hybridization should proceed to completion, just as it would in solution. On the other hand, target released during dissociation is diluted by the presence of the bulk phase thus requiring a higher degree of dissociation to occur to establish equilibrium than would be required if the reaction volume was not connected to the bulk solution. This effect can be expressed as a modification to the free energy as shown below in equation A.6, A.7 and A.8, where α , the dilution factor, is the ratio of the reaction volume, V_0 , around the DNA-functionalized particles to the total solution volume, V_T .



$$K_{general} = \frac{[PT]}{[P][T]} = e^{\frac{-\Delta G}{RT}} \tag{A.7}$$

$$K_{corrected} = \frac{[PT]}{([PT]_0 - [PT] + [P]_0)\alpha^{-1}([PT]_0 - [PT])} = K * \frac{1}{\alpha} = e^{\frac{-\Delta G}{RT}} e^{\ln \alpha} \quad (A.8)$$

The dilution factor can be calculated by considering the number of particles, N_p , diameter of the particles, d , and the height of the DNA layer, h , as shown in equation A.9. N_p , as shown in equation A.10, is dependent on the volume fraction of particles, f , as well.

$$\alpha = \frac{V_0}{V_T} = \frac{N_p \pi d^2 h}{(1-f)V_T} \quad (A.9)$$

$$N_p = \frac{fV_T}{\frac{1}{6} \pi d^3} \quad (A.10)$$

$$\alpha = \frac{6fh}{(1-f)d} \quad (A.11)$$

Since α is usually much less than one, the modification the the effective ΔG of hybridization is positive, thus making dissociation of DNA duplex on the surface is much more likely. Using a volume fraction of particle of 1.25×10^{-4} , height of probe DNA layer of 10 nm, and a particle diameter of 1 μm yields an α of 7.5×10^{-6} by equation A.11 and an effective change to the energy of 7 kcal/mol.

A.3 Kinetics of Hybridization

The equation used to calculate the fraction of primary target displaced by a competitive target, equation A.12 which is equivalent to equation 3.3, can also be expressed in terms of the

fraction of primary duplexes remaining, f_{pd} , shown in equation A.13 in which the terms are defined in Section 3.1.4. Through some simple manipulation one can then distinguish contribution of the dissociative and sequential pathways as shown in equation A.14. This form represents one of the simplest interactions between two simultaneous pathways. Furthermore, as long as the terms from the two pathways can be separated as in equation A.14, equation A.12 will only produce the fraction of primary target displaced.

$$f_d = (f_r - f_{r,nc}) / (1 - f_{r,nc}) \quad (\text{A.12})$$

$$f_d = (f_{pd,nc} - f_{pd}) / (f_{pd,nc}) \quad (\text{A.13})$$

$$f_{pd} = f_{pd,d} \cdot f_{pd,nc} = f_{pd, \text{only sequential pathway is active}} \cdot f_{pd, \text{only dissociative pathway is active}} \quad (\text{A.14})$$

Many others have modeled DNA hybridization as a two-state reaction and approximated it with simple reaction kinetics as discussed in Chapter 1. The most likely limiting reactions of the sequential and dissociative pathways in solution are listed below in equation A.15 and A.16.² On a surface, other intermediate steps involved in exchanging partner strands may become significant or dominate. For example, the approach of the target to a charged surface, the penetration of the target through the diffusion boundary layer and DNA brush, or conformational rearrangement in order to access a toehold region are more likely to become relevant on surfaces. The reactions below are assumed to be the limiting reaction for the purpose of this treatment in order to be consistent with solution work, thus making deviations caused by surface immobilization more evident. Both of these equations are strongly in toward the forward direction because $[T_1]$ is going to be very small (due to the dilution factor discussed earlier) and

the T_2 is a much more favorable binding partner than T_1 (in all cases but the **P15-F** primary target).



Equation A.17 is a simple description of the kinetics of these reactions. Since $[T_2]$ is in excess and is thus effectively constant in most of the conditions investigated in this work, the rate equation reduces to equations A.18 and A.19. The solution to equation A.19 is equation A.20. Equation A.21 is essentially a first order Langmuir adsorption equation. Second order Langmuir adsorption has also been suggested and appears to fit better under some conditions, however, treatments like equation A.21 appear to be the most common in literature²⁻⁵ and without clearer experimental and theoretical justification for other models we continue using it in the current work.

$$\frac{d[PT_1]}{dt} = -k_d[PT_1][T_2] - k_4[PT_1] \quad (\text{A.17})$$

$$\frac{d[PT_1]}{dt} = -(k_d[T_2] + k_4)[PT_1] \quad (\text{A.18})$$

$$\frac{d[PT_1]}{dt} = -k_{obs}[PT_1] \quad (\text{A.19})$$

$$[PT_1] = [PT_1]_0 e^{-k_{obs}t} \quad (\text{A.20})$$

Equation A.20 also satisfies the requirements of equation A.14. Based on this analysis, f_r and $f_{r,NC}$ can be determined by equations A.21 and A.22.

$$f_r = 1 - \frac{[PT_1]_{competitiveDNA}}{[PT_1]_0} = 1 - e^{-k_{obs}t} \quad (A.21)$$

$$f_{r,NC} = 1 - \frac{[PT1]_{NC}}{[PT1]_0} = 1 - e^{-k_4t} \quad (A.22)$$

In literature, f_d is has been expressed as by equation A.23²⁻⁴ but analysis was restricted to cases in which primary target dissociation (in the absense of a complementary target) was negligible. Upon substituting equations A.21 and A.22 into A.23, an expression is derived which takes into account both the displacement and dissociative pathways. The modification used in this work, equation A.24, successfully separates just the terms associated with sequential displacement of the primary target where k_2 equals $k_d[T_2]$.

$$f_r - f_{r,NC} = -e^{-k_{obs}t} + e^{-k_4t} \quad (A.23)$$

$$\frac{f_r - f_{r,NC}}{1 - f_{r,NC}} = \frac{-e^{-k_{obs}t} + e^{-k_4t}}{e^{-k_4t}} = 1 - e^{-k_2t} \quad (A.24)$$

Although the treatments in equations A.23 and A.24 are similar, using A.23 can lead to a local maximum that is not consistent with the assumptions above. Specifically, the “hump” in Figure A.2 (b) implies that the displaced DNA will either competitively displace the competitive DNA (eventually coming to an equilibrium) or that the competitive strand is less thermodynamically favorable bind partner than the primary target DNA and thus hybridizes to a lesser extent. Since neither of these possibilities is likely in the experimental system used in this

work, the local maximum generated by equation A.23 is purely an artifact of the analysis caused by slow but significant release in the presence of noncomplementary DNA as shown in Figure A.2 (a).

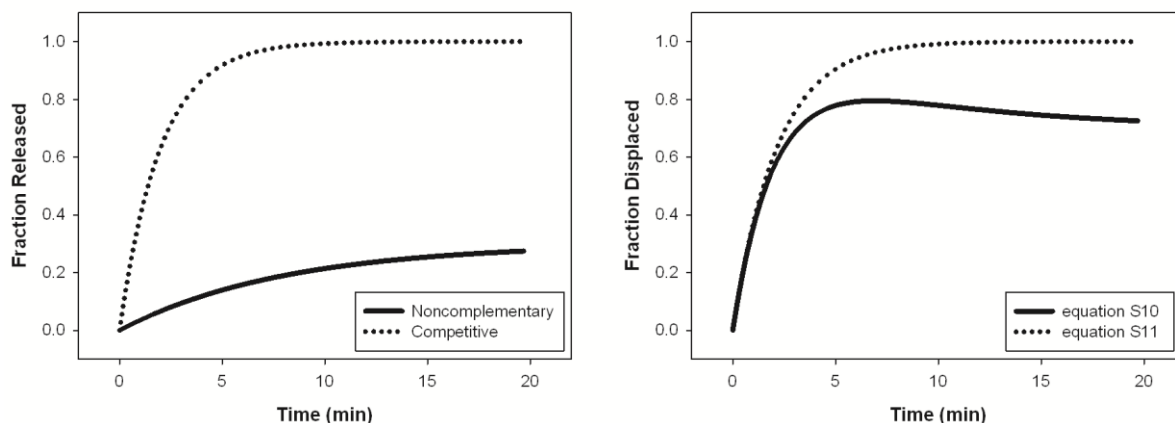


Figure A.2. (a) Examples of hypothetical fractions of primary target released in the presence of noncomplementary or competitive DNA based on equation A.21 and A.22 (limited to 30% of total strands). (b) Resulting fractions displaced using the examples in (a) and equation A.23 and A.24.

Equation A.24 also follows the form of an exponential rise to maximum. Others have suggested a double exponential rise to maximum.^{2, 3, 6} Such a form would imply two independent kinds of sites which seems unlikely unless one of the sites involves nonspecific adsorption events. In all of the cases displayed in Figure 3.6 the equilibrium fraction displaced remains significantly below 1, this equilibrium value represents a deviation from the behavior predicted in equation A.24 but fits to equation 3.5 still permit some quantitative assessment of competitive displacement rates. In conclusion, this treatment of the kinetics of competitive hybridization at a surface is simplistic, but more complete than previously done.

A.4 References

1. J. SantaLucia, Jr., *Proc. Natl. Acad. Sci. U. S. A.*, 1998, **95**, 1460-1465.
2. L. P. Reynaldo, A. V. Vologodskii, B. P. Neri and V. I. Lyamichev, *J. Mol. Biol.*, 2000, **297**, 511-520.
3. C. K. Tison and V. T. Milam, *Soft Matter*, 2010, **6**, 4446-4453.
4. B. A. Baker and V. T. Milam, *Nucleic Acids Res.*, 2011, **30**, doi:10.1093/nar/gkr1293.
5. D. Porschke, O. Uhlenbec and F. H. Martin, *Biopolymers*, 1973, **12**, 1313-1335.
6. J. Zeng, A. Almadidy, J. Watterson and U. K. Krull, *Sensors and Actuators B-Chemical*, 2003, **90**, 68-75.

VITA

James Hardin was raised in Statesboro, GA where he attended Georgia Southern University while completing his high school diploma in 2000. He then attended the Georgia Institute of Technology for undergraduate education and graduated with highest honors with bachelor degrees in Physics and Polymer and Fiber Engineering in 2005. After graduating from GaTech, James moved to the Massachusetts Institute of Technology for a Master of Engineering program in the Material Science and Engineering department. In his master's project at MIT, he evaluated the effectiveness of suspended microchannel resonator technology for detecting malaria and cancer. After graduating from MIT, James moved back to GaTech to work on a PhD in 2006 under Dr. Valeria Milam on using DNA intrinsic to a colloidal assembly to affect changes in its functionalization.